January 2012

Catalytic Tri-reforming of Biomass-Derived Syngas to Produce Desired H2:CO Ratios for Fuel Applications

Devin Mason Walker
University of South Florida, dmwalker@mail.usf.edu

Catalytic Tri-Reforming of Biomass-Derived Syngas to Produce Desired H_2:CO Ratios for Fuel Applications

by

Devin Walker

A thesis submitted in partial fulfillment
of the requirements for the degree of
Master of Science in Engineering Science
Department of Chemical and Biomedical Engineering
College of Engineering
University of South Florida

Major Professor: John Kuhn, Ph.D.
Babu Joseph, Ph.D.
Yogi Goswami, Ph.D.

Date of Approval:
February 22, 2012

Keywords: Gas to Liquid, Fischer Tropsch, Energy,
Biofuel, Solar Power, Hydrogen Production

Dedication

I would like to take the time here to thank all those who have inspired and encouraged me along the path towards completing this thesis. I would especially like to thank my mother and father, Linda and Kevin Walker, for inspiring the desire to be great and the persistence to achieve it. I also would like to thank all those that have encouraged/put up with me in this stressful time, especially Veronica Eltz and Reid Wilson. It has been a difficult time with the passing of Dr. John Wolan during this project, and I would especially like to express my appreciation to Dr. Kuhn and the Heterogenous Catalysis Group for welcoming me in with open arms and making the transition back to work much easier. I would like to thank Tim Roberge for his inspiration during the writing of this thesis. Tim silently proved through his actions that he could finish his thesis in a timely manner even when he had a family to provide for, a newborn child, and a second job. Lastly, I would like to thank my sister, Star Walker, for making feel like the best brother in the world even though I probably wasn't always there during the completion of this thesis.

Acknowledgements

I write this work in memoriam of Professor John T. Wolan who recently passed away during the completion of this project. I would also like to gratefully acknowledge funding from Hinkley Center for Solid and Hazardous Waste Management and the Florida Energy Systems Consortium. I thank USF's Nanotechnology Research and Education Center (NREC) for use of their facilities. I would also like to thank Sandra Pettit, Ali Gardezi, and Ben Rice for their help in obtaining XRD, XPS, and SEM-EDS data respectively. I thank the Heterogeneous Catalysis Group at USF for all their help and support both inside and outside the lab. I would also like to thank my lab partner Phil Saraneeyavongse for his help during this project. Lastly, I would like to acknowledge all of my committee members and professors that helped me throughout my years at USF, whom without I would not have been able to understand the complexities of catalysis and chemical engineering.

Table of Contents

List of Tables

List of Figures

Abstract

This study focuses on upgrading biomass derived syngas for the synthesis of liquid fuels using Fischer-Tropsch synthesis (FTS). The process includes novel gasification of biomass via a tri-reforming process which involves a synergetic combination of CO_2 reforming, steam reforming, and partial oxidation of methane. Typical biomass-derived syngas H_2:CO is 1:1 and contains tars that deactivate FT catalyst. This innovation allows for cost-effective one-step production of syngas in the required H_2:CO of 2:1 with reduction of tars for use in the FTS. To maximize the performance of the tri-reforming catalyst, an attempt to control oxygen mobility, thermal stability, dispersion of metal, resistance to coke formation, and strength of metal interaction with support is investigated by varying catalyst synthesis parameters. These synthesis variables include Ce and Zr mixed oxide support ratios, amount Mg and Ni loading, and the preparation of the catalyst. Reaction conditions were also varied to determine the influences reaction temperature, gas composition, and GHSV have on the catalyst performance. Testing under controlled reaction conditions and the use of several catalyst characterization techniques (BET, XRD, TPR, XAFS, SEM-EDS, XPS) were employed to better explain the effects of the synthesis parameters. This paper highlights the performance of the tri-reforming catalyst under various reaction conditions and explains results using catalyst characterization. A proof of concept solar powered BTL plant was designed by applying the resulting data.

1. Introduction

1.1 Renewable Energy

In today's environmentally conscious world, a recent shift towards using fuels produced from renewable resources has been seen. Rising fuel costs, instability in the Middle East, and rising greenhouse emissions are driving research towards finding alternative energies to petroleum. Recent developments in solar, wind, wave, and biofuel technologies are helping to make a sustainable and environmentally friendly energy solution possible. However each of these technologies have their disadvantages and it has become evident that a combination of alternative energy technologies will be needed to meet the world's energy demand.

Liquid hydrocarbon fuel derived from fossil fuels provides the majority of energy for transportation purposes around the world. The US alone currently has a total fossil fuel consumption of approximately 14.33 billion barrels (oil equivalent) per year [1]. Coal provides a large portion of energy for various purposes around the world with recent developments in coal to liquid fuel technologies. However, these fossil fuel resources are not sustainable and are limited in supply. The Energy Information Administration estimates that the US has 275 billion tons of coal resources and is capable of meeting domestic demand for 250 years at current rates of consumption [2]. It is estimated that the US oil reserves total 21.317 billion barrels while the world oil reserves total 1,342 billion barrels [3]. In 2009, the US consumed 19,150,000 bbl/day and the world consumed 84,213,000 bbl/day [4]. At this current consumption rate, the US would

deplete their own reserves in 3 years while the entire world reserves would be depleted in about 44 years. The greenhouse emissions from petroleum and coal-derived energies are also causing alarm with talks of global warming and pollution [5]. The problems mentioned above are things that are not an immediate threat and can be predicted or calculated to determine a specific time when these issues will cause a drastic problem. However, there are those problems that are unforeseen and cannot be predicted or calculated such as the recent Deepwater Horizon oil spill in the Gulf of Mexico or the earthquake that hit Fukushima Daiichi nuclear plant and caused a nuclear crisis. Therefore, it is recognized that there is a need to produce an alternative energy that reduces greenhouse emissions and provides a safer, environmentally friendly route towards sustainable energy. This need can be met through the use of bio-derived fuels. The use of biofuels creates a closed loop system in which carbon is taken up from the atmosphere and incorporated into the biomass framework [6]. The carbon from the biomass can then be converted into hydrocarbon fuels that when burned will release the carbon back into the atmosphere to continue the cycle. In doing so, no further carbon is added to the atmosphere leaving no carbon footprint.

Today, liquid biofuels are broken down into two main categories: fatty acid methyl ester (FAME) and non-ester biofuel. FAME fuel is mainly derived from the oils of plants and algaes. Methanol along with acid or base catalysts are added to processed plant and algae oils to convert the triglycerides to FAME's and glycerol in roughly a 9:1 ratio. The FAME product can then be used directly as a biodiesel type fuel. The disadvantages to this process are that FAME physical properties do not allow them to be used in cold environments and blending of the biodiesel with petroleum-derived fuel

must be done. The esters also provide sites of reactivity and the stability of the fuel must be conserved through the use of antioxidants, biocides, and other additives [7]. Other disadvantages are the large amounts of glycerol by-product produced and the large amounts of organic chemicals (methanol) that must be used. Research into ways to use the glycerol by-product to increase revenue is ongoing with hopes to use the glycerol as a feedstock in biological processes such as alcohol synthesis [8]. The second category of biofuel is non-ester renewable fuel (NERF). These biofuels can be derived through catalytic processing of plant and algae oils or gas to liquid technologies. The catalytic processing of oils usually involves nickel (Ni) catalyst along with hydrogen to decarboxylate, isomerize, and saturate the compounds found in plant and algae oils [9]. These fuels have the advantage of better physical properties over FAME's that can be tailored to fit the desired fuel cut. Some advanced biofuels have even met specification testing for JP-8 and Navy distillate fuels, resembling their petroleum counterparts [10]. These NERFs require large amounts of hydrogen usually derived by reforming of natural gas.

Recent developments in the reforming of biomass derived syngas has led to breakthroughs in producing hydrogen as well as syngas for industrial and environmental applications. Gas-to-liquid (GTL) technologies are seeing a resurgence in interest with expanding developments in the Middle East, Asia, and Africa [11]. Rahmim predicts growth in production capacity of GTL technologies though 2020 with increasing demands for GTL fuels built to serve local markets [12]. The EPA RFS2 alternative fuel mandate states that the US needs to produce 36 billion gallons/yr by the year 2022 [13]. The US federal government has set a target of displacing 30% of current US fuel

consumption, equating to 200 billion gallons/yr, of biofuels by 2030 [14]. The US military has stated goals to make changes to using renewable fuels with the Air Force planning on having 50% of its aviation fuels derived from domestically produced renewable fuels by 2016. This equates to 400 million gallons of synthetic fuels needed to be produced for the Air Force alone. The Air Force has also made intentions to fly solely on domestically produced alternative fuels from renewable resources, including biomass, by 2030 [15]. The Navy has stated goals to reduce its petroleum consumption 50% by 2020 [15-17]. It is clear a combination of renewable energy technologies will be needed to meet this demand with Fischer Tropsch synthesis (FTS) playing a major role. This requires that developments in the reforming of syngas for FT applications are necessary and highlights the need to develop those technologies utilizing biomass as a feedstock.

1.2 Biomass Feedstocks

Biomass is composed of the organic matter derived from living or recently living plants and animals. The main categories of biomass include food crops, grassy and woody plants, residues from agriculture or forestry, oil-rich algae, and the organic components of municipal and industrial wastes [18]. The use of biomass for energy can be dated back from the earliest of human existence, being burned to produce heat in the form of fire. The burning of biomass is still prevalent throughout the world supplying 15-20% of the total energy use in the world. In non-industrialized economies, biomass is mainly used for domestic heating and cooking while in industrialized countries biomass use as a fuel is mainly restricted to by-products from forestry, paper, and sugar industries [19]. Desires to produce a more efficient means of deriving energy from biomass have led to the developments of cellulosic ethanol processing. This led to large scale use of

food crops as feedstocks, such as corn, creating controversy in a food vs. fuel debate [20]. Prices of food began to escalate as more food crops were being used for energy applications. In 2008, corn reached a 10-year high at the price of $4.83 per bushel[21]. The US government recognized this and has called upon researchers to develop advanced biofuels from feedstocks that do not compete with the food industry and a shift towards using dedicated energy crops derived from non-food resources has begun. This includes utilization of the cellulosic portion of biomass already largely being produced in forestry and waste industries [22]. Some of the dedicated energy, non-food crops include jatropha, camelina, corn stover, fast growing grasses, bagasse, castor, tung, hardwoods, and pinewoods. "Black liquor" from papermaking processes is also seen as a potential biofuel resource. Each of the crops mentioned are grown with the intention of harvesting oil or cellulosic material from the plants to be converted into biofuel. However, biological conversion of low-value lignocellulosic biomass is still considered to be economically unfavorable with low efficiencies leading to new developments in biomass gasification [23].

Algae is recognized as a possible biomass feedstock with its ability to rapidly reproduce. Algae growing systems have seen an increase in research and development with goals of finding the optimum strain for energy applications. Open and closed systems are currently being used to grow various strains of micro and macro algae each with a specific niche in the biofuels market. Other areas of algae research include the use of algae to purify water and remove compounds such as fertilizers, CO_2, or industrial wastes [24, 25]. These open type systems usually involve the use of multiple indigenous algae strains that can be harvested as a biomass feedstock for gasification. This

overcomes the problem associated with complicated or economically challenging oil extraction processes and avoids the use of environmentally unfriendly chemicals by directly converting the dried algae biomass into valuable syngas for various energy and chemical applications.

As the human population increases, so has the amount of waste being produced. The accumulation of municipal solid waste (MSW) in landfills is causing concern with many waste companies offering incentives to safely remove and dispose of the accumulating waste. MSW is composed of everyday garbage consisting mainly of paper and paperboard, food scraps, yard trimmings, rubber, leather, textiles, wood, plastics, metals, and glass with biomass making up around 71% of the total. In 2009, the EPA estimated that 243 million tons of MSW were produced in the United States. This is an increase of 176% since 1960. It is estimated that it cost approximately $44/ton to bury landfill waste and therefore MSW provides the potential to use a negative value feedstock to create a high value product in the form of biofuel by recycling the biomass [26]. MSW provides an excellent opportunity as a major, near-term, carbon-neutral energy resource. Currently, less than 15% of MSW is being used to generate energy and the majority of MSW accumulates in landfills [27]. Florida has more MSW biomass resources than any other state, ~7% of the U.S. total. Harnessing these resources should be a key component of Florida's energy strategy. In today's industry, MSW used to generate energy is burned or incinerated creating environmentally unfriendly gases and particulates such as greenhouse gases, heavy metals, and organic compounds with well known negative environmental and public health effects [28]. The net efficiency for the generation of electricity from combustion is low at around 20-40%. Some facilities are co-firing

biomass and coal in existing combustors, but biomass is limited to 5-10% of the total feedstock due to concerns of plugging the coal feed system [23]. Pyrolysis of biomass to bio-oils also received some attention but due to difficulty in downstream processing, new routes to biomass energy conversion are more heavily researched. Evidence has shown gasification to be the more efficient and environmentally preferable way for thermal conversion of biomass and related organic feedstock to energy [23, 29]. Because of the natural biodegradation of landfill waste beneath the ground, large amounts of methane gas can also be collected. Stern et al states "Landfills are estimated to account for about 35% of anthropogenic CH_4 emissions in the United States and 5-10% of global CH_4 emissions to the atmosphere"[30]. Some landfills have taken advantage of this naturally occurring process and have refurbished their landfills to collect this methane as a value added side product. Here, it is proposed that this methane gas be used to supplement a reactant feed stream to an onsite reformer to optimize the syngas for FT applications. An onsite gasifier could provide crude syngas derived from the MSW to be delivered to the reformer. The upgraded syngas from the reformer could then be fed to a FT reactor to synthesize liquid hydrocarbon fuel to be sold or used onsite to power equipment. This overcomes the economic problems associated with transportation of the low energy density biomass (~3.7 GJ/m^3) by converting it to a high density transportable fuel onsite [19].

1.3 Gasification

Gasification creates synthesis gas (syngas) for the production of high value chemicals, electricity, and clean burning hydrocarbon fuels. This crude syngas is composed of CO_2, H_2O, CO_2, H_2, gaseous hydrocarbons, char, ash, and condensable

tars/oils. The main steps involved in gasification are drying, pyrolysis, oxidation, and reduction. The first step involves reducing the moisture content of the biomass by drying. The dried biomass is then fed to a pyrolysis zone where oxygen starved reactions occur to produces 75-90% volatile material. The remaining nonvolatile material is described as char or ash. The char is then oxidized to produce CO_2, CO, and H_2O while the ash is collected and removed from the process [31]. Ashes produced from biomass mainly consist of salts comprised of potassium, calcium, phosphorus, sodium, magnesium, iron, silicon, and other trace elements [19]. The ash has potential as a value added side product for the fertilizer industry. Reduction occurs in the presence of sub-stoichiometric O_2 and is driven by the heat produced from the exothermic oxidation reactions or an external source [23, 32-34]. Figure 1 shows a flow chart representing the major steps in the gasification process. The dominant reactions involved in gasification are listed in eq. 1-7 [19, 31, 35, 36].

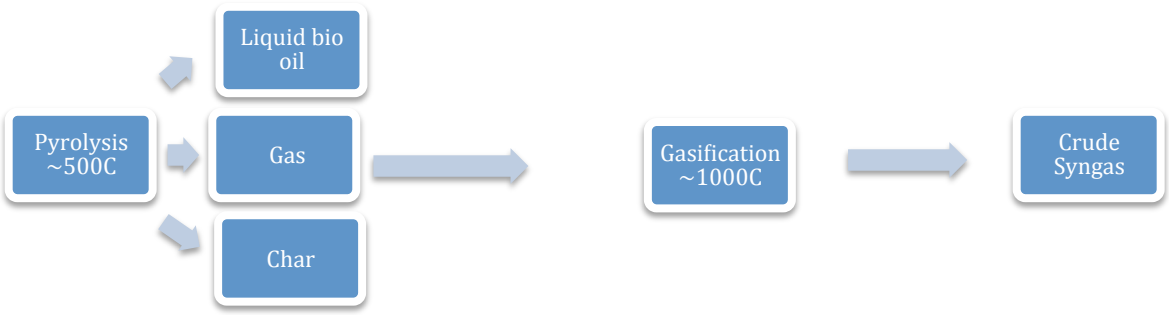

Figure 1: Flow chart representing major steps involved in gasification.

Exothermic Reactions

(1) Combustion $Biomass\ volatiles/char + O_2 = CO_2$

$$\Delta H° = -394\ {}^{kJ}/_{mol}$$

(2) Partial Oxidation $Biomass\ volatiles/char + O_2 = CO$

$$\Delta H° = -111\ {}^{kJ}/_{mol}$$

(3) Methanation $Biomass\ volatiles/char + H_2 = CH_4$

$$\Delta H° = -75\ {}^{kJ}/_{mol}$$

(4) WGS $CO + H_2O = CO_2 + H_2$

$$\Delta H° = -41\ {}^{kJ}/_{mol}$$

(5) CO Methanation $CO + 3H_2 = CH_4 + H_2O$

$$\Delta H° = -206\ {}^{kJ}/_{mol}$$

Endothermic Reactions

(6) Steam-Carbon rxn $Biomass\ volatiles/char + H_2O = CO + H_2$

$$\Delta H° = 122.6\ {}^{kJ}/_{mol}$$

(7) Boudouard rxn $Biomass\ volatiles/char + CO_2 = 2CO$

$$\Delta H° = 164.9\ {}^{kJ}/_{mol}$$

A variety of gasification processes have been developed including entrained-flow, fixed-bed, and fluidized-bed gasifiers. In the case of biomass gasification, fluid-bed processes are most often used [19]. Fluid-bed processes provide extremely good mixing between the feed and oxidant promoting heat and mass transfer with a good scale-up

potential. However, fluid-bed processes have the disadvantage of lower carbon conversions and higher tar production compared to other processes [19, 37, 38]. The composition of these tars can be complicated but mainly consists of organic molecules with larger molecular weights than benzene such as oxygenated aromatics [36]. Tars can create major problems in synthesis gas used for FT and Hydrogen applications [39]. Dayton states that removal and/or conversion of tars is one of the greatest technical challenges to overcome for successful development of biomass-derived fuels [40]. The tars can condense on cool surfaces causing plugging and fouling of pipes and other equipment. At higher temperatures, above 400°C, tars can form solid char and coke that can foul and plug the system or deactivate the catalyst being used [36]. This has led to the coupling of the gasification processes to reforming systems to remove the unwanted tars and optimize the syngas for the desired application [40, 41]. At University of South Florida (USF), current FTS experiments have shown that benzene not only leads to a less desirable FT product but deactivates the Co catalyst quickly. It is clear from the above information that there are a variety of ways to process biomass to produce a crude syngas. This leads to a broad range of possible crude biomass syngas compositions that result from the different process conditions. Typical crude biomass syngas compositions resulting from different process conditions are given in Table 1 [23, 42]. This introduces many variables to the reforming process that must be understood to make the production of liquid biofuels efficient and economical. Some of those variables will be discussed further in the text.

Table 1: Typical producer-gas composition and operating conditions for atmospheric bubbling fluidized-bed-gasifiers. Printed with permission from Elsevier [23].

	Air [105]	**Steam (pure) [42]**	**Steam-O_2 mixtures [177]**
Operating conditions			
ER	0.18-0.45	0.00	0.24-0.51
S/B (kg/kg daf)	0.08-0.66	0.53-1.10	0.48-1.11
T (°C)	780-830	750-780	785-830
Gas composition			
H_2 (vol%, dry basis)	5.0-16.3	38-56	13.8-31.7
CO (vol%, dry basis)	9.9-22.4	17-32	42.5-52.0
CO_2 (vol%, dry basis)	9.0-19.4	13-17	14.4-36.3
CH_4 (vol%, dry basis)	2.2-6.2	7-12	6.0-7.5
C_2H_n (vol% dry basis)	0.2-3.3	2.1-2.3	2.5-3.6
N_2 (vol%, dry basis)	41.6-61.6	0	0
Steam (vol%, dry basis)	11-34	52-60	38-61
Yields			
Tars (g/kg daf)	3.7-61.9	60-95	2.2-46
Char (g/kg daf)	na	95-110	5-20
Gas (Nm^3/kg daf)	1.25-2.45	1.3-1.6	0.86-1.14
LHV (MJ/Nm^3)	3.7-8.4	12.2-13.8	10.3-13.5

na: not available; daf: dry ash-free basis; ER: equivalence ratio; S/B; steam-to-biomass ratio (H2O (kg/hr)/biomass (kg/daf/hr).

1.4 Reforming

Reforming of methane has played a major role in the production of H_2 and syngas for transportation, industrial, and residential markets [43]. The need for H_2 and syngas has only increased in the developing world and three major classes of reforming technologies have been developed. These reforming technologies are classified as steam reforming (SR), CO_2 reforming (CR) or dry reforming, and partial oxidation of methane (POM). Each of these technologies offers advantages and disadvantages over the others.

SR is the most prominent form of reforming currently in the industry as it produces high levels of H_2 [11, 44, 45]. However, SR is energy intensive due to the endothermic nature of the reactions and excess steam that must be generated to reach high H_2O:CH_4 ratios in order to prevent carbon deposits [11, 46-51]. Syngas produced from SR has a high H_2:CO ratio, usually greater than 3, due to the side WGS reaction also lowering the selectivity and yield for CO. Therefore additional processing, often expensive and complex, must be done to adjust H_2:CO ratios for FT or methanol synthesis [48, 52].

Because of the growing concern about global warming and environmental impacts, many researchers have turned to CR as a way to reduce two major green house gases; CH_4 and CO_2 [53-64]. Other researchers justify CR due to its flexibility in niche applications such as the production of oxygenated chemicals from hydroformylation reactions requiring a H_2:CO ratio of 1:1 [19, 65]. Debates over the mechanism involved in dry reforming have occurred over the years. Some researchers believe that the mechanism involves a single rate-determining step (RDS). This rate-determining step has been argued to be CH_4 decomposition, the decomposition of CH_xO to adsorbed H and CO, or the reaction between carbon from CH_4 and oxygen from CO_2 to produce CO [66-70]. Other researchers believe there are two RDS, involving the dissociation of CH_4 and the CH_xO decomposition [57, 71, 72]. Nevertheless, a combination of the above reactions occurs and their order and role in the overall mechanism is more than likely influenced by catalyst and reaction variables such as support/promoters of the catalyst and temperature differences respectively [73]. The major reasons CR is impractical in industry is the highly endothermic nature of the reactions, the propensity of catalyst

deactivation by coking, and the formation of water through side reactions selective for H_2 [74-77]. Researchers believe that CH_4 decomposition and CO disproportionation are favorable on Ni catalysts and attribute the high rate of deactivation to these reactions [78-84].

The third process involves POM overcomes many of the disadvantages of the above two reforming technologies. POM creates syngas in the desired 2:1 ratio of H_2:CO with a high selectivity for H_2 and CO, good conversion of CH_4, and low residence times [47, 52, 85-94]. POM is also seen to have the advantage of being exothermic, thus lowering the energy demand and making the process more economical. However, due to nature of these exothermic reactions, the reactions are difficult to control with hot spots developing and risks of explosion dangers [50, 85, 95-98]. Under these conditions, the risk of combusting CO and H_2 also poses a challenge.

It is evident that the above reforming processes alone cannot overcome problems associated with H_2:CO ratios, deactivation, safety, and economics. The determination upon which process to use is also highly dependent upon the desired application of the resulting syngas produced [11]. Some researchers have turned to CO_2 sorbents and guard beds (quicklime, calcined dolomites, olivines, etc.) placed before the primary reforming bed [99-105]. These modifications to the reforming process can alleviate issues with catalyst deactivation and reduce the amount of tars and other catalyst poisons like S, Cl, P, NH_3, and alkali metals in the crude syngas [101, 106, 107]. However, these technologies also come with their disadvantages such as the requirements for regeneration, decrease in activity over calcination/carbonation cycles, and low activity for reforming of light hydrocarbons [54, 106, 108, 109]. Other researchers have focused on

to the development of technologies that combine reforming processes. This has led to combined CR and POM, SR and POM, CR and SR, and a mix of all three processes known as tri-reforming. The combining of reforming processes offer the ability to tailor H_2:CO ratios and selectivity of products by altering the feed gas composition. Combined CR/POM and SR/POM alleviate the problems associated with high energy input by coupling exothermic POM reactions with endothermic CR and SR reactions. This facilitates heat transfer and creates a safer work environment with more control over the process. In CR/POM and SR/POM, resistance to carbon formation is increased by introducing O_2 to the reactant feed while costs of steam generation are also reduced in the case of SR/POM [43, 48]. Combined CR/SR can aid in the resistance to catalyst deactivation due to carbon formation [52]. However, the CR/POM combined process falls short in the ability to produce optimum H_2:CO ratios for FT and methanol applications while the SR/POM combined process excludes the environmentally beneficial conversion of CO_2. The SR/CR combined process still requires high energy input making it economically unfavorable. Tri-reforming overcomes the above problems and offers the best of all three processes. An in-depth discussion on tri-reforming is included later in the text.

1.5 Fischer Tropsch Synthesis

FTS is a well-researched process playing a major role in GTL technology. The roots of FTS date back to 1902 when Sabatier and Senderens first discovered that CO could be hydrogenated to methane over Co, Fe, and Ni catalysts [110]. It wasn't until 1925 did the first reports of the synthesis of hydrocarbon liquids and waxes on Co and Fe catalyst by Franz Fischer and Hans Tropsch lead to the naming of this synthesis

technique [11]. During the 1930's and 40's Germany took advantage of FT synthesis as a way to produce liquid fuels from local coal reserves. Germany was cut off from foreign oil during WWII and had to develop technologies to produce liquid fuels from domestic coal reserves. This forced Germany to rapidly develop the FT process and spurred large amounts of research in this field. Many of the catalyst developments made at that time are still used widely today with a vast resource of data available publicly at Fischer-Tropsch.org [111]. The main reactions involved can be seen in eq. 1-3, 9. In simple terms, FT synthesis is a polymerization process in which hydrocarbons are added stepwise to a growing aliphatic chain on the catalyst surface (eq 8).

(8) $$CO + 2H_2 = {}^{1}/_{n}\, C_nH_{2n} + H_2O$$

There are two major catalysts used in FT synthesis and are classified as either Co or Fe catalyst. Comparisons of Co and Fe catalyst activities and selectivities can be found elsewhere [112, 113]. The use of metal promoters is widely practiced in both classes of FT catalysis. Some reduction promoters include Pt, Ru, Pd, Re, and Cu while K and Zr are used as activity/selectivity promoters. Supports usually include Al_2O_3, SiO_2, or TiO_2. Co and Fe catalyst each have their advantages, but supported/promoted Co catalyst have higher conversion activity, hydrocarbon selectivity, carbon efficiency, activity maintenance, and regenerability making them generally the more preferred catalyst for GTL processes [11]. Volcano plots of turnover frequency in FT reactions clearly show that Co is the most active catalyst [114]. However, Co catalysts must operate at H_2:CO ratios of 2 while Fe catalyst can operate in H_2:CO ratios of 0.6-1.0. This is due to Fe having a preference for the WGS reaction (eq. 11) while this is negligible in Co catalyst. Deactivation due to coking of the Co catalyst will occur at

lower H_2:CO ratios. Therefore, the use of Co catalyst in FTS from biomass feedstocks has been limited and new technological developments are needed to overcome this challenge. Other deactivation mechanisms involved in FTS include poisoning by sulfur and nitrogen compounds, fouling by hard waxes and carbon, formation of inactive catalytic phases (oxides, carbides, metal support compounds), hydrothermal sintering, and catalyst attrition [115, 116]. Controlling the H_2:CO ratio can help in reducing a lot of the deactivation mechanisms. Steam accumulation in the reactor is also a concern and leads to catalyst deactivation, more so in Fe catalyst [117-127]. Another main concern is the extreme local temperatures that can occur due to the highly exothermic nature of the FT reactions. Therefore, careful planning of reactor and process designs that distribute the heat effectively most be used in FT synthesis. Fe catalyst produce substantially greater amounts of CO_2, but have the advantage of costing significantly less than Co catalyst. Table 2 shows some of the current commercial GTL processes and the catalyst type used [11]. Note that only two of these processes use Fe catalyst.

Interest in FT synthesis has come in waves throughout history. Much of this is due to the availability and costs associated with petroleum. While recent interests in FT technologies have seen resurgence due to environmental concerns and the desires to replace fossil fuels with renewable fuels. FT fuels do not require a specific, new distribution infrastructure because the product specifications resemble those of conventional petroleum fuel markets. Biomass feedstocks can play a key role in making bio derived fuels a cost competitive option over traditional petroleum processing. Wolan et al has put considerable effort into finding commercially applicable technologies that overcome problems associated with the use of biomass and catalyst deactivation [128].

Table 2: Commercial GTL technology under development [11].

Company	Location	Syngas Production	Oxidant	FT Reactor	Catalyst	Bbl/day
BP	Nikiski, Alaska	Compact Steam Reforming	O_2	FBR[a]: SBCR planned	Co	300 (100[b])
Conoco Phillips	Ponca City, Oklahoma	CATPOX[c]	O_2	SBCR[d]	Co	400
Conoco Phillips	Qatar	CATPOX[c]	O_2	SBCR[d]	Co	160,000
Exxon Mobil	Qatar	CATPOX[c]	O_2	SBCR[d]	Co	100,000
Rentech	Colorado		O_2	SBCR[d]	Fe	800-1,000
Sasol	Mossel Bay, South Africa	Steam Reforming	O_2	CFB[e]	Fe (fused)	25,000
Sasol-Chevron-QP	Ras laffan, Qatar	ATR[f]	O_2	SBCR[d]	Co	100,000
Sasol-Chevron-Texaco	Escravos, Nigeria	ATR[f]	O_2	SBCR[d]	Co	34,000
Shell-MDS	Bintulu, Malaysia	Non-catalytic partial oxidation	O_2	FBR[a]	Co	14,000
Shell-QP	Ras laffan, Qatar	Non-catalytic partial oxidation	O_2		Co	140,000
Marathon/Syntroleum	Port of Catoosa, Oklahoma	Air-ATR[f]	Air	SBCR[d]	Co	70
Marathon/Syntroleum	Qatar	Air-ATR[f]	Air	SBCR[d]	Co	100,000

[a]Fixed Bed Reactor; [b]Already in production; [c]CATPOX (Catalytic Partial Oxidation); [d]Slurry Bubble Column Reactor; [e]Circulating Fluidized Bed; [f]Auto Thermal Reactor; [g]Printed with permission from John Wiley & Sons, Inc.

The development of a Co eggshell catalyst, to avoid mass transfer problems and hotspots occurring in the catalyst bed, has shown promising results [129]. The work presented here concentrates on upgrading the syngas produced in gasification by reducing the concentration of tars and adjusting the H_2:CO ratio to 2:1, needed in FT synthesis of hydrocarbon fuels, through the use of a tri-reforming catalyst.

1.6 Tri-reforming

The tri-reforming process has recently received attention in the research field for its ability to consume greenhouse gases like methane and CO_2 to produce syngas with a higher H_2:CO ratio desired for FTS. Tri-reforming involves a synergetic combination of

CO_2 reforming (eq 9), steam reforming (eq 10, 11, 12), and partial oxidation of methane (eq 13, 14, 15) in a single reactor.

(9) $CH_4 + CO_2 = 2CO + 2H_2$ $\Delta H° = 247.3\ {}^{kJ}/_{mol}$

(10) $CH_4 + H_2O = CO + 3H_2$ $\Delta H° = 206.3\ {}^{kJ}/_{mol}$

(11) $CO + H_2O = CO_2 + H_2$ $\Delta H° = -41\ {}^{kJ}/_{mol}$

(12) $C_nH_m + nH_2O = nCO + \left(n + {}^{1}/_{2}\, m\right)H_2$ $\Delta H° = 1175\ {}^{kJ}/_{mol}$ [a]

(13) $CH_4 + {}^{1}/_{2}\, O_2 = CO + 2H_2$ $\Delta H° = -35.6\ {}^{kJ}/_{mol}$

(14) $CH_4 + 2O_2 = CO_2 + 2H_2O$ $\Delta H° = -880\ {}^{kJ}/_{mol}$

(15) $CH_4 + 1\,{}^{1}/_{2}\, O_2 = CO + 2H_2O$ $\Delta H° = -520\ {}^{kJ}/_{mol}$

[a] For n-C_7H_{16} [11]

Using the tri-reform process eliminates the serious problem of carbon formation and high energy consumption commonly seen in CO_2 reforming by incorporating H_2O and O_2 (see equations 16-21). Heat is generated in-situ that can be used to increase energy efficiency and achieve a thermo neutral balance of reactions [78, 130, 131]. H_2 and CO selectivity can also be adjusted by controlling the amount of steam and CO_2 added to the reaction [45, 131-136]. Song and Pan compared tri-reforming to CR and SR and found that tri-reforming consumes less energy while producing less CO_2 per unit of desired syngas (H_2:CO=2). The review shows that tri-reforming uses 45.8% less energy and produces 92.8% less CO_2 compared to CR. When compared to SR, tri-reforming uses 19.7% less energy and produces 67.5% less CO_2 [131]. This provides an important role in both industrial and environmental applications allowing production of high value chemicals

via oxo-synthesis, electricity via solid oxide fuel cells or molten carbonate fuel cells, and clean burning hydrocarbon fuels via FT synthesis [137-141].

Coke Formation

(16) $CH_4 = C + 2H_2$ $\Delta H° = 74.9\ {}^{kJ}/_{mol}$

(17) $2CO = C + CO_2$ $\Delta H° = -172.2\ {}^{kJ}/_{mol}$

(18) $C_nH = nC + {}^{m}/_{2}\,H_2$ $\Delta H° = 188\ {}^{kJ}/_{mol}$

Coke Removal

(19) $C(ads) + CO_2 = 2CO$ $\Delta H° = 172.2\ {}^{kJ}/_{mol}$

(20) $C(ads) + H_2O = CO + H_2$ $\Delta H° = 131.4\ {}^{kJ}/_{mol}$

(21) $C(ads) + O_2 = CO_2$ $\Delta H° = -393.7\ {}^{kJ}/_{mol}$

Tri-reforming catalyst must be thermally stable, have a high surface area, provide resistance to coke formation, and be economically advantageous in order to be feasible as a renewable energy alternative. Metals that have shown to have a good activity and selective for reforming reactions include Ni, Pt, Rh, and Ru [55]. Ni based catalyst show good potential for reforming methane providing a more economically friendly option over noble metals and thus most research has focused on developing novel Ni catalyst formulations. However, Ni has the disadvantage of being susceptible to coke formation [55, 78]. This is attributed to methane decomposition and Boudard reactions being favorable over Ni catalyst (eq. 16, 17) [79-84]. Catalyst deactivation is even more of a hurdle to overcome in biomass gasification because of the high level of impurities associated with biomass-derived syngas. Some approaches to reduce these impurities include physical processes like filters and wet scrubbers or thermal type processes

associated with catalytic cracking [29]. Other researchers have become interested in developing "self cleaning" type catalyst that are more resistant to deactivation. This eliminates the accumulation of waste associated with physical removal methods and maintains energy content by converting problem tars into H_2 and CO.

Deactivation in reforming catalyst by coke formation; sintering; attrition; and poisoning by phosphorus, sulfur, and halides are all possible mechanisms associated with reforming catalyst. Deactivation is directly related to catalyst structure and composition and therefore recent research has been aimed at producing a suitable catalyst in the upgrading of biomass-derived syngas [17]. CeO_2 is reported to have a high oxygen storage capacity (OSC) and is often used as a promoter with Ni for methane conversion to syngas [142-144]. Addition of ZrO_2 to CeO_2 catalysts has shown to improve OSC, redox property, thermal stability, metal dispersion, selectivity, and catalytic activity [50, 145-149]. It's proposed these improved characteristics are attributed to the formation of a (Ce, Zr)O_2 solid solution [48, 97, 146, 147, 150-152]. Dong et al studied POM and CR on Ni/(Ce, Zr)O_2 and attributed better catalytic performance to the catalyst having two active centers, one for activating the CH_4 molecules and the other activating steam and O_2 molecules [48]. By incorporating CeO_x into the catalyst support, the reaction of steam with adsorbed species on the Ni surface, near the boundary between the metal and support, is accelerated. This improves coking resistance and stability of the catalyst, which is attributed to the increase OSC from modifying the local oxygen environment around Ce and Zr generating active oxygen [153]. Nagia et al explains this stating "the introduction of undersized Zr ions into the Ce framework (Zr^{4+}=0.84Å, Ce^{4+}=0.97Å) could compensate for the volume increase" associated with the valence change of Ce^{4+} to

Ce^{3+} (Ce^{3+}=1.14Å) easing the transition [154, 155]. Research has shown that the Ce/Zr mixed oxides consistently perform with higher activity compared to the pure oxide supports and Al_2O_3 due to the mixed oxide's ability to promote POM and steam reforming reactions [46, 88, 89, 92, 144, 146, 156, 157]. Because of this, $Ce_{1-x}Zr_xO_2$ support materials have received much attention with $0.6<x<0.8$ being preferred for catalytic applications [78].

Basic oxides, such as magnesia and zirconia, have shown to catalyze the gasification of coke with steam and to help prevent deposition of carbon in dry reforming [44, 53, 158, 159]. This may be attributed to the low concentration of Lewis sites and increase of oxygen vacancies by introducing ZrO_2 and MgO into the catalyst composition. Coupling these basic oxides with Ni catalyst helps in promoting CO_2 and H_2O adsorption leading to enhanced CO_2 conversion and H_2 production [131, 137]. It is postulated that MgO promotes the adsorption of steam by facilitating OH spillover to the Ni metal site [11]. Song and Pan also attribute the enhanced CO_2 conversion to a higher interface between Ni, MgO, and ZrO_2 resulting from NiO/MgO and ZrO_2/MgO solid solutions [131]. Evidence shows that using these basic promoters leads to ensemble control and prevention of sintering and carbon formation [56]. This work highlights the effects of ZrO_2, CeO_2, and MgO in Ni based tri-reforming catalysts and examines reaction selectivity due to variations in structure/composition and feed gas composition respectively.

2. Experimental Section

2.1 Catalyst Synthesis

Ce/Zr oxide supports were prepared using the co-precipitation method reported by Rossignol et al using $Ce(NO_3)_3x6H_2O$ and $ZrO(NO_3)_2xH_2O$ as precursors [160]. Co-precipitation of precursors provides an industrial scale up opportunity because of its simplicity. Pure Ceria and Zirconia oxides as well as the mixed oxides with Ce:Zr molar ratios of 0.16:0.84, 0.6:0.4, and 0.8:0.2 were all prepared using the same method. Appropriate quantities of the precursor salts were dissolved in deionized (DI) water and precipitated by the addition of NH_4OH to form hydrous zirconia, ceria, or Ce/Zr solution. This precipitate was vacuum filtered and re-dispersed into a 0.25M NH_4OH solution. The dilute, basic solution was again vacuum filtered and dried in an oven at 60°C for 1 hr followed by 120°C overnight. The dried powder was then calcined at 800°C for 4hr.

The loading of Ni and Mg to the oxide support was carried out using two different loading procedures: wet impregnation (WI) and deposition precipitation (DP). All metals were loaded on a mass basis to achieve desired wt. % of metal on the catalyst. For the WI method, appropriate amounts of $Mg(NO_3)_2xH_2O$ and $Ni(NO_3)_2x6H_2O$ were dissolved in deionized water to form a homogeneous solution. This solution was then added drop-wise to the support until incipient wetness and dried at 120°C for 2hr. This step was repeated until all of the metal nitrate solution had been added to the support. Following the final drying step, the catalyst was calcined at 500°C for 4hr. DP was carried out using a modified method adapted from Li et al [161]. Appropriate amounts of

$Mg(NO_3)_2xH_2O$ and $Ni(NO_3)_2x6H_2O$ where added to a volumetric flask and dissolved in 25ml DI water. The powder support was added to the metal salt solution and mixed with a stir plate to form a slurry. In a separate beaker, $CO(NH_2)_2$ (urea) was added in excess to 10ml of DI water to achieve a 1:4 ratio of total metal nitrates:urea. The urea solution was added drop-wise to the metal salt solution while stirring. The top of the volumetric flask was sealed to prevent evaporation of the solution and heated to 115°C while stirring at 600rpm on a heated stir plate. Urea hydrolyzes slowly at temperature allowing hydroxyl groups to react as rapidly as they form maintaining a constant pH and allowing precipitation on surface and interior of pores [11]. The solution was aged for 24hr and then cooled to room temperature before vacuum filtering with a Buchner funnel. Cold DI water was used to wash any remaining precursors and impurities from the filtered catalyst. The catalyst was then dried at 120°C for 4hr followed by calcination at 500°C for 4hr. Figure 2 shows a picture of a few of the catalysts made in this study.

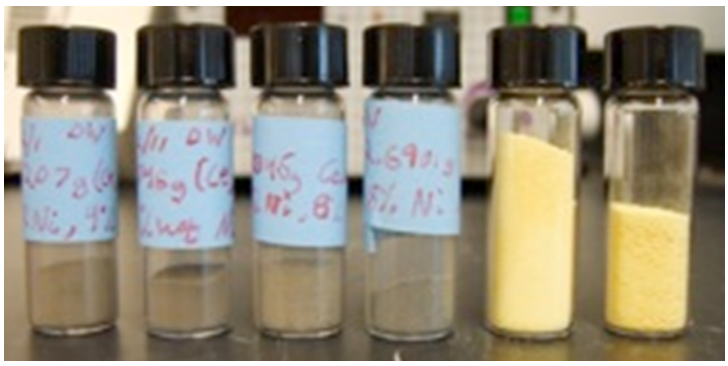

Figure 2: A picture of catalyst loaded with Ni and Mg (left side, grey samples) and the mixed oxide supports (far right, yellow samples).

2.2 Catalyst Characterization

BET, XRD, TPR, XAFS, SEM-EDS, and XPS were used to characterize catalysts. Each of these methods provides insight into the catalyst physical and chemical structure. The combination of these techniques provides valuable data that proves more

useful than any single characterization technique alone. These characterization techniques helped aid in the rational of the catalyst design and how to improve catalyst properties. A brief explanation of why and how these techniques were used is presented here.

2.2.1 BET Physisorption

Surface area was measured using the multipoint BET method. The BET theory explains the physical adsorption of gas molecules on a solid surface. Stephen Brunauer, Paul Hugh Emmet, and Edward Teller first published an explanation of BET theory in 1938 [162]. The naming of this technique was derived from each of their last names in combination. In BET analysis, a sample is enclosed in a glass cell and evacuated under an inert environment. The sample is then cooled with liquid N_2 and the partial pressure of N_2 in the cell is increased while the amount of adsorbed N_2 is recorded. The process is then reversed and the partial pressure of N_2 is decreased while measuring the desorption of N_2. The data collected can then be used to determine the number of N_2 molecules adsorbed for monolayer coverage and based upon the cross-sectional area of N_2 ($0.162nm^2$) the surface area can be calculated. The BET equation is found in eq. 22 and gives "the relationship between volume of N_2 adsorbed at given partial pressures and volume adsorbed at monolayer coverage" [11].

(22) $$\frac{\frac{P}{P_o}}{V(1-\frac{P}{P_o})} = \frac{1}{cV_m} + \frac{(c-1)\frac{P}{P_o}}{cV_m}$$

Where P is the partial pressure of N_2, P_o is the saturation pressure at experimental temperature, V is the volume adsorbed at P, V_m is the volume adsorbed at monolayer coverage, and c is the BET constant.

(23) $$V_m = \frac{1}{A+I}$$

(24) $c = 1 + \frac{A}{I}$

(25) $S_{BET,total} = \frac{V_m N s}{V_{molar}}$

From this data a BET plot with a slope of A and the y-intercept of I can be used to calculate the volume of monolayer adsorbed gas (V_m) and the BET constant (c) using eq 23, 24. The surface area can then be calculated from eq 25 where N is Avogadro's number, s is the cross section of the adsorbing species, and V_{molar} is the molar volume of adsorbate gas. A typical gas adsorption isotherm and the regions of the isotherm are given in Figure 3.

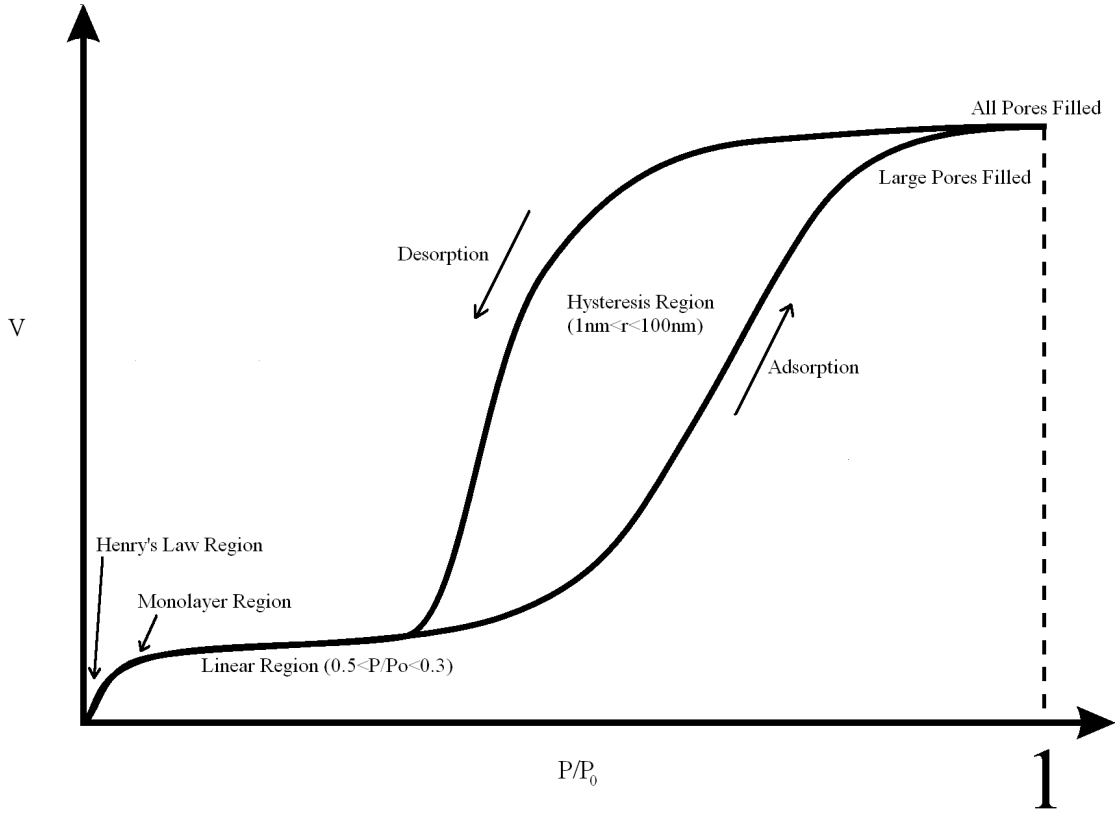

Figure 3: Nitrogen isotherm curve and labeled sections.

Physisorption experiments were performed using a Quantachrome Autosorb-iQ. Approximately 51mg of catalyst was loaded into a 6mm in diameter glass sample cell

with a spherical reservoir to hold the catalyst. No rod was used to reduce the void volume in the cell. The vacuum control was set to fine powder where the evacuation cross-over pressure was set to 3 torr. The sample was degassed from room temperature to a target temperature of 200°C at a rate of 25°C/min and allowed to soak for 2 hr. A backfill pressure of 800 torr was used. The sample was then cooled to room temperature and the degassed sample mass was then recorded. Following this measurement the sample was loaded into the analysis station and cooled to -196°C (77K) using a liquid N_2 bath. N_2 partial pressure and adsorption was then recorded by the sorption analyzer in P/P_o increments of 0.02. The BET surface area was calculated using data in the P/P_o range of 0.05-0.3. This is the region where the most reliable data is collected and a linear relationship for the BET plot is maintained.

2.2.2 X-Ray Diffraction

X-ray diffraction (XRD) is a bulk characterization technique commonly employed to measure the crystal structure of catalytic phases. Crystal structures are composed of planes made from repetitive arrangements of atoms. The miller indices further breaks down the orientation of these planes into vector notation and is the commonly used to describe crystal planes. Each of these planes is capable of diffracting X-rays at different angles. These diffracting angles are known as Bragg angles (2θ). Each compound has its own unique diffraction pattern due to the various planes that make up that particular crystalline structure. XRD works upon this principal and measures the angles of the diffracted X-rays from the radiated sample to produce a spectrum of characteristic peaks [11]. These peaks are interpreted by the analyst based upon their location (2θ), intensity, and width. This allows for qualitative and quantitative phase analysis of samples by

identifying the species, Miller's indices, and the relative intensity for each peak [163]. XRD analysis also allows for examination of crystallite size according to the Scherrer equation eq 26 where B is the width at half peak ht, d is the crystallite size, λ is the x-ray wavelength, θ is the Bragg angle/2, and κ is a constant.

(26) $$B = \frac{\kappa\lambda}{d\cos\theta}$$

However, XRD is limited to detecting crystallites that are larger than 3-5nm and make up more than 1% of the sample composition. Crystallites smaller than these are unable to diffract X-rays and are called X-ray amorphous. Nevertheless, the Scherrer equation allows a rough estimation of crystallite size to be made when diffraction peaks are detected.

XRD analysis was carried out with a Philips X'pert XRD using a powder x-ray diffraction technique. Before each sample was analyzed the instrument was calibrated to compensate for any differences in the positioning of the sample holder by adjusting θ, Φ, and Z angles of the x-ray beam. A 15mm mask was used to narrow the diffracted beam to the detector in the y-axis. A Cu plate was used to attenuate the x-ray beam during positioning as not to saturate the detector. After correct alignment of the instrument, the Cu plate was removed and a quick scan of the sample was made to optimize scanning parameters. The machine was operated in a Bragg angle (2θ) range of 15-80°. The step size was 0.06° and set at a dwell time of 1s for each step. These adjustments were made to maximize the intensity while keeping the signal to noise ratio high. X'pert Highscore software was used to assist in data analysis.

2.2.3 Temperature-Programmed Reduction

Temperature-programmed reduction (TPR) is a widely used tool to characterize the reducibility of the oxide form of a catalyst. This is done by flowing a reducing gas mixture, usually diluted hydrogen in an inert gas, over a catalyst while the temperature is ramped over a particular range. H_2 adsorption occurs on metal or metal oxide surfaces, due to the reduction of the species, and the consumption of H_2 is measured as a function of temperature. H_2 consumption is usually measured by a thermal conductivity detector (TCD). In doing so, a TPR profile can be made and conclusions reached about the reduction kinetics of the species. The areas under the curve are proportional to the extent of reduction. Species that are reduced at lower temperatures are indicative of metal or metal oxides with weaker interactions between the catalyst support and/or other metals loaded onto the surface. Those species that are reduced at higher temperatures are a result of more stable or strongly interacting species making up the catalyst. Thus, from TPR measurement, one can determine the optimum reduction temperature and how species in the catalyst are influencing each other.

TPR was carried out using 50 mg of catalyst loaded into a glass sample cell. Each sample was pretreated with helium while ramping the temperature 10°C/min from 25°C to 110°C and holding at temperature for 30minute. The sample was then cooled to 50°C. Following pretreatment the carrier gas was switched to 5% H_2/N_2 and the temperature ramped to 1100°C at 10°C/min. Gas analysis was performed using a thermal conductivity detector (TCD) measuring the uptake of H_2 under the temperature-programmed conditions.

2.2.4 EXAFS

X-ray absorption fine structure (EXAFS) spectroscopy is a characterization method to determine detailed local structures of solids. It works upon the principal that photoelectrons are created upon X-ray absorption by the sample. These photoelectrons are scattered by nearby atoms causing fine structure that can be identified in X-ray absorption spectrum as interference fringes. The frequencies of these fine structure interference fringes are related to interatomic distances between absorbing neighboring atoms. The amplitude of the fine structure is related to the number, type, and order of neighboring atoms [11]. Therefore, information on structure and the coordination of atoms on the surface of the catalyst can be deduced. However, this characterization technique is very complex and expensive and a synchrotron facility is required. Very few facilities in US are capable of performing EXAFS characterizations. The data collected must be carefully modeled and require appropriate software packages (ATHENA, ARTEMIS, HEPHAESTUS). This can be a time consuming process and great effort must be used to decipher the sometimes ambiguous results.

X-ray absorption spectroscopy (XAS) was performed at DuPont-Northwestern-Dow (DND) Collaborative Access Team (CAT) beamline 5-BM-D (BM = bending magnet, http://www.dnd.aps.anl.gov/) at the Advanced Photon Source, Argonne National Laboratory. Approximately 50mg of catalyst were ground with a mortar and pestle and pressed onto a 13 mm diameter pellet using a Carver press operated at 12,500psi for 20s. Adjustment of pellet thickness was made to obtain a linear absorption coefficient close to 1. For these experiments the storage ring energy was 7.0 GeV and the circulating current was 100.6 mA. A Si(111) monochromator was used to filter for the desired X-ray

wavelengths. Spectra were collected in transmission mode at the Ni K absorption edge (8333 eV) under ambient conditions. Energies were scanned from 150 eV to 30 eV before the edge in 10 eV steps (background region) and then to 975 eV (representing k = 16 Å-1) after the edge in 2 eV steps (pre-edge/edge region). The absorption was measured using ionization chambers before and after the sample. Following the second ionization chamber, the Ni foil and a third ionization chambers were positioned so this reference could be examined simultaneously. Multiple scans (typically 3 per sample) were taken to improve the signal-to-noise ratio. Merging of individual scans and data reduction were performed with the Athena software package [164, 165]. The background region (-150 to -30 eV before the edge) was extrapolated and subtracted from the data. Edge energies were selected as energy yielding the maximum absorption derivative. Spectra were normalized with a polynomial spleen operation by the absorption over the Δk range of 2 to 14 Å-1. Finally, the spectra were Fourier transformed with a Hanning window from k-space into R-space over the Δk range of 3 to 14 Å-1. A previous study was used to help analyze the results [22].

2.2.5 SEM-EDS

Scanning electron microscopy (SEM) allows topographical analysis of solid surfaces. Images can presently be produced at resolutions down to 5nm. SEM works upon the principal that when a sample is bombarded with excited electrons this causes secondary electrons to be produced and detected. These secondary electrons are produced as the electron beam passes over the sample allowing variations in the topology and composition to be measured by the intensity of the secondary electrons produced [11]. Energy dispersive X-ray spectroscopy (EDS) allows the capability to detect

characteristic X-rays produced by specific elements in the sample when an electron beam passes over the sample. Coupling of these two technologies are commonly used to collect information on the topography and elemental composition of a catalyst surface.

SEM coupled with EDS was used to characterize catalyst surface topography and composition. A Hitachi S-800 SEM coupled to an Ametek EDAX was utilized to conduct these experiments. An excitation energy of 10 keV, a magnification of 1010, and a tilt angle of 30° was used in this analysis. Apertures were fully opened to allow max current. For EDS elemental mapping, a matrix of 256x200 was used with each pixel representing a size of approximately 0.45 μm. Samples were first scanned to generate an EDS spectrum. For elemental mapping the excitation energy was based upon the highest intensity peak in the EDS spectrum and doubling the excitation energy needed for this species. In this case, Ce at 5 keV was used, therefore an excitation energy of 10keV was used for elemental mapping.

2.2.6 XPS

X-ray photoelectron spectroscopy (XPS) measures bonding energies to give information on surface chemical states including oxidation states, surface composition, surface phases, and dispersion of the tested catalyst. This technique uses X-ray photons to bombard the surface and measures the emitted core photoelectrons as a function of electron energy. These binding energies can be used to fingerprint elements and their oxidation states present in the catalyst, allowing conclusions to be drawn about the chemical states of the species present [166-168]. "Several important catalytic properties can be studied by this technique, including oxidation state of the active species, interaction of a metal with an oxide, support, changes in oxidation state upon activation

of the catalyst, and the nature of surface impurities such as chemisorbed poisons [catalyst book].

XPS was performed on the reduced and oxide forms of catalyst with the Ce:Zr mixed oxide ratio of 0.6:0.4 and a metal loading of 8% Ni and Mg for both the WI and DP metal loading methods. XPS measurements were taken with a Perkin-Elmer PHI 560 ESCA/SAM system under vacuum using a Mg filament. Binding energies were scanned in the 0-1030 eV range initially. A high resolution scan was performed on the Ni2p3 peak in the binding energy rang of 849-869 eV. RBG AugerScan 3 software was used for data analysis of the resulting spectrum. A curve fit summary was produced from the resulting high resolution scans.

2.3 Catalytic Testing

Catalytic reactions were carried out in a fixed-bed quartz u-tube reactor (i.d.=4mm) at 1 atm. Feed gas composition was controlled using Alicat Scientific mass flow controllers and adjusting the flow rates accordingly. Online analysis of the product gas was taken with a MKS Spectra (Cirrus) mass spectrometer (MS) connected in-line with the reactor. Before each experiment, the quartz reactor was loaded with 75.2 mg of catalyst into the bottom third of the quartz tube and supported on either side by inert quartz wool. The reaction vessel was positioned inside a Thermoscientific Thermolyne tube furnace. Reaction temperature was controlled by adjusting the furnace temperature program to the desired ramp rate or fixed temperature. Heat tape was used to heat reactant and product lines to prevent condensation from occurring prior to the catalyst bed and MS detector. H_2O was delivered to the reactant gas mixture through a heated water bubbler using helium as a carrier gas. A picture of the apparatus used to deliver H_2O to the composite

gas feed is shown in Figure 4. Similarly, tar-reforming experiments were carried out using toluene delivered to the reactant gas mixture by a glass bubbler using helium as a carrier gas. Toluene was chosen as a model compound for tars because of its aromatic structure with one methyl group attached and fairly low boiling point. This was a safer option over benzene since toluene is considered less toxic and also provides a means to track decomposition mechanisms such as dealkylation by measuring the amount of methane in the product gas. The Antione equation (eq. 27) was used to calculate vapor pressures at various temperatures to determine the amount of H_2O and Toluene in the feed gas. Where P is the vapor pressure; T is temperature; and A, B and C are component-specific constants.

(27) $$P = 10^{\left(A-\frac{B}{C+T}\right)}$$

A picture of the reactor set up can be seen in Figure 5. All catalysts were first reduced with 10% H_2 in He while ramping the temperature from room temperature to 800°C at 10°C/min and holding for 2hr. After reducing the catalyst, by-pass valves were used to stop flow through the reactor while the reforming gas mixture was adjusted to the desired composition. The valves were then reopened after the MS gave stable responses for each of the reactants. A gas hourly space velocity (GHSV) of 61000 hr^{-1} was employed for all tri-reforming reactions, unless otherwise specifically stated. Conversion of CH_4 and CO_2 were calculated using the following formula:

(28) $$CH_4\ conv. = 1 - (mol\ CH_4\ in\ product \div mol\ CH_4\ in\ feed)$$

(29) $$CO_2\ conv. = 1 - (mol\ CO_2\ in\ product \div mol\ CO_2\ in\ feed)$$

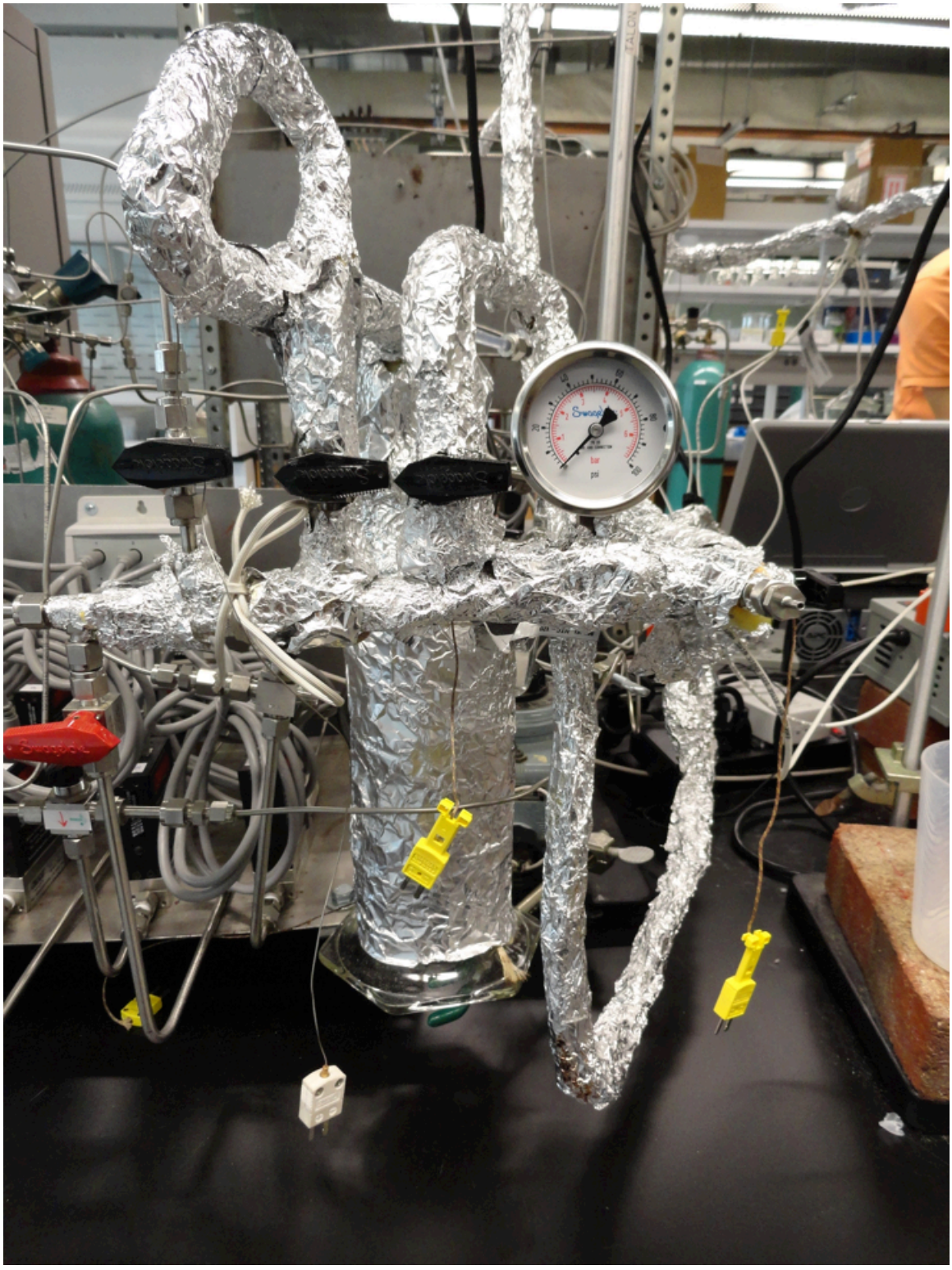

Figure 4: H_2O bubbler wrapped in heat tape and thermally insulated for H_2O delivery to feed gas.

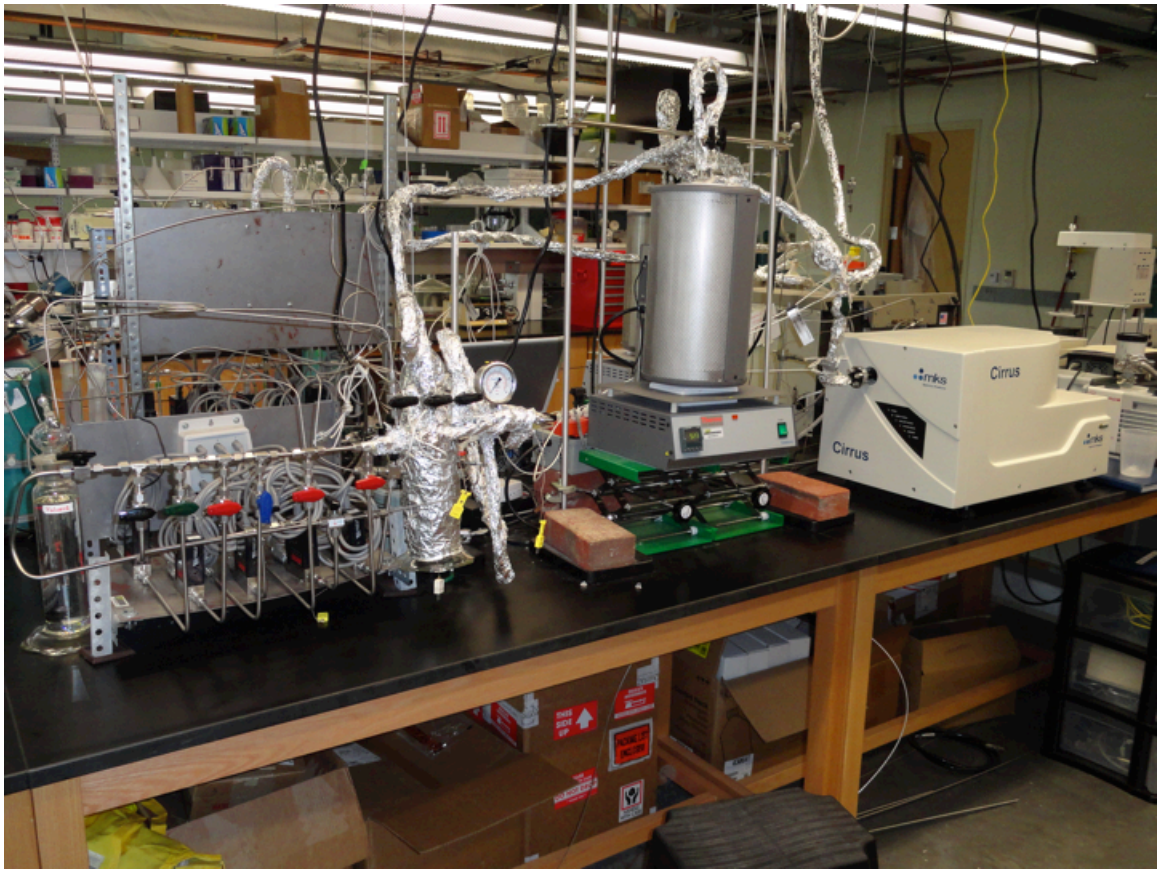

Figure 5: Reactor used in tri-reforming experiments.

2.4 TPO Coke Studies

Immediately following each tri-reforming reaction a temperature-programmed oxidation (TPO) was performed to quantify any coke present on the surface of the catalyst. After tri-reforming, catalyst were quickly cooled to 115°C under an inert (He) environment. The temperature was then ramped at 10°C/min to 700°C and held for 1hr as flow rates of O_2=2.5ml/min and He=50ml/min were used to oxidize the catalyst and convert surface coke to CO_2. Essentially all carbon was converted to CO_2 with insignificant amounts of other carbon containing species produced. An example of the typical data collected during TPO studies is seen in Fig. 6. The product gas was analyzed by a MS detector and quantified by integrating the peak areas to determine the amount of carbon present as coke. TPO was used to measure the amount of coking and is reported

in this study as the % coke. This number is given as the % of total carbon in reactants that ended up as coke.

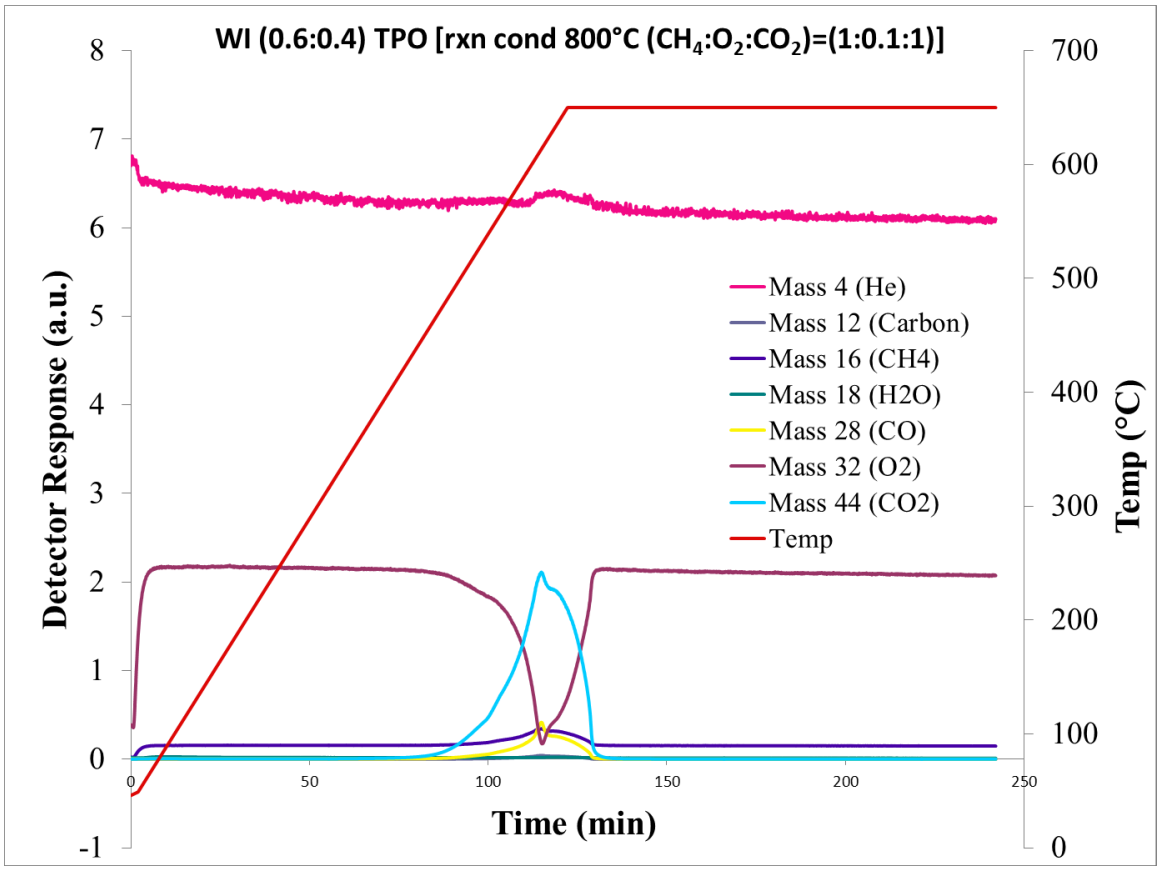

Figure 6: Typical data collected during TPO studies.

3. Results and Discussion

3.1 Structure of the Catalyst

The structure of the catalyst plays a significant role in many of the physical and chemical characteristics of the catalyst. Catalyst performance can be directly related to the structure of the catalyst. Therefore, characterization methods must be employed to understand the structural differences in the catalyst. Interpretation of the data from the various characterization techniques is presented here. This discussion identifies the structure and composition of catalyst used in this study.

3.1.1 Surface Area

To understand how support composition, metal loading, and preparation influenced the surface area of the catalyst, BET analysis was performed and compared on multiple samples. These results are found in Table 3. It was interesting to find that each of the pure oxide species had significantly lower surface areas than any of the mixed oxide supports. This indicates that the mixed oxide supports are not simply a mechanical mixture of the two species. Instead, a new oxide material with very different physical properties from either of its pure components had been synthesized, which suggests that a solid solution of Ce and Zr oxides was formed using the co-precipitation technique. Similar results are reported by Song and Pan [131]. By comparing the surface areas of oxide supports with different Ce:Zr ratios, the surface area is directly related to the percentage of Ce in the support material. As more Ce is introduced into the structure of the catalyst, the surface area also increased.

Table 3: BET surface area for various catalyst compositions.

Catalyst	BET Surface Area (m^2/g)
Pure Ceria Oxide	28.27
Pure Zirconia Oxide	12.02
$Ce_{0.16}Zr_{0.84}$ support	30.52
$Ce_{0.6}Zr_{0.4}$ support	48.65
$Ce_{0.8}Zr_{0.2}$ support	50.05
$Ce_{0.6}Zr_{0.4}$-8Ni8Mg (wet impreg.)	34.53
$Ce_{0.6}Zr_{0.4}$-8Ni8Mg (dep. Precip.)	43.29
$Ce_{0.8}Zr_{0.2}$-8Ni8Mg (wet impreg.)	33.21
$Ce_{0.8}Zr_{0.2}$-8Ni8Mg (dep. Precip.)	44.06

This effect reaches a maximum at a Ce:Zr ratio between 0.8:0.2 and 1:1 because the pure Ce oxide material has a dramatically lower surface area than the highest Ce content sample tested here (Ce:Zr=0.8:0.2). Upon loading of the Ni and Mg metals to the surface of each mixed oxide support material, the surface area decreased slightly. Metal crystals forming within pores of the support and sometimes blocking the pathway may be an explanation for this. The DP method consistently gave higher surface areas when compared to the WI method. This suggests that the DP method forms smaller metal clusters on the surface of the support and therefore fewer pores are being blocked than compared to the WI method. These results are consistent with previous studies [11].

3.1.2 Crystal Structure

XRD analysis was utilized to identify the differences in crystal structure for various catalysts. Catalyst support materials were analyzed by XRD and compared to elucidate structural differences as the composition was altered.

Figure 7 shows a comparison of the pure oxide species and the mixed oxide support with a Ce:Zr ratio of (0.6:0.4). Miller indices are also represented for each peak in Figure 7.

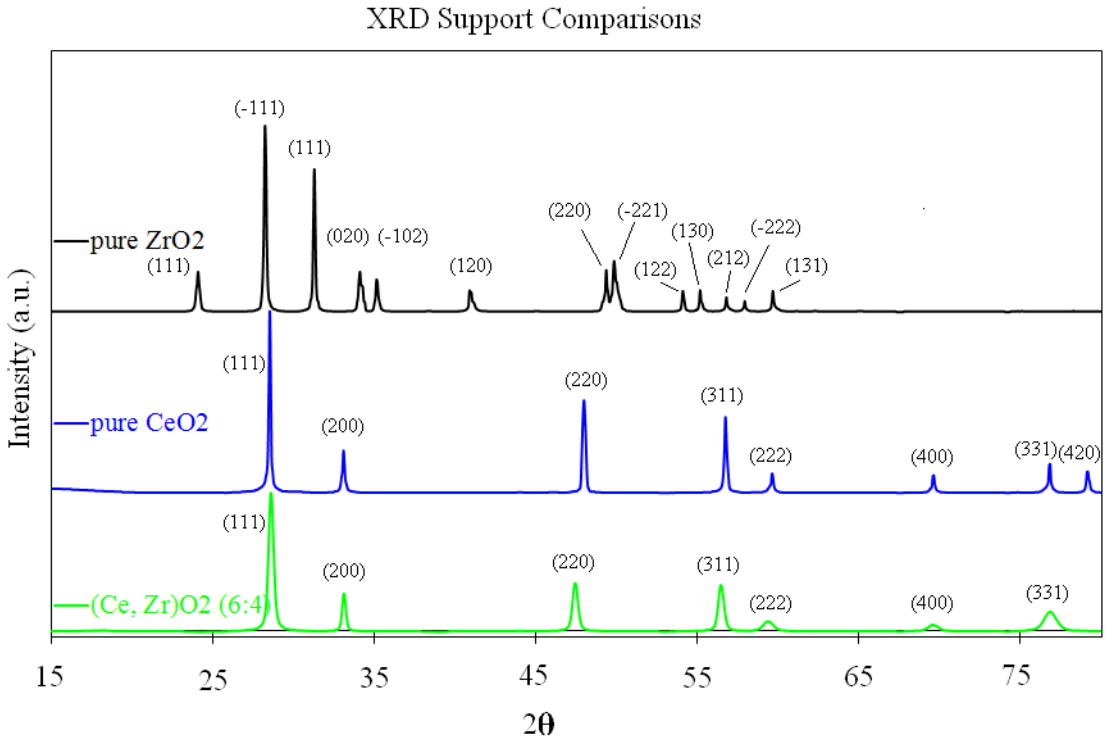

Figure 7: XRD comparison of support materials with miller indices for each peak.

Pure ZrO_2 is known to exist in the tetragonal and monoclinic phases. The XRD pattern of pure ZrO_2 in this study closely resembles characteristic peaks of the monoclinic phase. This is typical of ZrO_2 samples that have been calcined at higher temperatures [169]. The XRD pattern from the pure CeO_2 shows characteristic peaks for a cubic fluorite structure. However, when these two pure oxide species were co-precipitated no peaks could be identified that indicated a monoclinic ZrO_2 species and all peaks resembled the cubic fluorite structure found in pure CeO_2. This suggests that ZrO_2 is incorporated into the CeO_2 lattice and that a solid solution formed from the combination of these two oxide species. Peak broadening is seen in the mixed oxide sample compared to the pure oxides

and is most likely due to lattice defects from the insertion of the smaller Zr cation into the CeO_2 lattice. Similar results are reported in previous literature [87, 131, 144, 170]. The lower Ce:Zr ratio supports were not analyzed here by XRD but previous studies show that upon increasing the Zr content in the support the lattice size shrinks and diffracting peaks are shifted to higher angles [87, 144].

XRD analysis was also performed to identify structural differences arising from different catalyst preparation techniques. The Ce:Zr ratio was held constant at 0.6:0.4 and the oxide support used in both metal loading methods were taken from the same batch. The XRD patterns for the oxidized and reduced forms of samples prepared by WI and DP are compared in Figure 8. Identification of the species is also given in Figure 8. The oxidized form of catalyst prepared by both techniques show peaks characteristic to (Ni,Mg)O solid solution (reference pattern 00-003-0988). However, the oxidized WI sample shows sharper and more intense peaks for the (Ni, Mg)O species. This may be attributed to smaller crystallites of the metal species or that less Mg is loaded on the surface of the DP prepared catalyst. The later was confirmed in SEM-EDS experiments. DP typically results in smaller crystallite size and better dispersion compared to the wet impregnation method [11]. The reduced form of both catalyst show peaks characteristic to reduced Ni species (reference pattern 00-001-1260) but the WI sample gave higher intensity peaks for the Ni species. This may be attributed to the higher dispersion associated with DP. Both the oxidized and reduced forms of the catalyst gave characteristic peaks for the cubic fluorite structure of the $(Ce, Zr)O_2$ solid solution (reference pattern 00-002-1311) indicating the stability of the cubic phase under the reduction conditions employed (800°C).

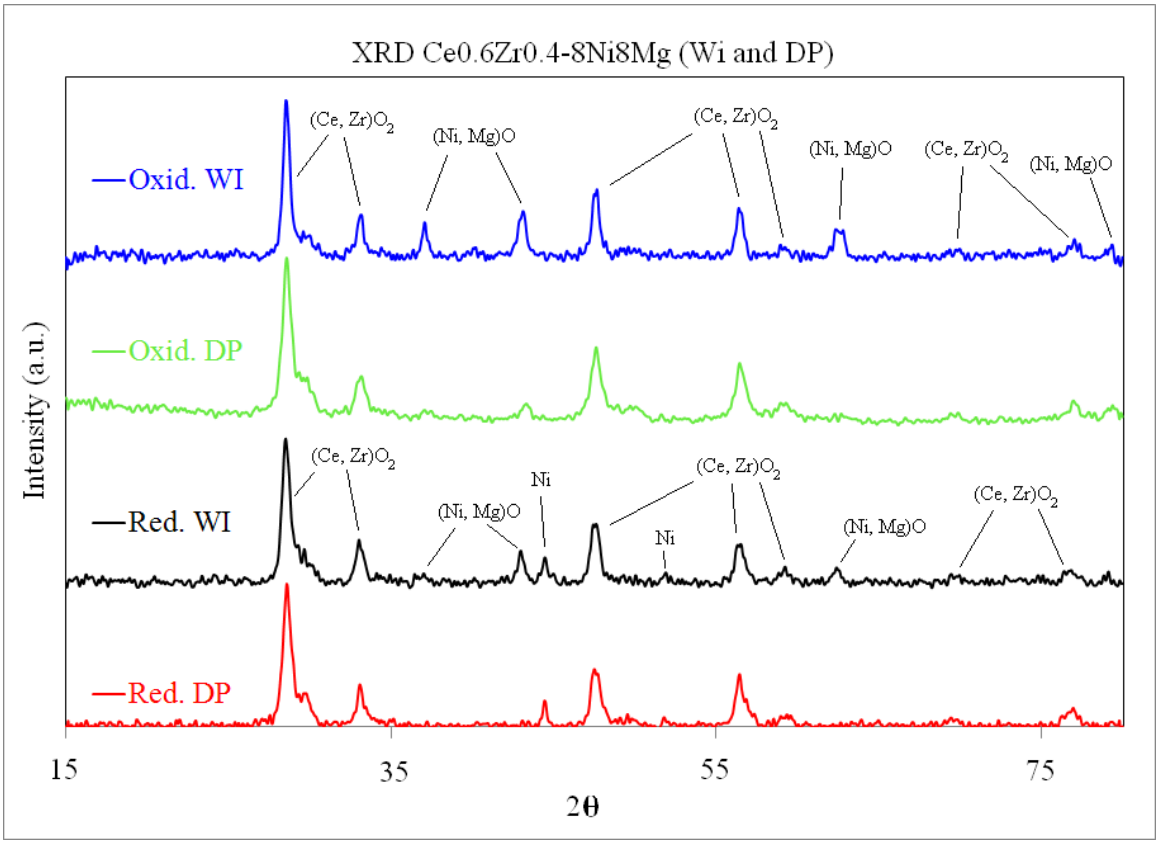

Figure 8: XRD spectrum for oxidized and reduced catalysts samples.

Pre- and post-reaction samples of the Ce0.6Zr.04-8Ni8Mg WI catalyst were also compared using XRD analysis. The comparisons of XRD spectra are seen in Figure 9. Identification of the species and Miller indices are also given in Figure 9. No evidence of crystalline carbon is present in the XRD pattern of the post reaction sample. The post-reaction sample shows Ni in the reduced form and is expected due to the high production of H_2 during the reforming reaction. Peaks characteristic of reduced Ni show higher intensity while the characteristic peaks for (Ni,Mg)O decreased in the post-reaction sample, which indicates that Ni species in the (Ni, Mg)O solid solution are reducible under reaction conditions for those catalyst prepared by WI. This was an excellent result since Yung-Kuhn attributes the deactivation of Ni reforming catalysts to the inability to reduce Ni in an inactive oxide phase thus loosing activity due to fewer reduced Ni active

sites [22]. Post-reaction samples showed the same (Ce, Zr)O_2 pattern as the pre reaction sample indicating that the cubic fluorite phase is stable under the reaction conditions employed.

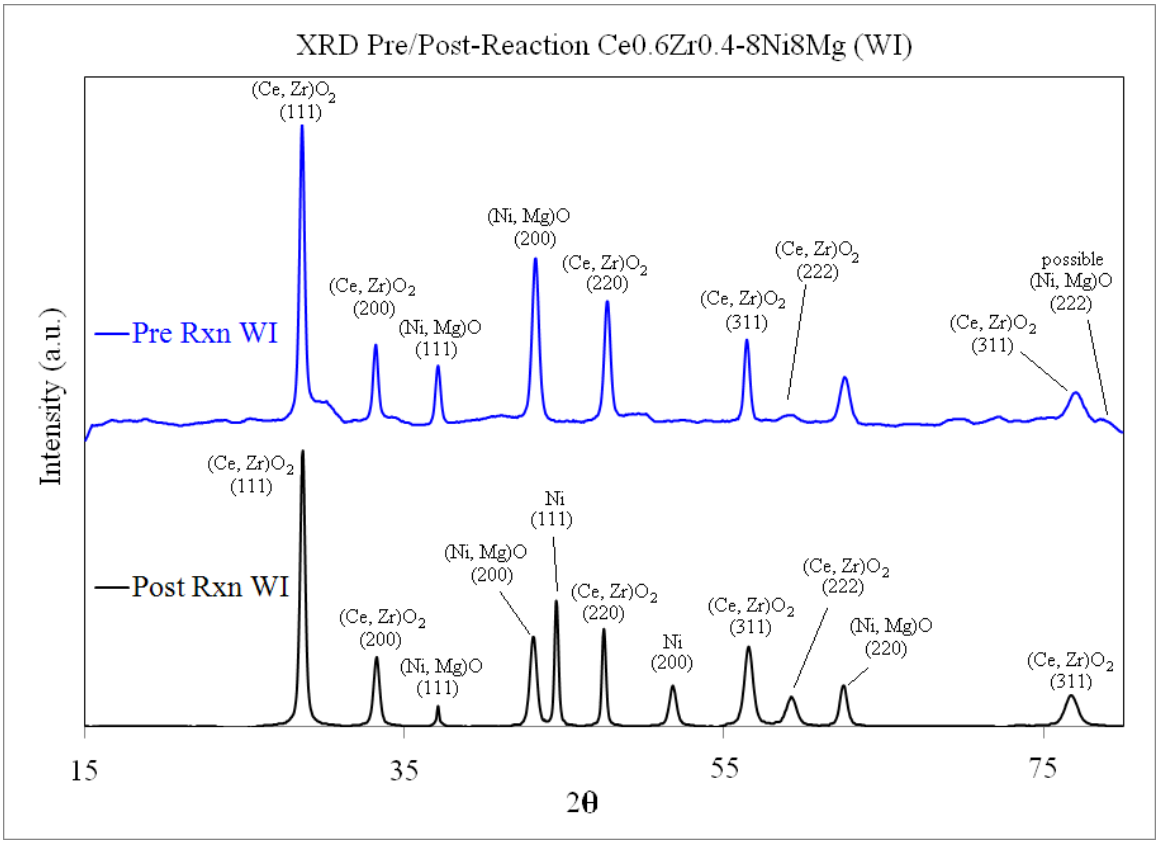

Figure 9: XRD spectrum for pre- and post-reaction WI catalyst.

3.1.3 Reducibility

Figure 10 shows different reduction peaks for the pure and mixed oxide supports. Both the pure CeO_2 and ZrO_2 show much higher temperatures needed to reduce these species compared to the mixed oxide. The pure CeO_2 support shows a max reduction peak around 865°C while the pure zirconia support shows no reduction occurring at temperatures up to 1100°C.

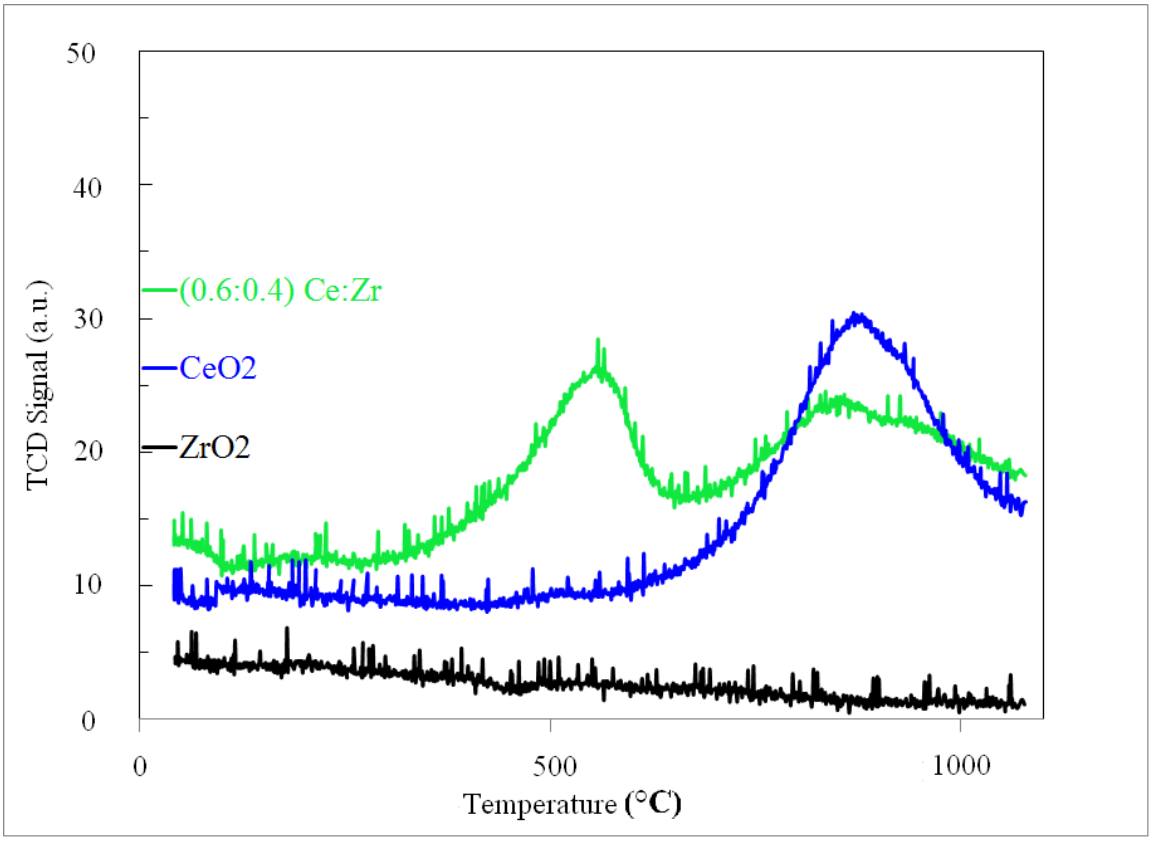

Figure 10: Reduction profiles for support materials.

When these pure species were combined to form a mixed oxide support, a much lower reduction peak is seen to occur between 300-650°C with a max adsorption peak at 555°C. This lower reduction temperature is attributed to a (Ce, Zr)O_2 solid solution forming with similar trends seen for other Ce:Zr ratios. The first and second reduction peaks seen in the mixed oxide are due to the surface and bulk reduction, respectively, and can be explained by the Binet et al model for ceria reduction [171]. The explanation given earlier by Nagia also explains this shift. Incorporation of Zr ions facilitates the valence change of Ce by enabling the volume change associated with the reduction of Ce (Figure 11) [154]. By incorporating Zr within support framework, oxygen mobility is increased allowing oxygen migration between nearby cation channels. This channeling effect is further explained by Ranga et al. [172]. From the TPR experiments, it is seen that

incorporating ZrO_2 into CeO_2 to form a mixed oxide improves oxygen storage capacity (OSC) and redox properties.

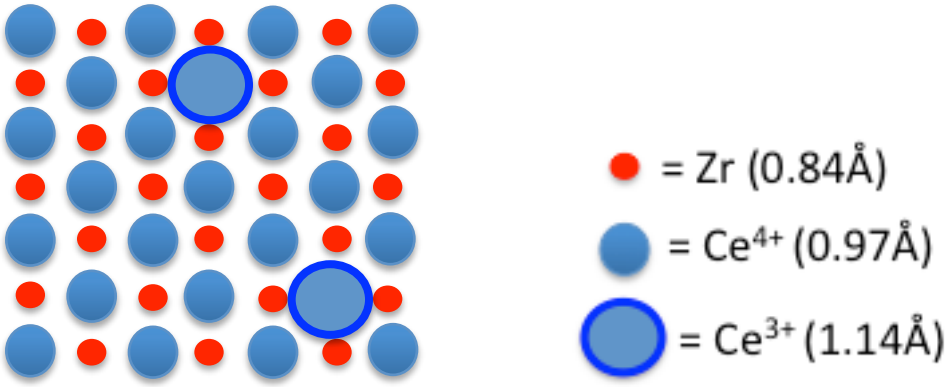

Figure 11: Representation of the Ce valence change facilitation by incorporating Zr into the catalyst framework [151].

ZrO_2 is also a more thermally stable compound that improves the mixed oxides catalytic activity at the elevated temperatures used in reforming reactions.

TPR was also utilized to gain a better understanding of how the Ni interactions between Mg and the support are affected when using different metal loading techniques. Figure 12 and 13 compare the TPR profiles of catalysts loaded with Ni and Mg using WI and DP methods. A catalyst with only Ni loaded via wet impregnation was also compared in Fig 12. Interestingly, when Ni and Mg were loaded by DP the reduction profile closely resembled that of the catalyst with only Ni loaded onto the surface (Fig 12).

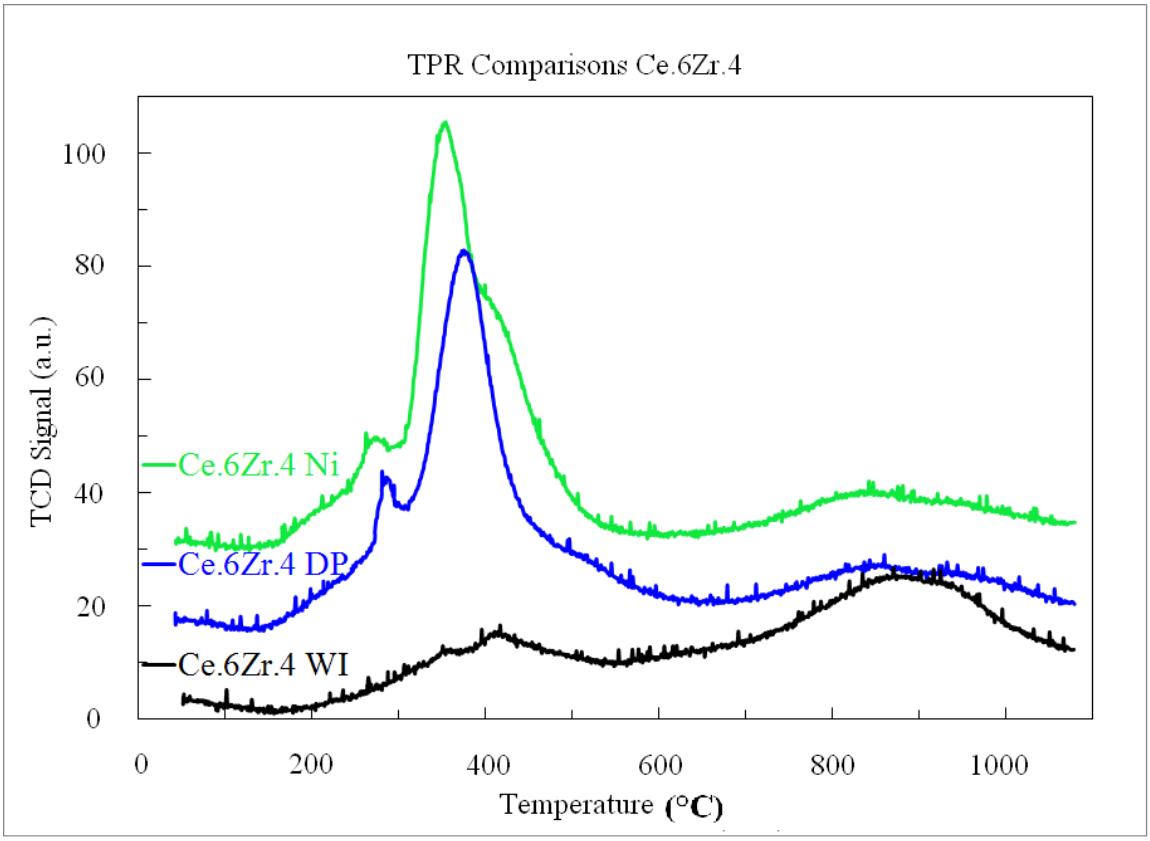

Figure 12: Ce.6Zr.4 support TPR comparison.

When Ni and Mg were loaded by WI most of the reduction occurred at higher temperatures. The lower temperature reduction peaks seen are associated with isolated Ni and weakly interacting Ni with the support and Mg. The higher temperature reduction seen in the WI catalyst is indicative of a strong interaction occurring between Ni and Mg. This was found as a surprise since DP is usually associated with higher dispersion of smaller particles and thus stronger interactions. Initially, it was proposed that the lower reduction peak in the DP prepared catalyst was attributed to higher dispersion causing fewer interfaces between the Ni and Mg particles and thus weaker interactions.

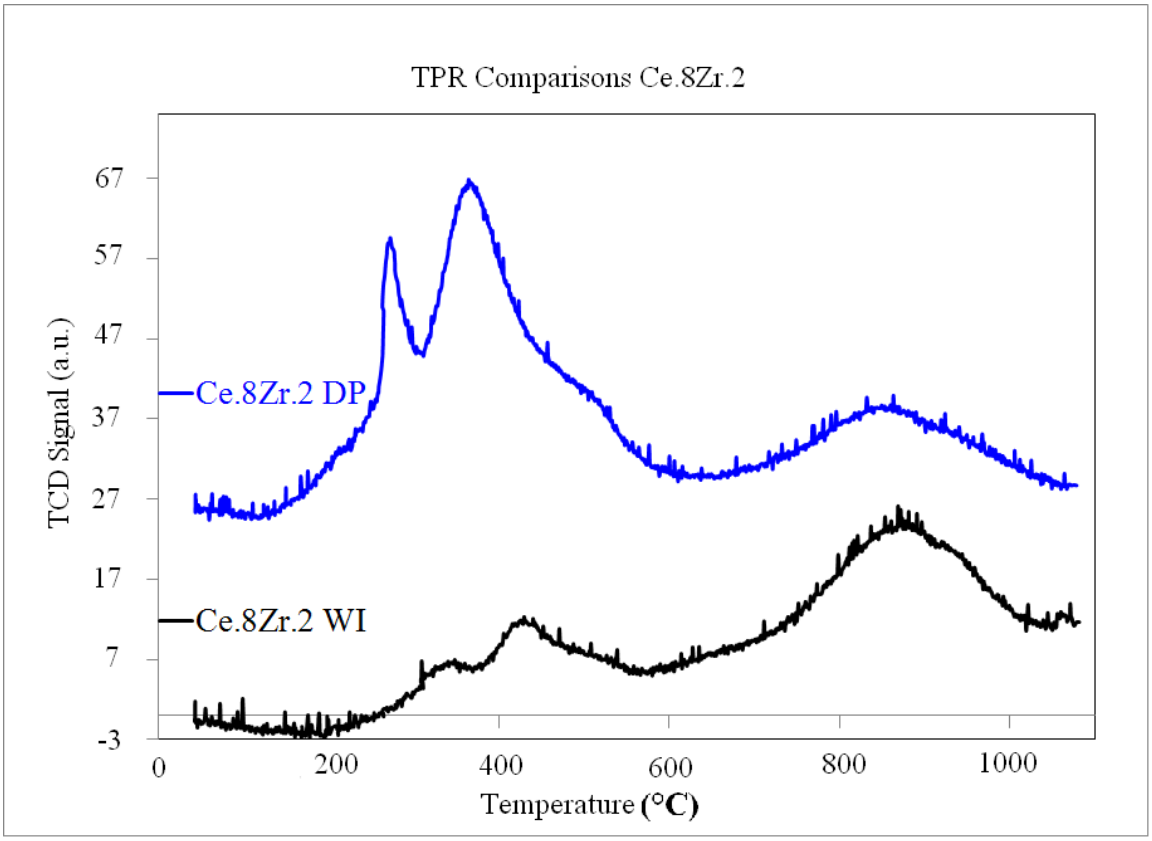

Figure 13: Ce.8Zr.2 support TPR comparison.

Upon further experimentation, it was determined that less Mg had been loaded onto the DP prepared catalysts compared to the WI prepared catalyst. This is why the reduction peak of DP catalyst resembled the catalyst with only Ni loaded onto the surface by WI. The high temperature reduction shift in the WI catalyst containing Ni and Mg species is thus attributed to more interfaces between Ni and Mg with stronger interactions between them.

3.1.4 Neighboring Atoms

To examine the influence of different Ni:Mg ratios loaded onto the catalyst, EXAFS characterization was utilized. Catalysts with Ni:Mg ratios of 1:1 and 2:1 were analyzed by EXAFS and the results can be seen in Fig. 14. Both of the catalysts were freshly calcined and, therefore, species were in the oxide form. Examination of the first

two peaks gives data upon the neighboring atoms of Ni. The first peak represents structures resulting from Ni-O bonds. The second peak represents Ni-Ni bonds in an

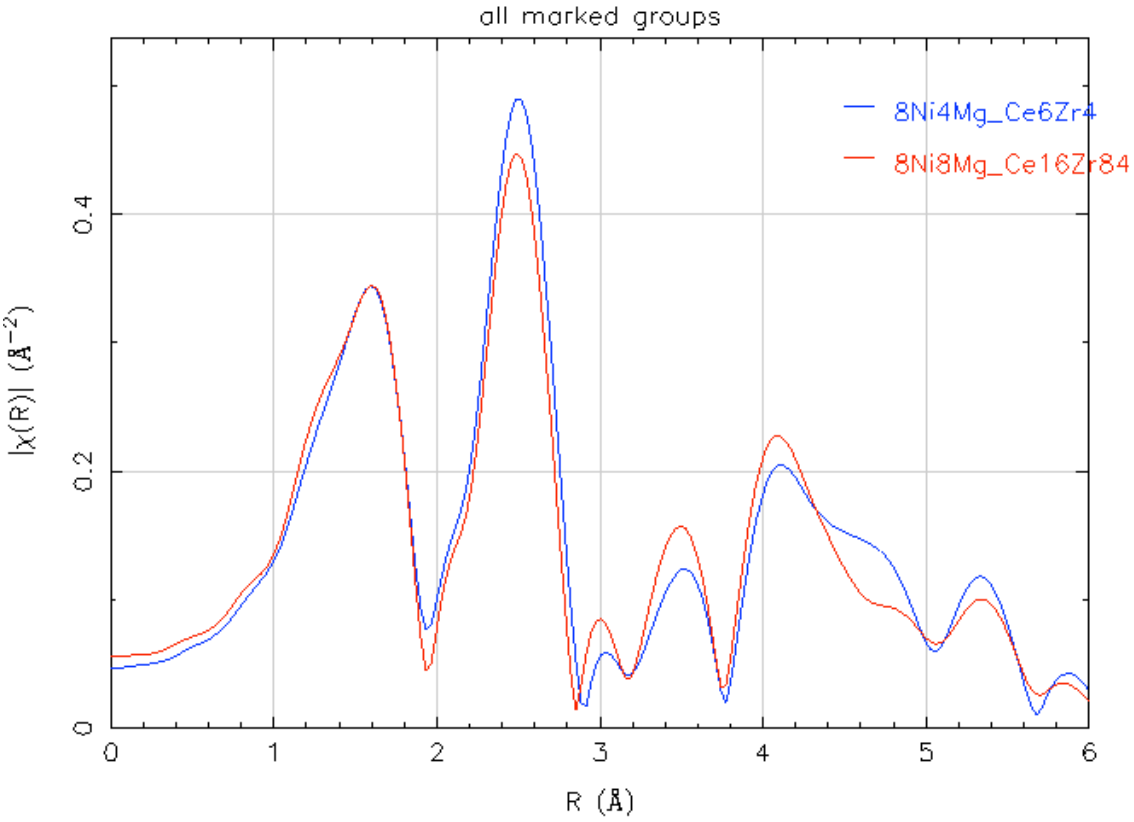

Figure 14: EXAFS spectrum of Mg loading comparison.

oxide structure. The first peak of both catalysts was nearly identical indicating that the same amount of Ni was loaded onto both surfaces and similar particle sizes. However, the second peaks varied indicating a difference in the number of Ni-Ni bonds. Catalyst that were loaded with a Ni:Mg ratio of 1 showed less Ni-Ni bonds while catalyst loaded with the Ni:Mg ratio of 2 showed more Ni-Ni bonds. This indicates that upon increasing the amount of Mg to give a Ni:Mg ratio closer to 1, more Ni/Mg interactions occur.

This result was expected since an increase in Mg content increases the likelihood for Ni species to be in close proximity to Mg and thus increasing the potential to interact with Mg.

3.1.5 Surface Morphology and Composition (SEM-EDS)

A scanning electron microscope allowed the surface topography of the catalysts to be analyzed. By coupling SEM and EDS the confirmation of the metal species, their relative dispersion, and their approximate wt% on the surface of the catalysts could be made. Catalysts prepared by WI and DP with the same support makeup ($Ce_{0.4}Zr_{0.6}O_2$) were compared using SEM-EDS and the results are found in Figure 15 –18. Figure 15 and 16 show the image of the catalysts surface and the elemental mapping at this particular location on the catalyst. From these two figures, it is seen that both Ni and Mg appear well dispersed over the catalyst surface for both metal loading methods (WI and DP). Upon examining the elemental map for Zr in the DP sample, it appears that there might be some segregated Zr particles. This was confirmed to be topographical effects versus an elemental effect because this segregation was not seen in the DP catalyst and the same batch of support was used in both loading methods. XRD analysis further proved that the ZrO_2 was well dispersed in a solid solution with CeO_2. The EDS results for both catalysts were compared and are seen in Figure 17 and Figure 18.

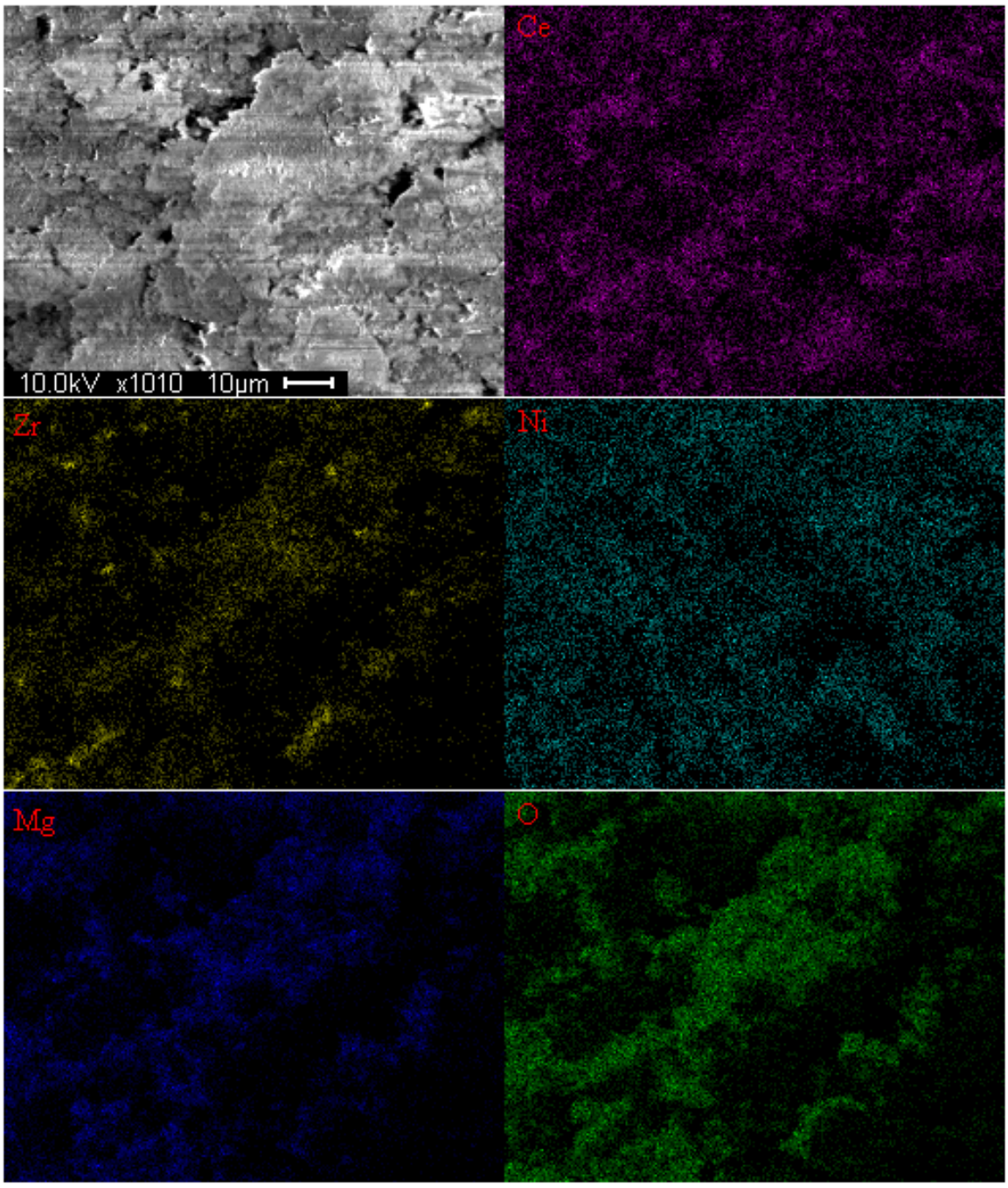

Figure 15: SEM-EDS metal mapping of WI sample.

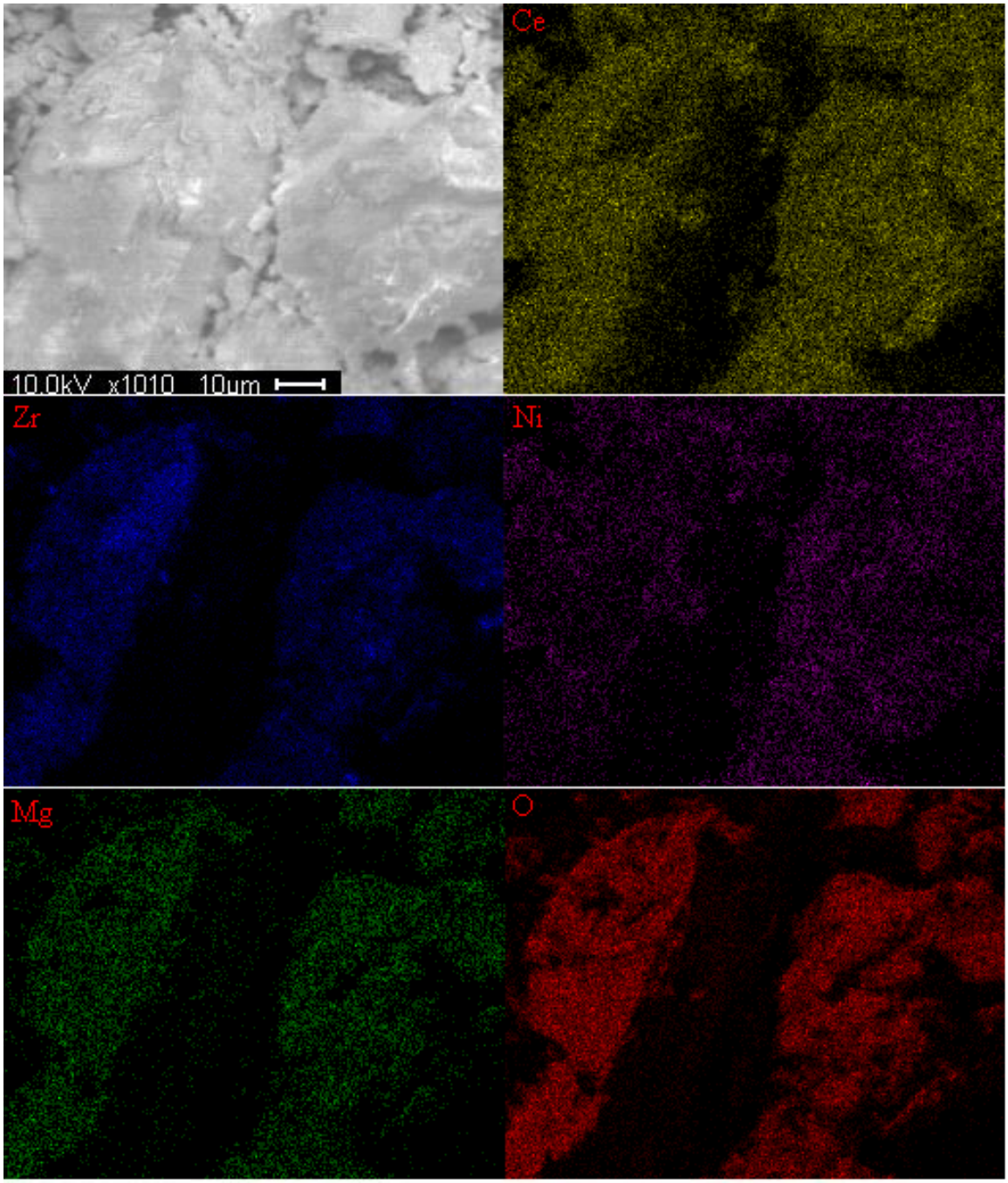

Figure 16: SEM-EDS metal mapping of DP sample.

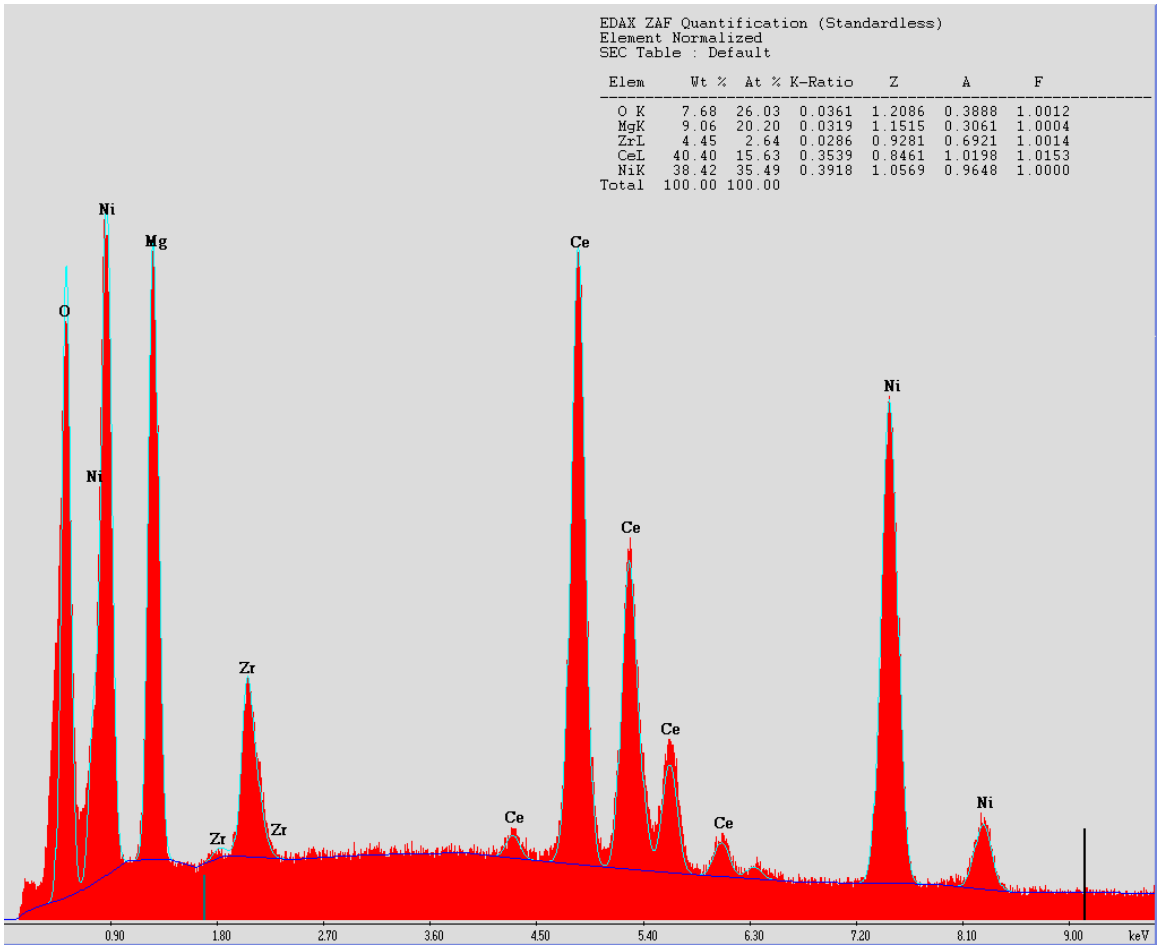

Figure 17: EDS spectrum and approximate elemental wt % for WI sample.

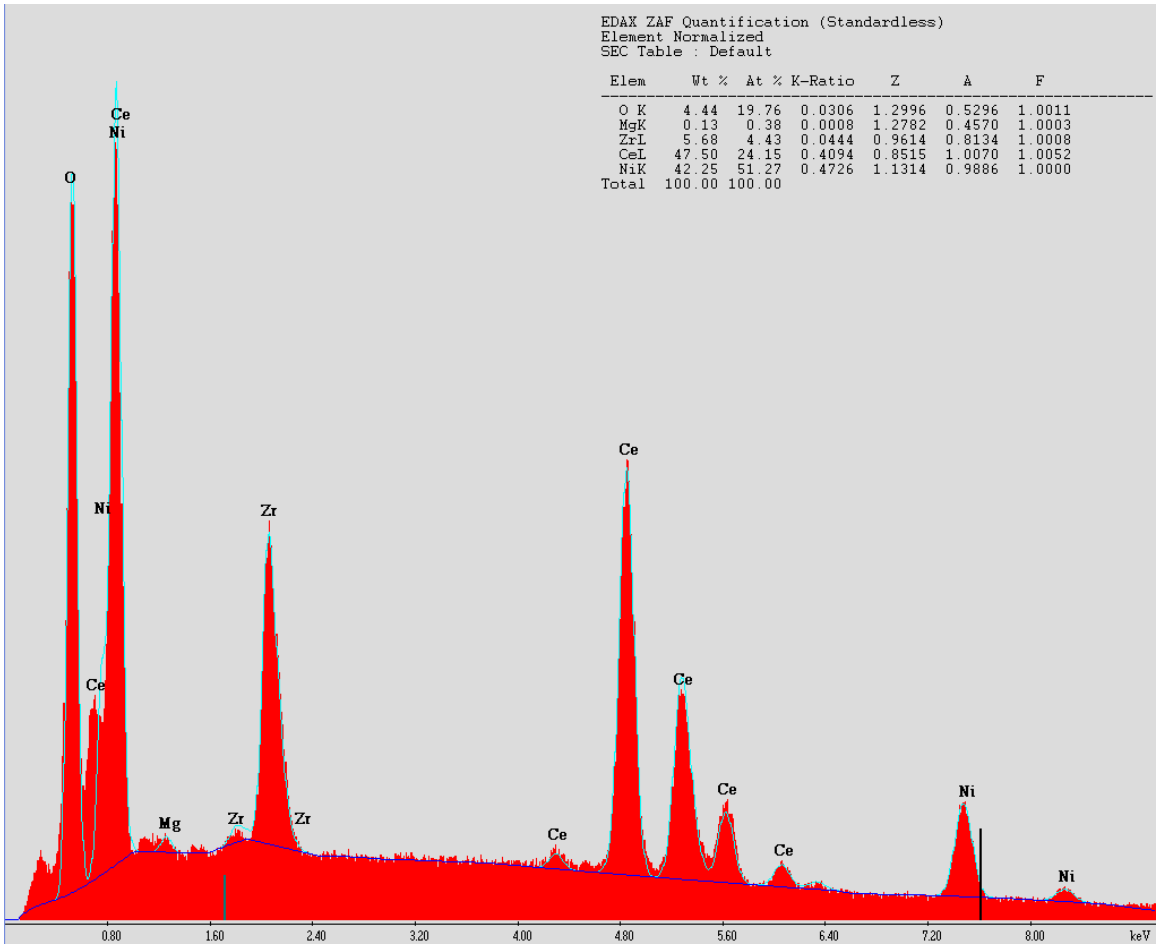

Figure 18: EDS spectrum and approximate elemental wt % DP sample.

The elemental wt% calculated by the EDS are not an accurate method for determining bulk composition because this is a surface technique that only examines a very small area of the catalyst and is influenced heavily by topographical effects. However, from these spectra some approximate ratios can be inferred. Therefore, upon comparing the different metal loading methods it was reasoned that the DP catalyst had less Mg loaded onto the surface than the WI catalyst. Further investigations into why Ni readily precipitated onto the surface, in the presence of excess urea, while Mg did not will have to be made.

3.1.6 Binding Energies and Surface Phases

XPS was utilized to measure the binding energies of species present in the catalyst. An initial broad range scan was performed to identify the major species present and the binding energies associated with these species. Catalysts prepared by WI and DP with the same support makeup ($Ce_{0.4}Zr_{0.6}O_2$) were compared using XPS. The results of which can be found in Figure 19.

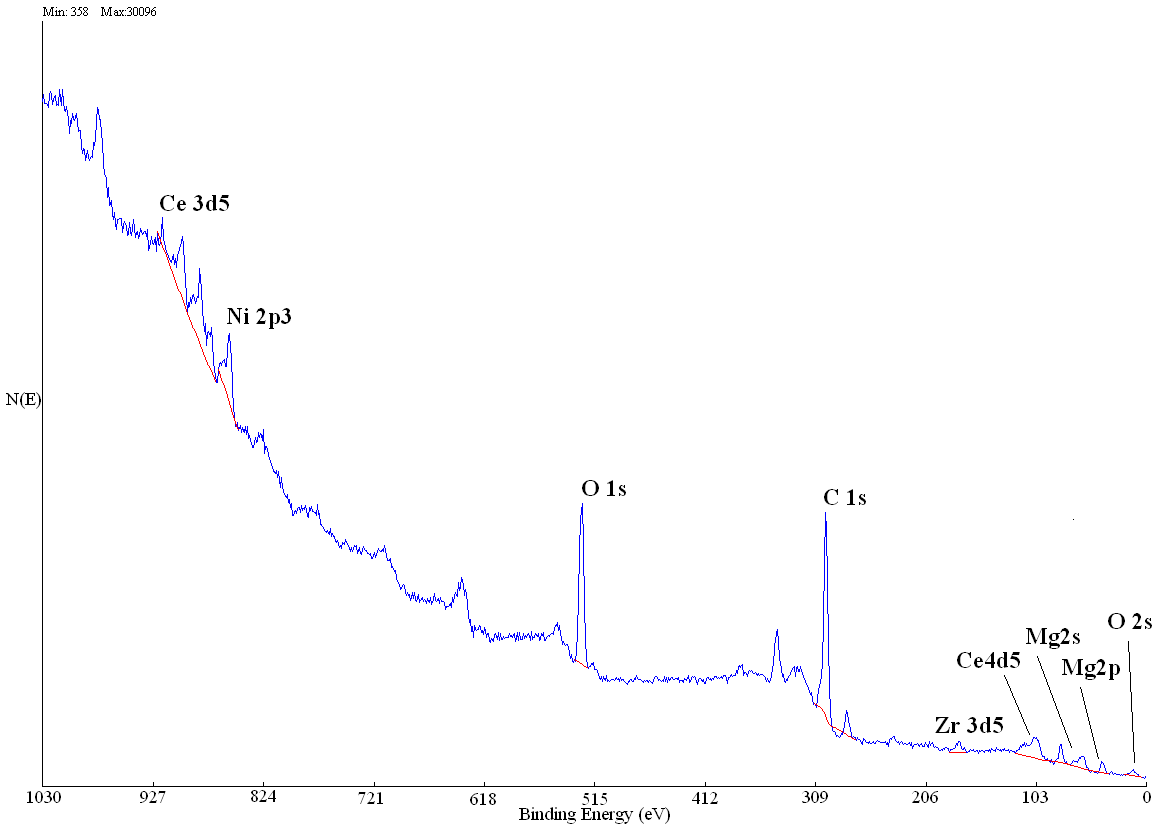

Figure 19: XPS spectrum of reduced WI catalyst with 8 wt. % Ni and Mg loadings.

The binding energies of all species expected to be present in the catalyst were found and the compositions of the mixed oxide support and metal loading % were confirmed. Upon further examination, it was determined to run a high resolution scan of the Ni2p3 peak occurring at a binding energy of 856 to identify the interactions between the Ni, mixed

oxide support, and MgO of the catalyst loaded with 8 wt % Ni and Mg. A curve fit summary was produced from this scan and the results of which can be found in Figure 20.

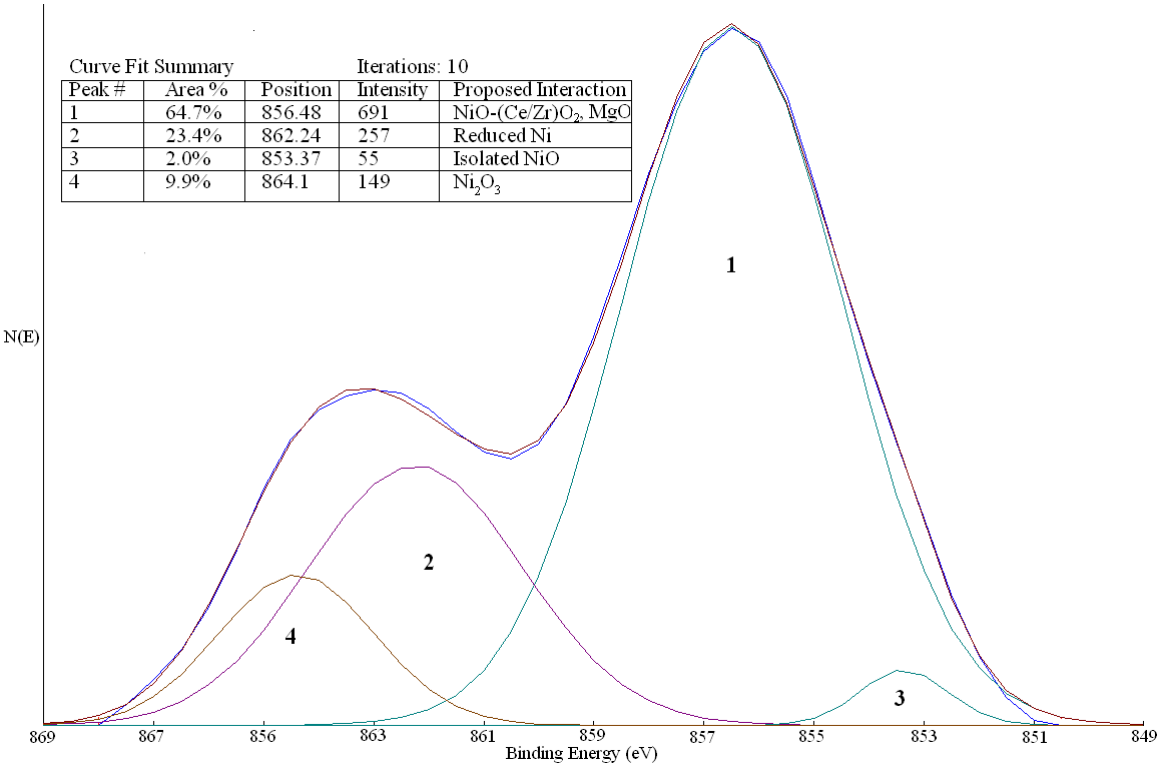

Figure 20: High resolution XPS spectrum of Ni2p3 peak in reduced WI catalyst.

From figure 20 it can be seen that the majority of Ni is found to be interacting with the mixed oxide support or the MgO present in the catalyst. Both of these binding energies occur at 856 and therefore, cannot be resolved. The second largest peak occurs at a binding energy of 862 and is attributed to Ni in the active reduced state. It is important to note that the catalyst tested here was reduced one month prior to XPS testing and it is expected that a larger portion of reduced Ni species would be found in freshly reduced catalyst. Only a small amount of isolated and bulk NiO species was found and suggests that the majority of the Ni remains in the desired active states.

3.2 Examination of the Reaction Conditions on Catalyst Performance

Reactions were studied under controlled temperature programs with the optimum temperature range found between 750-850°C. At the lower end of this range, higher H_2:CO ratios were produced due to the steam reforming and WGS reactions (eq.10, 11) being more favorable at these temperatures. However, lower CO_2 conversions were seen at the lower temperatures. Because CO_2 reforming is favorable at high temperatures, it was determined that CO_2 conversion could be increased by raising the temperature to the higher end of this range. This was confirmed by experiments. At 800°C, CO_2 conversions remained high and desired H_2:CO ratios could be achieved without catalyst deactivation. At this temperature, coke gasification reactions can occur while maintaining high levels of steam reforming and POM to produce desired H_2:CO ratios. At higher temperatures, CO_2 conversion increases but H_2:CO ratios dropped not only due to the increase in CO production, but also to less H_2 production. This is because H_2 production decreases as CO_2 reforming dominates the reaction making steam reforming and POM reactions less favorable at higher temperatures. Similar findings have been seen in previous studies [43, 173].

Gas composition greatly affects the reaction products. In tri-reforming, many reactions are occurring at one time and finding the correct ratios of reactants is not trivial. During tri-reforming reactions, it was found that conversion of O_2 was the highest of all oxidants, completely being consumed. O_2 seems to have a high affinity for active sites on the catalyst and tend to react quickly. Remaining active sites or those where O_2 had disassociated already are available for the other reactants. This finding is similar to the results of Amin et al thermodynamic equilibrium analysis [43]. H_2O and CO_2 compete

for the same active sites so experiments were performed to understand how altering these two reactant concentrations influenced product ratios. Table 4 helps to explain these effects and shows that increasing the H_2O ratio in the feed will increase the H_2:CO ratio.

Table 4: Gas composition comparison table.

Gas Composition (CH_4:CO_2:H_2O:O_2)	Rxn Time	H_2:CO	CH_4 Conv. (%)	CO_2 Conv (%)	Coke (%)
(1:1:0:0.1)	30 min	1.09	74.7	71.1	-
	4 hr	0.91	60.9	59.8	0.35
(1:0.7:0:0.2)	30 min	1.76	99.13	87.4	-
	4 hr	1.73	99.06	87.99	4.1E-02
(1:0.7:0.085:0.2)	30 min	2.06	98.9	86.94	-
	4 hr	2.03	98.85	87.83	1.1E-02
(1:0.7:0.23:0.2)	30 min	2.21	98.84	76.25	-
	4 hr	2.12	97.33	77.6	8.9E-03
(1:0.7:0.3:0.2)	30 min	2.287	99.45	69	-
	4 hr	2.13	99.38	70.24	6.2E-03
(1:0.7:0.5:0.2)	30 min	2.33	99.58	66.27	-
	4 hr	2.19	99.59	65.55	6.3E-03

However, there is a point were higher H_2O ratios led to a decrease in CO2 conversion. One of the goals in tri-reforming is to maintain high CO_2 conversions while still producing desired H_2:CO ratios. High CO_2 conversions make the process more environmentally friendly and improve efficiency in FTS for liquid hydrocarbons. The results in Table 4 suggests that the adsorption of H_2O blocks the CO_2 adsorption sites leading to higher H_2:CO ratios and inhibition of CO_2 reforming. Surprisingly, it was found that lower than expected H_2O concentrations in the feed gas could produce high concentrations of H_2 without sacrificing CO_2 conversion greatly. From Table 4, it is seen that at a CH_4:CO_2:H_2O:O_2 ratio of 1:0.7:0.23:0.2 the reaction produced desired H_2:CO ratios above 2. This suggests that optimum syngas compositions for FT applications could be achieved while maintaining high CO_2 conversions at lower H_2O ratios. At these conditions, the catalyst still showed a high resistance to coke formation on the catalyst

surface. This is an added benefit for FTS since H_2O is reported to deactivate catalysts [117-127]. Xu et al also reports higher than expected H_2:CO and attributes this to the WGS reaction contributing at a higher than expected level to the H_2 production [174]. At the reaction temperature of 800°C and the composition ratio mentioned above, tri-reforming over Ce0.6Zr0.4-8Ni8Mg produced an upgraded syngas with desired H_2:CO ratios for FT applications that achieved CO_2 conversions above 86% and maintained resistance to coke formation at lower steam ratios. Negligible levels of coke were detected in TPO experiments and catalyst activity remained high at the above reaction conditions. The ability to maintain high levels of CO_2 conversion without deactivation becomes a highly attractive option since CO_2 in FT feedstock syngas increases the H_2 demand and higher H_2:CO ratios than 2 will be needed to produce low concentrations of olefins and oxygenates in the FT synthesized product.

Tar reforming experiments were also conducted at reaction conditions similar to previous runs but with the addition of toluene to the system. The reaction temperature was held constant at 800°C while toluene was introduced to the reactant feed gas mix. The ratios of the other reactants were held constant at CH_4:CO_2:H_2O:O_2 ratios of 1:0.7:0.4:0.2. A higher H_2O:CH_4 ratio was chosen to make up for the hydrogen deficiency of toluene. Therefore, H_2:CO product ratios would remain above 2 at the desired ratio for FT applications. Table 5 shows the results from these experiments. Because the mass ionization spectrum for toluene gives the largest response at mass 91, this was the chosen mass to analyze for the conversion of toluene.

Table 5: Tar reforming chart.

Tar Reforming Analysis (CH_4:CO_2:H_2O:O_2=1:0.7:0.4:0.2)				
Toluene (% feed)	Toluene Conv. (%)	Hydrocarbon Conv. (%)	CO_2 Conv. (%)	H_2:CO
2.2	99.9	99.6	72.5	2.58
4.4	99.9	99.2	82.6	2.44
6.7	99.9	98.2	90.9	2.33
8.9	99.9	93.1	97.5	2.28
11	99.9	89.3	99.5	2.33

The results indicate that as more toluene is introduced to the system the conversion or decomposition of the larger molecule remained constant a 99.9%. Thus, the conclusion was reached that all toluene compounds are at least partially decomposed at the various levels of toluene addition tested here. To examine whether complete decomposition of toluene was occurring the mass of 15, indicative of hydrocarbon species, was recorded by the MS. At higher toluene % in the feed gas, the conversion of the hydrocarbon species (mass 15) decreased. At lower % of toluene (toluene additions between 2.2-6.7%) in the feed gas, detection of hydrocarbon species remained fairly low. However, there seemed to be a threshold where the hydrocarbon conversion was influenced to a greater extent by larger toluene additions. This threshold was found to occur between 6.7-8.9% toluene in the feed gas. At toluene addition of 8.9% and 11%, conversions of mass 15 were 93.1% and 89.3% respectively. Feed gas with 6.7% toluene resulted in a 98.2% conversion of mass 15. These findings indicate that, at concentrations of toluene in the reactant feed above 8.9%, the toluene is only partially being decomposed and could possibly lead to adverse effects in FT processing. Possible species could include benzene, methane, alkenes, and other hydrocarbons species

typically associated with the decomposition of toluene. Further testing and investigations into what species are forming must be conducted to gain a clear understanding of how this impacts downstream processes like FT synthesis. MS analysis for mass 78, the largest peak in the mass ionization spectrum for benzene, would indicate if benzene compounds are still present in the product gas and provide more precise data for total tar reduction. Initial investigations are still promising though, and indicate that biomass derived crude syngas containing less than 6.7% total tars can effectively be tri-reformed resulting in a desired syngas for FT applications.

In an effort to determine how the gas hourly space velocity (GHSV) influenced the composition of the product and what reactions might be taken place, the amount of catalyst was increased. The increase in catalyst amount forced reactant gas residence times to be longer. The amount of catalyst used in this study ranged from 2.5-2.9 times (186-218mg) the amount used in previous studies (75mg). A feed gas CH_4:CO_2:H_2O:O_2 ratio of 1:0.7:0.5:0.2 was fed to the reactor. GHSV were calculated to be approximately 21000 $hr^{-1}$and 25000 hr^{-1} when 218 mg and 186 mg catalyst respectively were used to carry out the reforming reaction. The results of which can be found in Table 6. It was interesting to find that while CH_4 conversions remained relatively unchanged, CO_2 conversions were slightly lower and H_2:CO ratios were significantly reduced compared to the previous studies in which the GHSV~61000hr^{-1}. This suggests that, as the feed gas travels through the catalyst bed, different reaction zones are being formed. It is proposed that as the feed gas initially reacts and creates higher H_2 concentration, the reverse WGS reaction becomes more favorable further down the catalyst bed.

Table 6: GHSV comparison chart at CH_4:CO_2:H_2O:O_2 gas feed ratio of ratio of 1:0.7:0.5:0.2 and reactor temperature of 800°C.

(Ce.6Zr.4 Ni+Mg 8%) GHSV Comparisons				
GHSV (hr^{-1})	**Rxn Time**	**H_2:CO**	**CH_4 Conv. (%)**	**CO_2 Conv. (%)**
61000	Init.	2.33	99.58	66.27
	4 hr	2.19	99.59	65.55
25000	5 min	1.57	99.4	63.3
	4 hr	1.55	99.5	62.7
21000	5 min	1.66	98.3	57.2
	4 hr	1.6	98.3	54.7

This could be an of steam reforming reactions (eq. 3, 4) approaching equilibrium. This suggests that there may be an advantage to using higher GHSV to maintain higher H_2 production. By decreasing residence time, the ability to limit reactions that consume H_2 may be possible. Understandably, as this process is scaled up or with turbulent gas flows, reaction equilibrium may be unavoidable. However, even at the lower GHSV conditions, H_2:CO ratios were maintained between 1.55-1.66. Therefore, if H_2 supplementation is needed for FT processing of the tri-reformed gas the amount of H_2 needed to be added to the tri-reforming process will be significantly lower than compared to more traditional reforming processes. These other reforming processes will also be significantly more expensive as higher amounts of steam will be needed and/or coking reactions will limit catalyst lifetime.

Through experimentation, it is seen that control over the feed gas composition is extremely critical in producing a desired syngas composition with a H_2:CO ratio of 2:1. It is clear that analytical analysis of the feed gas coming from the gasifier is extremely important to determine the degree of supplementation of CH_4, O_2 and H_2O needed to reach a CH_4:CO_2:H_2O:O_2 ratio of 1:0.7:0.23:0.2. However, because larger hydrocarbons

and tars have a lower H:C ratio, this will impact product H_2:CO ratios and further studies will be needed to determine how to adjust feed gas supplementation when various amounts of these longer chain hydrocarbons are present. Crude biomass-derived syngas typically contains between 0.2-9.5% total tars and therefore a broad range of possible feed gas compositions for tri-reforming need to be tested [23]. From the studies presented here, it is proposed that lower than previously reported water ratios can be used to reach desired H_2:CO ratios for FT applications. Also, by examining how much CO_2 is present in the crude biomass syngas sent to the reformer, one can significantly reduce the total cost by supplementing with CH_4 or natural gas instead of a pure H_2 stream produced from processes utilizing the WGS reaction or other costly processing to produce higher H_2 content syngas. The amount of CO_2 present determines how to correctly adjust feed gas composition ratios since typical crude biomass syngas contain less CH_4 than CO_2 (Table 1). Significant energy, costs, and environmental advantages can be achieved in using a tri-reforming process that supplements with a CH_4 or natural gas stream and reduces the amount total steam needed. This can be achieved using the Ce/ZrO_2-Ni-Mg catalyst described here. Further discussion to prove this is provided later in the text.

3.3 Examination of the Catalyst Formulation on Catalyst Performance

Various catalyst formulations were tested during this research to study the consequences of altering the support mixture and the ratios/amounts of metals loaded onto the catalyst. These catalysts were each tested under the same conditions while steadily ramping the temperature. All catalysts were prepared using the same WI preparation technique. Results were compared in Figure 19 showing the H_2 production from various catalysts tested while steadily ramping the temperature at 10°C/min. H_2

production is only shown in Figure 19 for ease of interpretation but CO_2 and CH_4 conversions were also analyzed. The effects of varying the support makeup ratio were

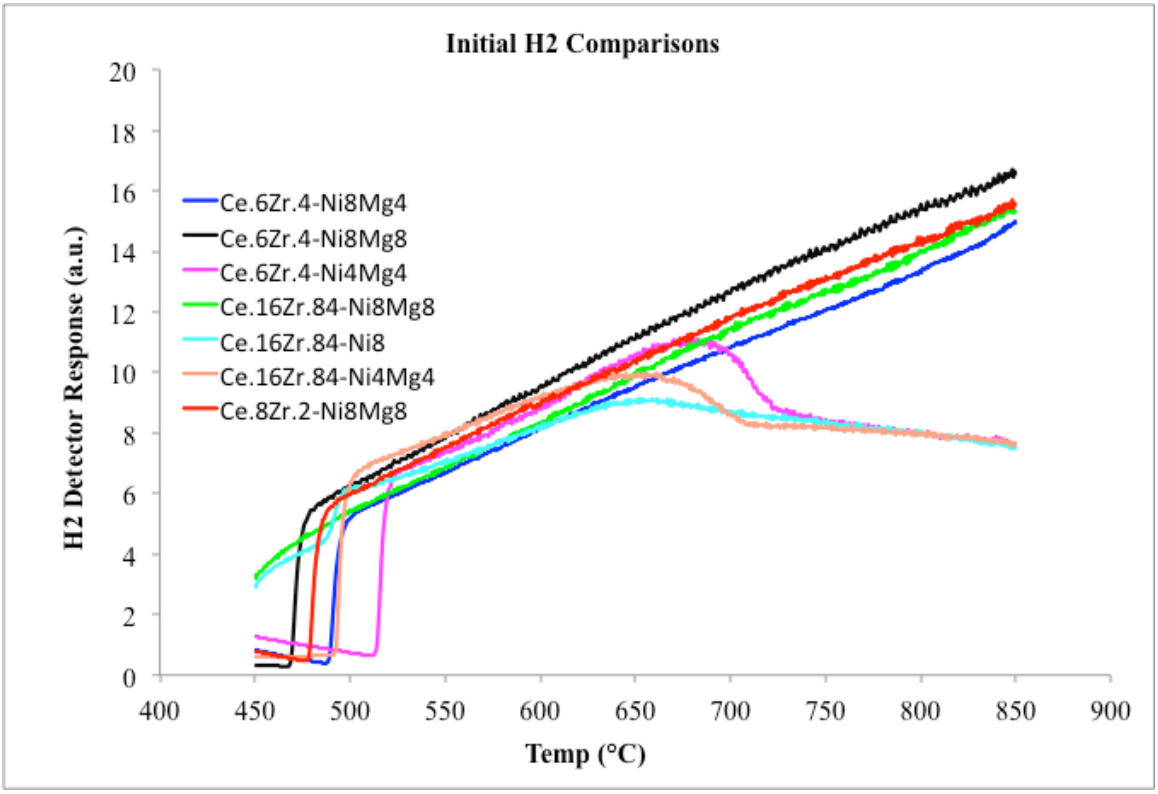

Figure 21: H_2 production chart for initial catalytic testing.

compared by holding the metal wt% and ratios constant. The lower Ce:Zr ratios of 0.16:0.84 in the support led to lower H_2 production, CH_4 conversion, and CO_2 conversion. When Ce:Zr ratios were increased to 0.8:0.2, the H_2 production, CH_4 conversion, and CO_2 conversion slightly increased. Adjusting Ce:Zr ratios to a more even ratio of 0.6:0.4 gave the best results with the highest H_2 production, CH_4 conversion, and CO_2 conversions. This can be explained by the charge channeling effect created by nearby cations. By incorporating a more even ratio of Ce:Zr, oxygen mobility and redox properties are improved allowing transport of oxygen to appropriate sites preventing coking on the Ni metal surface. These results were also reported by Ranga et al. who discovered the even Ce:Zr support ratios give the optimum channel size for

oxygen mobility [172]. Thermal stability was seen in all mixed oxide support ratios and is attributed to ZrO_2 high thermal stability. By incorporating this compound into the support, it improves the mixed oxides catalytic activity at the elevated temperatures used in reforming reactions. This is supported by the XRD data showing that the crystallite structure and size are unchanged at reduction and reaction conditions (Fig 8, Fig. 9) at temperatures of 800°C.

The impacts of metal loading ratios and wt% on the catalyst were explored by holding the support ratio constant and varying the metal loading quantities. Two different Ni amounts of 4% and 8% were loaded onto the same support composition. In all cases, the lower wt% of Ni lead to a plateau effect and a low H_2 production was seen. The plateauing effect describes the tendency of the production of a certain compound, in this case H_2, to remain unchanged even when temperature is increased. This can be explained by the occupancy of all active sites. As the reaction temperature is increased, more active sites become occupied by reactants until all active sites are occupied and higher conversions can no longer be achieved. When 8% Ni was loaded onto the catalyst, the plateauing effect on H_2 production at higher temperatures is no longer seen. The amounts and ratios of Mg were also varied to study its effect on catalyst performance. Again, catalysts with the same support composition and metal loading technique were compared while varying the metals loaded onto the surface. The catalyst with no Mg loaded onto the surface had the slowest rates of H_2 production and quickly plateaued even when higher Ni amounts were loaded onto the surface. This can be explained by the deactivation of the catalyst due to coking. At a Ni:Mg wt% ratio of 2:1, H_2 production rates were increased and no plateauing of the H_2 production was seen with

a steady rise in production as temperatures were increased. Higher amounts of H_2 and the fastest rate of H_2 production were seen when Ni:Mg wt% ratios of 1:1 were loaded onto the catalyst surface. This effect can be explained by the facilitation of the redox mechanism involved in methane reforming with increased interface between Ni and Mg. Metal wt % ratios approaching unity gave more interfaces between Ni and Mg. This facilitates CO_2 adsorption/dissociation and oxygen movement to the reduced Ni surface were it could react with the adsorbed carbon from CH_4. Basic promoters like MgO have an affinity for CO_2 due to its acidic nature [131]. This is an added advantage in CO_2 reforming since CO_2 is normally a very stable molecule and a catalytic reaction is needed for quick dissociation. XAFS data given in Figure 14 supports this explanation showing that increased Ni-Mg interactions were found in the sample with a Ni:Mg ratio of 1. Further support for advantages using Ni:Mg ratios approaching 1 is given in section 3.4.

TPO studies of catalyst reacted with feed gas CH_4:CO_2:H_2O:O_2 ratios of 1:0.7:0.23-0.5:0.2 and even ratios of Ni:Mg show very little amounts of coke formation (Table 4). This is attributed to the self-cleaning capabilities of the catalyst. These de-coking mechanisms are attributed to the desirable OSC and redox properties associated with the mixed (Ce,Zr)O_2 support and basic promoter (MgO) present in this Ni tri-reforming catalyst. Similar results of negligible deactivation due to coke formation have been reported for Mg promoted catalyst [22]. This further proves that the mixed oxide support and MgO promoter play a critical role in extending catalyst lifetime and promoting CO_2 conversions in Ni reforming catalyst.

3.4 Examination of the Preparation Technique on Catalyst Performance

In an attempt to compare different metal loading methods, catalysts prepared by WI and DP were examined under the same tri-reforming conditions. Table 7 shows the total % carbon species in the feed gas that ended up as coke on the catalyst surface. These amounts were measured by TPO immediately following each reaction after rapid cooling. Unfortunately, a direct comparison between these two catalyst preparation techniques is unable to be made. It was found through characterization that those catalyst prepared by deposition precipitation resulted in less MgO loaded onto the surface. Therefore, the results shown here are more indicative of the influence higher MgO loadings have on catalyst performance. WI catalysts consistently had a higher resistance to coke formation in every case where support mixture, Ni loading, and reacting conditions were held constant. This trend becomes more dramatic as higher concentrations of carbon containing species where supplied to the reaction feed gas and in some cases forced the reaction to be aborted due to coking on the DP prepared catalyst. XRD data of the pre- and post-reaction WI samples show a definitive peak for the reduced Ni species. The presence of the reduced Ni species in the post reaction sample shows that deactivation, due to unreduced (Ni,Mg)O species, was limited and Ni species remained in the reduced form after a time on stream of 4hr for WI catalyst.

Table 7: Catalyst preparation method coke comparison chart.

Support and Metal Loading Method Comparison	
(Ce:Zr) Loading Method	**Coke (%)**
(0.6:0.4) Wet Impreg	0.007138
(0.6:0.4) Dep Precip	0.05943
(0.8:0.2) Wet Impreg	0.008836
(0.8:0.2) Dep Precip	0.02016

4. Solar Application (proof of concept)

4.1 Solar Introduction

Solar power is seen as a very promising sustainable energy source. However, the storage of the sun's energy for long periods of time is a large hurdle to overcome in order to make this the solution to our world's energy crisis. To overcome this problem, it is proposed here to combine biomass gasification (BTL) processes with solar power to create hydrocarbon fuels via FT synthesis. It is the goal of this section to prove the concept of this idea and create a preliminary reactor design for this process. In doing so, this provides a means to store the suns energy for long periods of time in the form of liquid fuel for future use.

The use of a solar concentrator and an appropriate heating media will be implemented to transfer heat to a set of reaction vessels. The location of the power plant is designed for Phoenix, AZ and will be next to a municipal solid waste (MSW) landfill where methane gas is being produced via biodegradation. The reason for this is that around 71% of the MSW can be used as a biomass feedstock to the gasifier and a supply of methane to run the reactors can be supplied during the night-time or when sunshine is unavailable. This allows for 24/7 operations. When sunshine is unavailable, the heating media will be heated using methane or natural gas in order to reach the desired temperatures needed to run the reactors. In doing so, it will cut down on start up time when the sun is available by keeping the media at the desired temperature. This media will be used to directly/indirectly heat a gasifier (1000°C), reformer (750-900°C), and FT

(250-350°C) reactor. The media will directly heat to the reforming reactor first and the energy provided from the exit stream of the reformer and FT reactor will provide sufficient energy heat the gasifier indirectly. Steam will also be generated in the process to deliver to the gasifier, reformer, and possibly a turbine by using the extra heat from the reformer product gas and FT reaction. The product will be a clean, sustainable liquid fuel for military and civilian applications.

4.2 Reactor Scheme

4.2.1 Fischer Tropsch Synthesis

The goal for this proof of concept project is to design a 4,000 barrel JP8/day facility. The Fischer Tropsch synthesis will produce liquid hydrocarbon fuel using a syngas feed composition of H_2:CO=1.7-2.15. Reaction products and their reaction equations are listed in eq. 5, 30-32.

(5) Methanation $CO + 3H_2 \rightarrow CH_4 + H_2O$

(30) Paraffins $nCO + (2n + 1)H_2 \rightarrow C_nH_{2n+2} + nH_2O$

(31) Olefins $nCO + 2nH_2 \rightarrow C_nH_{2n} + nH_2O$

(32) Alcohols $nCO + 2nH_2 \rightarrow C_nH_{2n+1}OH + (n-1)H_2O$

For simplicity, we will only consider making undecane (C11) since this is the average carbon chain length in JP-8 fuels. Fischer Tropsch reactions are known to be highly exothermic and according to eq. 30 the heat produced will be 164.9 kJ/mol CO. Considering the average carbon number in the product fuel is 11, then 1.8 MJ/mol C11 will be produced. The MW of C11 paraffin is 156.31g/mol and the average density of JP8 is 0.8kg/L, therefore the following calculation can be made:

$$\left(^{4000\ bbl\ JP8}/_{day}\right)\times\left(^{157\ L}/_{bbl}\right)\times\left(^{0.8\ kg}/_{L}\right)\times\left(^{1000\ g}/_{1kg}\right)\left(^{1\ mol}/_{156.31\ g}\right)$$

$$=\ ^{3.21E6\ mol\ JP8}/_{day}$$

$$\left(^{1.8MJ}/_{mol\ JP8}\right)\times\left(^{3.21E6\ mol\ JP8}/_{day}\right)=\ ^{5.785E6\ MJ}/_{day}\ or\ 66.96\ MW$$

The 66.96 MW of heat produced from the FT reactions can be used to create steam to run a turbine or heat the feed gases flowing to the gasifier and reforming reactions. The later is explained further in the text. Since the heat of vaporization of steam is 40.56 kJ/mol and the specific heat of water is 4.190 J/kg-K, it is possible to calculate for the production of steam from 30°C water we would need around 2.26 MJ/m^3 liquid water. If you are using the steam to run a turbine, then electricity could be produced to run pumps, drives, controls, etc. Considering a steam turbine efficiency of 40% you could produce around 26.78 MW electricity from the excess heat generated by the FT reaction. This is a very nice contribution to the overall process and lowers production cost.

Using cobalt as the FT catalyst, 200°C is the typical operating temperature for this type of FT reaction. Reaching these temperatures will be no problem as the exit gas from the reformer will be ~800°C. Another opportunity to create more steam can be taken advantage of in the cooling of these gases from the reformer. It may also be a good opportunity to provide heat to the gasifier through another heating media (air, steam, O_2). Therefore, no heat needs to be provided directly by solar or natural gas to run the FT reactor. Instead, the FT reactor produces heat that can generate 26.78 MW to help in the overall process. The reforming and gasification reactions, on the other hand, are very energy intensive.

4.2.2 Reforming

To provide the ratio of H_2:CO needed in the FT synthesis, the crude syngas produced in the biomass gasifier needs to be reformed. A reforming reactor temperature of ~800°C will be needed in this process. Calculations based on my research suggest that 14,418 mol/min of CH_4 will need to be reacted for a 4,000 barrel/day facility. This is a rough calculation based upon the amount of CH_4 and CO_2 consumed to produce enough moles carbon to synthesize C11 paraffins at 100% efficiency. Energy needed for this idealized process is 2.60E6 kJ/min (1.56E5MJ/hr) or 43,333 kJ/s or 43.33 MW. These calculations have been made below and are based upon my research and eq. 9, 10, 13, and 14.

(9) $CH_4 + CO_2 = CO + 2H_2$ $\Delta H° = 247.3\ {}^{kJ}/_{mol}$

(10) $CH_4 + H_2O = CO + 3H_2$ $\Delta H° = 206.3\ {}^{kJ}/_{mol}$

(13) $CH_4 + {}^{1}/_{2}\,O_2 = CO + 2H_2$ $\Delta H° = -35.6\ {}^{kJ}/_{mol}$

(14) $CH_4 + 2O_2 = CO_2 + 2H_2O$ $\Delta H° = -880\ {}^{kJ}/_{mol}$

26.1% of methane is converted by steam reforming[a]

$$0.261 \times 206.3\ {}^{kJ}/_{mol} = 53.84\ {}^{kJ}/_{mol}$$

53.9% of methane is converted by CO_2 reforming[a]

$$0.539 \times 247.3\ {}^{kJ}/_{mol} = 133.3\ {}^{kJ}/_{mol}$$

20% of methane is converted by POM[a]

$$0.20 \times \left(-35.5\ {}^{kJ}/_{mol}\right) = -7.12\ {}^{kJ}/_{mol}$$

$Total = 180.02\ {}^{kJ}/_{mol\ CH_4}$[b]

[a] The percentage of CH_4 converted by each reforming mechanism was calculated based upon the complete consumption of O_2, 77% conversion of CO_2, and the remaining balance due to steam reforming.

[b] Song and Pan report 217.3KJ/mol CH_4 needed [131].

$$\left(3.21E6\ mol\ JP8/_{day}\right)\times\left(11\ mol\ C1/_{mol\ C11}\right)$$

$$= 35.31E6\ mol\ C\ containing\ cmpd/_{day}$$

$$= 24520\ mol\ C\ containing\ cmpd/_{min}$$

$$Ratio\ of\ C\ containing\ species\ (CH_4{:}\ CO_2) = 1{:}\ 0.7$$

$$\Longrightarrow 41.2\%\ mol\ C\ as\ CO_2$$

$$\Longrightarrow 58.8\%\ mol\ C\ as\ CH_4$$

$$(0.588)\times\left(24520\ mol\ C\ containing\ cmpd/_{min}\right) = 14418\ mol\ CH_4/_{min}$$

$$\left(14418\ mol\ CH_4/_{min}\right)\times\left(180.02\ kJ/_{mol\ CH_4}\right) = 2.60E6\ kJ/_{min}\ or\ 43333\ kJ/_{sec}$$

$$\left(4333kJ/_{s}\right)\times\left(1000J/_{1kJ}\right)\times\left(1W/_{1\ J/_{s}}\right) = 43.33\ E6\ W\ or\ 43.3MW$$

During the day, the use of solar power will be employed along with a hybrid type system. This hybrid system would incorporate the use of the methane or syngas produced in biodegradation and gasification respectively to heat the system during cloud cover or night hours. Steam turbines could also be used to provide heat when sunshine is unavailable. The reformer reactor will consist of a bank of tubes containing the molten salt that will transfer heat to a fixed bed of catalyst (Ce:Zr 8% Ni+Mg) where the crude syngas from biomass gasification will be fed through. In this way, the molten salt can transfer heat to the catalyst bed in a more uniform manner using the catalyst to aid in heat transfer directly to the gas. The product syngas will be free of tar and contaminants that

would otherwise deactivate the cobalt FT catalyst and also contain the desired H_2:CO ratio of 2:1 needed for FT synthesis.

4.2.3 Gasification

The gasifier also requires a heat input considering the main reactions (eq. 9-15). For this process, around 2,740 ton/day of biomass will be fed to an indirectly heated gasification technology. This involves the use of hot solid particles (sand) fluidized with steam. The char and sand are separated from the syngas via a cyclone and transported to a second fluidized bed reactor. The second reactor is O_2/H_2O blown and acts as a char combustor, generating hot gases and particles (sand). The hot sand is then separated from the hot gases and recirculated to the gasifier to provide heat for pyrolysis [31]. The heating value of this gas is ~15MJ/m^3 and could be used to provide heat when sunshine is unavailable. The O_2/H_2O provided to the second part (exothermic zone) of this reactor will be preheated by the exit gas from the reformer or heat produced from FT reaction. Exit gas from the gasifier will approach ~1000°C and can be used to regulate the temperature of the molten salt coming from the receiver to stabilize the temperature at the desired inlet reaction temp~ 900°C. Therefore, the reforming step is the only reactor directly heated by solar power in this process while the other reactors are indirectly heated by the solar power.

4.3 Plant Design

A central tower solar receiver was chosen for this proof of concept. Therefore monthly insolation/day values most be calculated to design the power plant. Using the Collares-Pareira and Rabl equation (eq. 33) for two-axis tracking and the monthly averaged insolation per day in Phoenix, Az, the monthly averaged insolation per day on a

collector surface in Phoenix, Az was calculated [175]. These values are given in Table 8. See Appendices A for full list of calculated solar values for Phoenix, AZ.

(33) $$H_c = \left[r_t - r_d \left({}^{D_h}/_{H_h}\right)\right] H_h$$

Table 8: Monthly averaged insolation per day on a collector surface in Phoenix, AZ.

Month	H_c (kJ/m^2-day)
January	18600
February	19107
March	18507
April	18085
May	14195
June	16345
July	15375
August	16574
September	18164
October	19536
November	19291
December	18335

The H_c (monthly averaged insolation per day on a collector surface) design value chosen is 19107kJ/m^2-day and occurs 17% of the time. This design value was chosen in order to reduce cost and prevent overheating of the heat media. In times of less insolation (values lower than 19107kJ/m^2-day) during the year, the auxiliary power system will be used. This auxiliary power system will operate from either the natural gas being collected from the nearby landfill through biodegradation, the steam turbine if chosen to incorporate into plant, or the syngas being produced in the process.

Due to the extreme temperatures needed for the reforming reaction, it is difficult to decide on the most appropriate type of salt to be used as the heating media. A cavity type receiver was chosen to reduce heat loss through convection and conduction and needs a fluid media. Therefore, the heating media (molten salt) chosen needs to be in a

liquid state to provide flow through the bank of tubes in the receiver and reactor. Table 9 lists possible salts that could be applicable and Table 10 lists the cost associated with some of these salts [176, 177].

Table 9: Salt properties.

Salt Sytem	Composition (wt%)	Literature mp (°C)	Heat fusion (kJ/kg)	Thermal Conductivity (W/m-K)	Cp liq (kJ/Kg-K)	Density (Kg/m3)
Li_2CO_3-$CaCO_3$	44.3-55.7	662	274.5	-	-	-
Na_2-$BaCO_3$	52.2-41.8	686	172.1	-	-	-
K_2CO_3-Na_2CO_3-Li_2CO_3	48.8-50-1.2	706	162.8	1.73	1.549	2400
K_2CO_3-Na_2CO_3	50-50	710	162.8	1.73	1.549	2400
Li_2CO_3	100	726	607.1	1.96	2.512	2108
Na_2CO_3-K_2CO_3	81.3-18.7	790-737	253.5	-	-	2513
$Na2CO_3$	100	858	265.2	1.83	1.005	2528
K_2CO_3	100	891	200	1.73	1.507	2428
$AlSi_{12}$	100	576	560	160	1.038	2700
$AlSi_{20}$	100	585	460	-	-	-
$MgCl_2$	100	714	452	-	-	2140
LiF-CaF_2	80.5-19.5	767	790	1.7/5.9	1.97/1.84	2100/2670
NaCl	100	800	492	5	-	2160
$NaCO_3$-$BaCO_3$/MgO	-	500-850	-	5	-	2600
LiF	100	850	1800MJ/m3	-	-	-
Na_2CO_3	100	854	275.7	2	-	2533
KF	100	857	452	-	-	2370

Table 10: Salt prices.

Salt	Description	Cost ($/kg)
Li_2CO_3	Powder, bags	2.06
Na_2CO_3	Pwder	0.07
K_2CO_3	Granulated, purified/Calcined	0.44/0.42
$MgCO_3$	Powder, bags	0.22
$CaCO_3$	Ultrafine USP bags/natural dry air floated bags	0.20/0.02
$SrCO_3$	Glass ground, bags	0.62
$BaCO_3$	precipitated, bags/photo grade, bags/ elctroics grad, bags	0.46/0.37/0.37

Li_2CO_3 was decided upon because of its reasonable melting point (726°C) occurring below the operating minimum temperature of 750°C and because of its higher energy

density of 1.47kWh/m^3-K. Other possible salts that take advantage of the latent heat may be possible. Another option is the use of extremely hot air as the heating media.

In section 4.2.2, it was calculated that 43.3 MW or 1.56E8 kJ/hr needed to be generated to successfully run the reforming reaction. To determine the amount of salt needed to run the reactor at the desired temperature range (750-900°C), the following calculations have been made:

$$Q = (Li_2CO_3\ density)\times(Volumetric\ flow\ rate)\times(Heat\ capacity\ of Li_2CO_3\ )\times (900-750°C) = {}^{1.56\ E8\ kJ}/_{hr}$$

$$(Volumetric\ flow\ rate) = \left[\left({}^{1.56E8\ kJ}/_{hr}\right)\times\left({}^{1000J}/_{1kJ}\right)\right] \div \left[\left({}^{2108kg}/_{m^3}\right)\times\left({}^{2512.1\ J}/_{kg\cdot K}\right)\times(150°C)\right] = {}^{196.4m^3}/_{hr}\ or\ {}^{3.32m^3}/_{min}$$

A flow rate of 720.5 m^3/min of inlet gas (CH_4:CO_2:H_2O:O_2=1:0.7:0.3:0.2) to the reformer will be needed, based on 22.4L/mol gas and 14418 mol CH_4/min needed to react for 4,000 barrel/day production. Using a GHSV of 61000 hr^{-1}, this would equate to a catalyst bed volume of 1001m^3. Although scale up to this size is not a trivial feat, it is not impossible. Boger reports that "commercial applications and stationary environmental application have been successfully employed in reactors ranging from several cubic meters up to 1000 m^3 bed volumes [178].

For this process, a bank of tubes will be placed inside the cavity receiver and absorb the solar energy. Thin walled stainless steel or Incoloy 800 tubes, painted with black pyromark paint to optimize absorbance with minimal heat loss, will be used inside

the receiver. These materials have a high resistance to corrosion but other materials may have to be looked at considering the high temperatures involved in this process. The tubes will be placed along a serpentine path inside the cavity receiver and then flow to a 400m^3 thermal storage tank allowing 2hr of thermal storage. The molten salt will then be pumped to a bank of tubes inside the reformer reactor to provide the heat for reaction. The lower temperature salt (750°C) will then be pumped from the reactor either directly to the cavity receiver or to a heated zone where it can be reheated to the appropriate 900°C. This second heated zone allows heating of the salt by other means (methane, electricity, syngas), which can then bypass the receiver when sunlight is unavailable. Based upon the receiver and auxiliary heated zone containing~5m^3 molten salt each, the reactor containing~100m^3, the thermal storage container ~400 m^3 molten salt, and molten salt flowing through the piping system~5m^3; a total of ~514m^3 of salt would be adequate for this process. The sizing of the catalyst bed was based upon similar GHSV used in my laboratory experiments. Scaling up from lab to commercial is unpracticed in the field and is usually done in orders of magnitude. Therefore, the rough estimations done to size this reactor system are susceptible to large error. Based upon the prices of salts listed in Table 10 the cost of the $LiCO_3$ salt needed would be around $2.23 million.

$$(514m^3)\times\left(2108\ kg\ LiCO_3/_{m^3}\right)\times\left(\$2.06/_{kg}\right)=\$2.23\ million$$

Heliostats with an area of 150m^2 will be used to provide heat at a theoretical 90% efficiency. These larger area heliostats may prove to be better than their smaller counterparts due to the reduction in the number of drive system and mechanical parts needed. This may help reduce the likelihood of mechanical failure. Based upon the design value chosen for H_c and the heliostats area, the total radiation each heliostat

receives is 2866.1MJ/day or 119.4MJ/hr. Therefore, at a 90% efficiency, 107.5MJ/hr can be generated for each heliostat. Based upon the energy needed for the reforming reaction of 1.56E5 MJ/hr a total of 1452 heliostats will be needed in this power plant design. Therefore the total heliostat area will be 220500 m^2. Due to shading issues in the heliostat field, it was determined that the mirrors should occupy 40-50% of total land area. Based upon 50% land coverage by mirrors, the total land area needed will be 441000 m^2. Table 11 gives heliostat prices at an estimated production of 50,000units/yr facility [6].

Table 11: Heliostat costs.

148m^2 ATS Glass/Metal Heliostat Price ($/$m^2$)	
Mirror Module	23.06
Support Structure	21.21
Drive	27.11
Drive electrical	1.78
Controls	1.94
Pedestal	16.96
Total Direct Cost:	**92.06**
Overhead/Profit (20%)	18.41
Total Fabricated Price:	**110.47**
Field wiring	7.4
Foundation	2.28
Field alignment/checkout	6.34
Total Installed Price:	**126.5**

These prices are lower than current heliostat prices but will be used because of the possibility that these prices can be reached if a company chooses to increase the production line on heliostats. From the values listed in Table 11, the total cost for the heliostats is $27.9 million. The heliostats will focus on a 325m^2 surface area inside the central receiver cavity and thus the CR (concentration) is equal to (220500m^2)/(325m^2)= 678.

4.4 Economics

The estimated cost of this central receiver power plant is based upon [179, 180] and are listed in Table 12.

Table 12: Estimated plant cost.

	Cost ($ million)	**% Total**
Heliostats	27.9	3.1
Reciever	13	1.5
Tower/piping	13	1.6
Contols	1	0.1
Land	0.5	0.1
Feedstock Prep	15	1.8
Structure/Improvements	10	1.2
Thermal Storage	18	2.2
Thermal Heater	1	0.1
Air Separation Unit	250	30.1
Gasifier	190	22.9
Reformer	190	22.9
FT reactor	150	18.0
O and M	5.4	0.6
Salt	2.23	0.3
Total	**887.03**	

At the estimated $44/ton to bury landfill waste, the conversion of this waste to energy would actually save the landfill around $44 million/year if the plant were operated year round. This is a significant savings for MSW facilities alone. Factoring in that 4,000 barrel/day of JP-8 will be produced and at a selling price of $3.5/gallon, the plant can generate around $215 million/yr if the plant is operated year round. Thus, from the savings by the MSW facility and the profit from selling the JP8 fuel, the company can bring in $255 million/yr. The capital needed to build the power plant is estimated at $887 million. Therefore, the possibility of paying off the capital and producing a profit within 4 years is promising. If the plant has a downtime of 1 month out of the year, the plant

would lose around $18 million in fuel sales and still be looking to pay off the capital cost within 4 years. These estimates are based upon no outside electricity while sunlight is unavailable and energy would be provided by methane from biodegradation and crude syngas from biodegradation. Because of the complexity of this plant design, there may be factors that have been overlooked, along with errors in cost estimates that could make this a less profitable process. But from the data presented here, this plant stands to make a substantial contribution to sustainable alternative energy solutions.

4.5 Solar Conclusion

This central receiver power plant attempts to collect solar energy and store the energy for long-term periods in a stable liquid form as hydrocarbon fuel. Jet fuel (JP-8) was chosen as the desired end product due to the large consumption rates in the US and the military's need to provide alternative fuels to its fleets. The Air Force and Navy have both expressed goals to reduce their petroleum consumption. The design of this plant in close proximity to a landfill also creates a waste to energy process that can take a negative value feedstock (MSW) and convert it into a high value liquid fuel. This process is designed to be totally sustainable and is a proof of concept. Further research and development will be needed to make this plant feasible but the concepts presented here prove the possibility of designing such a process in the near future.

5. Conclusion

The support Ce:Zr ratio, metal loading techniques, metal wt %, and Ni Mg ratios all had a pronounced influence on the catalyst performance. Even ratios of metal oxides making up the support and even ratios of Ni:Mg gave the best performance. The wet impregnation method consistently showed more resistance to coke formation when compared to the deposition precipitation method but was later attributed to higher Mg loadings. Lower than previously reported H_2O concentrations in the feed gas composition also led to desired H_2:CO ratios needed for FT reaction while maintaining high conversions of CO_2 and resistance to coke formation. Reactions involving tar reforming indicate that biomass derived crude syngas containing less than 6.7% total tars can effectively be tri-reformed resulting in a desired syngas for FT applications. Higher GHSV around 61000 hr^{-1} gave significantly higher H_2:CO ratios when compared to reactions run at lower GHSV around 25000 hr^{-1}. These results suggest that steam reforming reactions are kept further from equilibrium at higher GHSV and result in higher than expected H_2 production at lower steam ratios. Moreover, in gasification of biomass, CH_4 and H_2O supplementation of the product gas, prior to reforming, may be needed to produce desired H_2:CO ratios for FT applications. The amounts of which can be determined based upon CO_2:CH_4 ratios in the crude syngas from the biomass gasification process. Further experiments are needed to determine how the amount of tars present in the feed gas will influence the degree of CH_4 and H_2O supplementation needed for tri-reforming. The proof of concept design of a solar powered GTL plant

using MSW as a feedstock shows a realistic opportunity for long term storage of the sun's energy in the form of liquid fuels without outside energy sources (electricity from the grid). Tri-reforming with the above tested catalyst and reaction conditions offers the advantage of producing desired H_2/CO ratios with minimal deactivation, high reactant conversions, and extended catalyst lifetime.

Works Cited

1. Whitney, G., C.E. Behrens, and C. Glover. *US Fossil Fuel Resources: Terminology, Reporting, and Summary*. 2010; Available from: http://epw.senate.gov/public/index.cfm?FuseAction=Files.view&FileStore_id=04212e22-c1b3-41f2-b0ba-0da5eaead952.

2. *About Coal*. 2012; Available from: http://www.clean-energy.us/facts/coal.htm.

3. Corporation, P., Oil & Gas journal, 2008. **106**.

4. *World Crude Oil Consumption by Year (Thousand Barrels per Day)*. 2011; Available from: http://www.indexmundi.com/energy.aspx.

5. Lashof, D.A. and D.R. Ahuja, *Relative contributions of greenhouse gas emissions to global warming*. Nature, 1990. **344**(6266): p. 529-531.

6. Schlamadinger, B. and G. Marland, *Full fuel cycle carbon balances of bioenergy and forestry options*. Energy Conversion and Management, 1996. **37**(6–8): p. 813-818.

7. Tyson, K.S., *Biodiesel Handling and Use Guidelines*. 2001, National Renewable Energy Laboratory: Golden, CO.

8. Zheng, Y., X. Chen, and Y. Shen, *Commodity Chemicals Derived from Glycerol, an Important Biorefinery Feedstock*. Chemical Reviews, 2008. **108**(12).

9. Kalnes, T., *Green diesel: a second generation biofuel*. International journal of chemical reactor engineering, 2007. **5**(5): p. 48.

10. Li, L., et al., *Catalytic Hydrothermal Conversion of Triglycerides to Non-ester Biofuels*. Energy & Fuels, 2010. **24**(2): p. 1305-1315.

11. Bartholomew, C.H. and R.J. Rarrauto, *Industrial Catalytic Processes*. 2nd ed. 2005, Hoboken, New Jersey: John Wiley & Sons, Inc.

12. RAHMIM, I.I., *Stranded gas, diesel eds push GTL work*. Vol. 103. 2005, Tulsa, OK, ETATS-UNIS: Pennwell. 9.

13. EPA. *Renewable Fuel Standard (RFS) | Fuels & Fuel Additives | Transportation & Air Quality | US EPA*. 2012 2011-11-15; Available from: http://www.epa.gov/otaq/fuels/renewablefuels/index.htm.

14. Simmons, B.A., D. Loque, and H.W. Blanch, *Next-generation biomass feedstocks for biofuel production*. Genome Biology, 2008. **9**.

15. Jean, G.V. *Air Force Tells Biofuels Industry to 'Bring It'*. 2011; Available from: http://www.nationaldefensemagazine.org/archive/2011/January/Pages/AirForceTellsBiofuelsIndustrytoBringIt.aspx.

16. Vasden, B. *USCJO - Biomass & Biofuel Feedstock Farming*. 2010; Available from: http://www.uscjo.com/.

17. Bowen, H., *Air Force wants 50% use of biofuel by 2016*, in *Moscow-Pullman Daily News*. 2011: Moscow, Idaho.

18. NREL. *Learning - Biomass Energy Basics*. 2012; Available from: http://www.nrel.gov/learning/re_biomass.html.

19. Higman, C. and M. van der Burgt, *Gasification*. 2nd ed. 2008, Burlington, MA: Elsevier.

20. Sunderasan, S., *The food v. fuel debate: A nuanced view of incentive structures*. Renewable Energy, 2009. **34**(4): p. 950-954.

21. Service, U.E.R. *ERS/USDA Data - Feed Grains Database: Custom Queries*. 2012; Available from: http://www.ers.usda.gov/Data/FeedGrains/CustomQuery/.

22. Yung, M.M. and J.N. Kuhn, *Deactivation Mechanisms of Ni-Based Tar Reforming Catalysts As Monitored by X-ray Absorption Spectroscopy†*. Langmuir, 2010. **26**(21): p. 16589-16594.

23. Puig-Arnavat, M., J.C. Bruno, and A. Coronas, *Review and analysis of biomass gasification models*. Renewable and Sustainable Energy Reviews, 2010. **14**(9): p. 2841-2851.

24. Wang, L., et al., *Cultivation of Green Algae <i>Chlorella</i> sp. in Different Wastewaters from Municipal Wastewater Treatment Plant*. Applied Biochemistry and Biotechnology, 2010. **162**(4): p. 1174-1186.

25. Ruiz-Marin, A., L.G. Mendoza-Espinosa, and T. Stephenson, *Growth and nutrient removal in free and immobilized green algae in batch and semi-continuous cultures treating real wastewater*. Bioresource Technology, 2010. **101**(1): p. 58-64.

26. *Waste Business Journal : Information for the Waste Industry | Data and Research*. Waste Business Journal.com 2012; Available from: http://www.wastebusinessjournal.com/.

27. EPA, *Municipal Solid Waste Generation, Recycling, and Disposal in the United States Tables and Figures for 2010*. 2011, EPA.

28. *Waste Gasification Impacts on the Environment and Public Health*. 2009; Available from: http://www.bredl.org/pdf/wastegasification.pdf.

29. Li, J., et al., *Development of a supported tri-metallic catalyst and evaluation of the catalytic activity in biomass steam gasification*. Bioresource Technology, 2009. **100**(21): p. 5295-5300.

30. Stern, J.C., et al., *Use of a biologically active cover to reduce landfill methane emissions and enhance methane oxidation*. Waste Management, 2007. **27**(9): p. 1248-1258.

31. Ciferno, J.P. and J.J. Marano, *Benchmarking Biomass Gasification Technologies for Fuels, Chemicals and Hydrogen Production*. 2002, U.S. Department of Energy National Energy Technology Laboratory.

32. Peter, M., *Energy production from biomass (part 3): gasification technologies*. Bioresource Technology, 2002. **83**(1): p. 55-63.

33. Peter, M., *Energy production from biomass (part 1): overview of biomass*. Bioresource Technology, 2002. **83**(1): p. 37-46.

34. Li, X.T., et al., *Biomass gasification in a circulating fluidized bed*. Biomass and Bioenergy, 2004. **26**(2): p. 171-193.

35. Galletti, C., et al., *CO Methanation as Alternative Refinement Process for CO Abatement in H2-Rich Gas for PEM Applications*. 2007, The Berkeley Electronic Press.

36. Rezaiyan, J. and N.P. Cheremisinoff, *Gasification Technologies*. 2005, Boca Raton, FL: CRC Press Taylor & Francis Group.

37. A.V, B., *The technical and economic feasibility of biomass gasification for power generation*. Fuel, 1995. **74**(5): p. 631-653.

38. A.A.C.M, B., *Biomass gasification in moving beds, a review of European technologies*. Renewable Energy, 1999. **16**(1–4): p. 1180-1186.

39. Devi, L., K.J. Ptasinski, and F.J.J.G. Janssen, *Pretreated olivine as tar removal catalyst for biomass gasifiers: investigation using naphthalene as model biomass tar*. Fuel Processing Technology, 2005. **86**(6): p. 707-730.

40. Dayton, D., *A review of the Literature on Catalytic biomass Tar Destruction*, in *Milestone Completion Report*. 2002, NREL: Golden, Colarado.

41. Nakamura, K., et al., *Promoting effect of MgO addition to Pt/Ni/CeO2/Al2O3 in the steam gasification of biomass*. Applied Catalysis B: Environmental, 2009. **86**(1–2): p. 36-44.

42. Herguido, J., J. Corella, and J. Gonzalez-Saiz, *Steam Gasification of lignocellulosic residues in a fluidized bed at a small pilot scale. Effect of the Type of Feedstock*. Ind. Eng. Chem. Res., 1992. **31**: p. 1274-1282.

43. Amin, N.A.S. and T.C. Yaw, *Thermodynamic equilibrium analysis of combined carbon dioxide reforming with partial oxidation of methane to syngas*. International Journal of Hydrogen Energy, 2007. **32**(12): p. 1789-1798.

44. Rostrup-Nielsen and R. Jens, *Steam reforming catalysts: An investigation of catalysts for tubular steam reforming of hydrocarbons*. 1975, Copenhagen: Teknisk Forlag. 240.

45. Li, Y., et al., *Oxidative reformings of methane to syngas with steam and CO2 catalyzed by metallic Ni based monolithic catalysts*. Catalysis Communications, 2008. **9**(6): p. 1040-1044.

46. Roh, H.-S., H.S. Potdar, and K.-W. Jun, *Carbon dioxide reforming of methane over co-precipitated Ni–CeO2, Ni–ZrO2 and Ni–Ce–ZrO2 catalysts*. Catalysis Today, 2004. **93–95**(0): p. 39-44.

47. PENA, et al., *New catalytic routes for syngas and hydrogen production*. Vol. 144. 1996, Kidlington, ROYAUME-UNI: Elsevier.

48. Dong, W.-S., et al., *Methane reforming over Ni/Ce-ZrO2 catalysts: effect of nickel content*. Applied Catalysis A: General, 2002. **226**(1–2): p. 63-72.

49. Wang, S., G.Q. Lu, and G.J. Millar, *Carbon Dioxide Reforming of Methane To Produce Synthesis Gas over Metal-Supported Catalysts: State of the Art*. Energy & Fuels, 1996. **10**(4): p. 896-904.

50. Roh, H.-S., et al., *Highly stable Ni catalyst supported on Ce–ZrO2 for oxy-steam reforming of methane*. Catalysis Letters, 2001. **74**(1): p. 31-36.

51. Pompeo, F., et al., *Study of Ni catalysts on different supports to obtain synthesis gas*. International Journal of Hydrogen Energy, 2005. **30**(13–14): p. 1399-1405.

52. Koo, K.Y., et al., *Coke study on MgO-promoted Ni/Al2O3 catalyst in combined H2O and CO2 reforming of methane for gas to liquid (GTL) process*. Applied Catalysis A: General, 2008. **340**(2): p. 183-190.

53. Horiuchi, T., et al., *Suppression of carbon deposition in the CO2-reforming of CH4 by adding basic metal oxides to a Ni/Al2O3 catalyst*. Applied Catalysis A: General, 1996. **144**(1–2): p. 111-120.

54. Martavaltzi, C.S., et al., *Hydrogen Production via Steam Reforming of Methane with Simultaneous CO2 Capture over CaO−Ca12Al14O33*. Energy & Fuels, 2010. **24**(4): p. 2589-2595.

55. Rostrupnielsen, J.R. and J.H.B. Hansen, *CO2-Reforming of Methane over Transition Metals*. Journal of Catalysis, 1993. **144**(1): p. 38-49.

56. Bradford, M.C.J. and M.A. Vannice, *CO2Reforming of CH4over Supported Pt Catalysts*. Journal of Catalysis, 1998. **173**(1): p. 157-171.

57. Bradford, M.C.J. and M.A. Vannice, *Catalytic reforming of methane with carbon dioxide over nickel catalysts II. Reaction kinetics*. Applied Catalysis A: General, 1996. **142**(1): p. 97-122.

58. Efstathiou, A.M., et al., *Reforming of Methane with Carbon Dioxide to Synthesis Gas over Supported Rhodium Catalysts: II. A Steady-State Tracing Analysis: Mechanistic Aspects of the Carbon and Oxygen Reaction Pathways to Form CO*. Journal of Catalysis, 1996. **158**(1): p. 64-75.

59. Ruckenstein, E. and Y.H. Hu, *Carbon dioxide reforming of methane over nickel/alkaline earth metal oxide catalysts*. Applied Catalysis A: General, 1995. **133**(1): p. 149-161.

60. Yamazaki, O., K. Tomishige, and K. Fujimoto, *Development of highly stable nickel catalyst for methane-steam reaction under low steam to carbon ratio*. Applied Catalysis A: General, 1996. **136**(1): p. 49-56.

61. Mark, M.F. and W.F. Maier, *CO2-Reforming of Methane on Supported Rh and Ir Catalysts*. Journal of Catalysis, 1996. **164**(1): p. 122-130.

62. Erdohelyi, A., J. Cserenyi, and F. Solymosi, *Activation of CH4 and Its Reaction with CO2 over Supported Rh Catalysts*. Journal of Catalysis, 1993. **141**(1): p. 287-299.

63. Tomishige, K., Y.-g. Chen, and K. Fujimoto, *Studies on Carbon Deposition in CO2Reforming of CH4over Nickel–Magnesia Solid Solution Catalysts*. Journal of Catalysis, 1999. **181**(1): p. 91-103.

64. Bradford, M.C.J. and M.A. Vannice, *CO2 Reforming of CH4*. Catalysis Reviews, 1999. **41**(1): p. 1-42.

65. Hao, Z., et al., *CH4–CO2 reforming over Ni/Al2O3 aerogel catalysts in a fluidized bed reactor*. Powder Technology, 2008. **182**(3): p. 474-479.

66. Schuurman, Y., et al., *Unraveling mechanistic features for the methane reforming by carbon dioxide over different metals and supports by TAP experiments*. Catalysis Today, 1998. **46**(2–3): p. 185-192.

67. Wei, J. and E. Iglesia, *Isotopic and kinetic assessment of the mechanism of reactions of CH4 with CO2 or H2O to form synthesis gas and carbon on nickel catalysts*. Journal of Catalysis, 2004. **224**(2): p. 370-383.

68. Chang, J.-S., et al., *Catalytic Behavior of Supported KNiCa Catalyst and Mechanistic Consideration for Carbon Dioxide Reforming of Methane*. Journal of Catalysis, 2000. **195**(1): p. 1-11.

69. Luo, J.Z., et al., *CO2/CH4 Reforming over Ni–La2O3/5A: An Investigation on Carbon Deposition and Reaction Steps*. Journal of Catalysis, 2000. **194**(2): p. 198-210.

70. Osaki, T. and T. Mori, *Role of Potassium in Carbon-Free CO2 Reforming of Methane on K-Promoted Ni/Al2O3 Catalysts*. Journal of Catalysis, 2001. **204**(1): p. 89-97.

71. Nandini, A., K.K. Pant, and S.C. Dhingra, *Kinetic study of the catalytic carbon dioxide reforming of methane to synthesis gas over Ni-K/CeO2-Al2O3 catalyst*. Applied Catalysis A: General, 2006. **308**(0): p. 119-127.

72. L.M, A., *Transient Isotopic Studies and Microkinetic Modeling of Methane Reforming over Nickel Catalysts*. Journal of Catalysis, 1997. **165**(2): p. 262-274.

73. Cui, Y., et al., *Kinetic study of the catalytic reforming of CH4 with CO2 to syngas over Ni/α-Al2O3 catalyst: The effect of temperature on the reforming mechanism*. Applied Catalysis A: General, 2007. **318**(0): p. 79-88.

74. Wilhelm, D.J., et al., *Syngas production for gas-to-liquids applications: technologies, issues and outlook*. Fuel Processing Technology, 2001. **71**(1–3): p. 139-148.

75. Nagaoka, K., et al., *Carbon Deposition during Carbon Dioxide Reforming of Methane—Comparison between Pt/Al2O3 and Pt/ZrO2*. Journal of Catalysis, 2001. **197**(1): p. 34-42.

76. Li, M.-w., et al., *Carbon Dioxide Reforming of Methane Using DC Corona Discharge Plasma Reaction*. The Journal of Physical Chemistry A, 2004. **108**(10): p. 1687-1693.

77. Kim, T., S. Moon, and S.-I. Hong, *Internal carbon dioxide reforming by methane over Ni-YSZ-CeO2 catalyst electrode in electrochemical cell*. Applied Catalysis A: General, 2002. **224**(1–2): p. 111-120.

78. Sukonket, T., et al., *Influence of the Catalyst Preparation Method, Surfactant Amount, and Steam on CO2 Reforming of CH4 over 5Ni/Ce0.6Zr0.4O2 Catalysts*. Energy & Fuels, 2011. **25**(3): p. 864-877.

79. Wang, S. and G.Q. Lu, *Role of CeO2 in Ni/CeO2–Al2O3 catalysts for carbon dioxide reforming of methane*. Applied Catalysis B: Environmental, 1998. **19**(3–4): p. 267-277.

80. Ermakova, M.A., et al., *New Nickel Catalysts for the Formation of Filamentous Carbon in the Reaction of Methane Decomposition*. Journal of Catalysis, 1999. **187**(1): p. 77-84.

81. Wang, J.B., Y.-S. Wu, and T.-J. Huang, *Effects of carbon deposition and de-coking treatments on the activation of CH4 and CO2 in CO2 reforming of CH4 over Ni/yttria-doped ceria catalysts*. Applied Catalysis A: General, 2004. **272**(1–2): p. 289-298.

82. Huang, T.-J., H.-J. Lin, and T.-C. Yu, *A Comparison of Oxygen-vacancy Effect on Activity Behaviors of Carbon Dioxide and Steam Reforming of Methane over Supported Nickel Catalysts*. Catalysis Letters, 2005. **105**(3): p. 239-247.

83. Huang, T.-J. and T.-C. Yu, *Effect of steam and carbon dioxide pretreatments on methane decomposition and carbon gasification over doped-ceria supported nickel catalyst*. Catalysis Letters, 2005. **102**(3): p. 175-181.

84. Iwasa, N., M. Takizawa, and M. Arai, *Preparation and application of nickel-containing smectite-type clay materials for methane reforming with carbon dioxide*. Applied Catalysis A: General, 2006. **314**(1): p. 32-39.

85. Ashcroft, A.T., et al., *Partial oxidation of methane to synthesis gas using carbon dioxide*. Nature, 1991. **352**(6332): p. 225-226.

86. Choudhary, V.R., A.S. Mammon, and S.D. Sansare, *Selective Oxidation of Methane to CO and H2 over Ni/MgO at Low Temperatures*. Angewandte Chemie International Edition in English, 1992. **31**(9): p. 1189-1190.

87. Dajiang, M., et al., *Catalytic Partial Oxidation of Methane over Ni/CeO2 -ZrO2 -Al2O3*. Journal of Rare Earths, 2007. **25**(3): p. 311-315.

88. Choudhary, V.R., B.S. Uphade, and A.S. Mamman, *Oxidative Conversion of Methane to Syngas over Nickel Supported on Commercial Low Surface Area Porous Catalyst Carriers Precoated with Alkaline and Rare Earth Oxides*. Journal of Catalysis, 1997. **172**(2): p. 281-293.

89. Tang, S., J. Lin, and K. Tan, *Partial oxidation of methane to syngas over Ni/MgO, Ni/CaO and Ni/CeO<sub>2</sub&gt*. Catalysis Letters, 1998. **51**(3): p. 169-175.

90. Diskin, A.M., R.H. Cunningham, and R.M. Ormerod, *The oxidative chemistry of methane over supported nickel catalysts*. Catalysis Today, 1998. **46**(2–3): p. 147-154.

91. Hickman, D.A. and L.D. Schmidt, *Production of Syngas by Direct Catalytic Oxidation of Methane*. Science, 1993. **259**(5093): p. 343-346.

92. Ruckenstein, E. and Y. Hang Hu, *Methane partial oxidation over NiO/MgO solid solution catalysts*. Applied Catalysis A: General, 1999. **183**(1): p. 85-92.

93. Jones, R.H., et al., *Catalytic conversion of methane to synthesis gas over europium iridate, Eu₂Ir₂O<sub>7</sub >: An<i>in situ</i> study by x-ray diffraction and mass spectrometry*. Catalysis Letters, 1991. **8**(2): p. 169-174.

94. Hickman, D.A. and L.D. Schmidt, *Synthesis gas formation by direct oxidation of methane over Pt monoliths*. Journal of Catalysis, 1992. **138**(1): p. 267-282.

95. Rabe, S., T.-B. Truong, and F. Vogel, *Low temperature catalytic partial oxidation of methane for gas-to-liquids applications*. Applied Catalysis A: General, 2005. **292**(0): p. 177-188.

96. Roh, H.-S., et al., *Partial Oxidation of Methane over Ni/θ-Al2O3 Catalysts*. Chemistry Letters, 2001. **30**(7): p. 666-667.

97. Roh, H.-S., et al., *Partial Oxidation of Methane over Ni Catalysts Supported on Ce-ZrO2 Mixed Oxide*. Chemistry Letters, 2001. **30**(1): p. 88-89.

98. Koh, A.C.W., et al., *Hydrogen or synthesis gas production via the partial oxidation of methane over supported nickel–cobalt catalysts*. International Journal of Hydrogen Energy, 2007. **32**(6): p. 725-730.

99. Johnsen, K., et al., *Sorption-enhanced steam reforming of methane in a fluidized bed reactor with dolomite as -acceptor*. Chemical Engineering Science, 2006. **61**(4): p. 1195-1202.

100. Balasubramanian, B., et al., *Hydrogen from methane in a single-step process*. Chemical Engineering Science, 1999. **54**(15–16): p. 3543-3552.

101. Harrison, D.P., *Sorption-Enhanced Hydrogen Production: A Review*. Industrial & Engineering Chemistry Research, 2008. **47**(17): p. 6486-6501.

102. Li, Z.-s., N.-s. Cai, and J.-b. Yang, *Continuous Production of Hydrogen from Sorption-Enhanced Steam Methane Reforming in Two Parallel Fixed-Bed Reactors Operated in a Cyclic Manner*. Industrial & Engineering Chemistry Research, 2006. **45**(26): p. 8788-8793.

103. Corella, J., A. Orío, and P. Aznar, *Biomass Gasification with Air in Fluidized Bed: Reforming of the Gas Composition with Commercial Steam Reforming Catalysts*. Industrial & Engineering Chemistry Research, 1998. **37**(12): p. 4617-4624.

104. Corella, J., et al., *Biomass Gasification in Fluidized Bed: Where To Locate the Dolomite To Improve Gasification?* Energy & Fuels, 1999. **13**(6): p. 1122-1127.

105. Narváez, I., J. Corella, and A. Orío, *Fresh Tar (from a Biomass Gasifier) Elimination over a Commercial Steam-Reforming Catalyst. Kinetics and Effect of Different Variables of Operation*. Industrial & Engineering Chemistry Research, 1997. **36**(2): p. 317-327.

106. Yung, M., et al., *Demonstration and Characterization of Ni/Mg/K/AD90 Used for Pilot-Scale Conditioning of Biomass-Derived Syngas*. Catalysis Letters, 2010. **134**(3): p. 242-249.

107. Ding, Y. and E. Alpay, *Adsorption-enhanced steam–methane reforming*. Chemical Engineering Science, 2000. **55**(18): p. 3929-3940.

108. Abanades, J.C. and D. Alvarez, *Conversion Limits in the Reaction of CO2 with Lime*. Energy & Fuels, 2003. **17**(2): p. 308-315.

109. Juan Carlos, A., *The maximum capture efficiency of CO2 using a carbonation/calcination cycle of CaO/CaCO3*. Chemical Engineering Journal, 2002. **90**(3): p. 303-306.

110. Sabatier, P. and J.B. Senderens, *Hydrogenation of CO Over Nickel to Produce Methane*. J.Soc. Chim. Ind., 1902. **21**.

111. *Fischer-Tropsch Archive*. 2012; Available from: http://fischer-tropsch.org/.

112. van Berge, P.J. and R.C. Everson, *Cobalt as an alternative Fischer-Tropsch catalyst to iron for the production of middle distillates*, in *Studies in Surface Science and Catalysis*, R.L.E.C.P.N.J.H.S.a.M.S.S. M. de Pontes, Editor. 1997, Elsevier. p. 207-212.

113. Raje, A., J.R. Inga, and B.H. Davis, *Fischer-Tropsch synthesis: Process considerations based on performance of iron-based catalysts*. Fuel, 1997. **76**(3): p. 273-280.

114. Anderson and Boudart, *Vannice, in Catalysis: Science & Technology*. Vol. 3, Berlin: Springer-Verlag.

115. GRUVER, et al., *The role of accumulated carbon in deactivating cobalt catalysts during FT synthesis in a slurry-bubble-column reactor*. Vol. 50. 2005, Washington, DC, ETATS-UNIS: American Chemical Society. 3.

116. Tsakoumis, N.E., et al., *Deactivation of cobalt based Fischer–Tropsch catalysts: A review*. Catalysis Today, 2010. **154**(3–4): p. 162-182.

117. Schanke, D., et al., *Study of the deactivation mechanism of Al₂O₃-supported cobalt Fischer-Tropsch catalysts*. Catalysis Letters, 1995. **34**(3): p. 269-284.

118. Kogelbauer, A., J.C. Weber, and J.G. Goodwin, *The formation of cobalt silicates on Co/SiO₂ under hydrothermal conditions*. Catalysis Letters, 1995. **34**(3): p. 259-267.

119. van Berge, P.J., et al., *Oxidation of cobalt based Fischer–Tropsch catalysts as a deactivation mechanism*. Catalysis Today, 2000. **58**(4): p. 321-334.

120. Hilmen, A.M., et al., *Study of the effect of water on alumina supported cobalt Fischer–Tropsch catalysts*. Applied Catalysis A: General, 1999. **186**(1–2): p. 169-188.

121. Li, J., et al., *Fischer–Tropsch synthesis: effect of water on the catalytic properties of a ruthenium promoted Co/TiO2 catalyst*. Applied Catalysis A: General, 2002. **233**(1–2): p. 255-262.

122. Li, J., et al., *Fischer–Tropsch synthesis: effect of water on the catalytic properties of a Co/SiO2 catalyst*. Applied Catalysis A: General, 2002. **236**(1–2): p. 67-76.

123. Li, J., et al., *Fischer–Tropsch synthesis: effect of water on the deactivation of Pt promoted Co/Al2O3 catalysts*. Applied Catalysis A: General, 2002. **228**(1–2): p. 203-212.

124. Huber, G., et al., *Gd promotion of Co/SiO2 Fischer–Tropsch synthesis catalysts*. Catalysis Letters, 2001. **74**(1): p. 45-48.

125. Jacobs, G., et al., *Fischer–Tropsch synthesis: deactivation of noble metal-promoted Co/Al2O3 catalysts*. Applied Catalysis A: General, 2002. **233**(1–2): p. 215-226.

126. Jacobs, G., et al., *Fischer–Tropsch synthesis XAFS: XAFS studies of the effect of water on a Pt-promoted Co/Al2O3 catalyst*. Applied Catalysis A: General, 2003. **247**(2): p. 335-343.

127. Kiss, G., et al., *Hydrothermal deactivation of silica-supported cobalt catalysts in Fischer–Tropsch synthesis*. Journal of Catalysis, 2003. **217**(1): p. 127-140.

128. Gardezi, S., J. Wolan, and B. Joseph, *An Integrated Approach to the preparation of effective Catalyst for Biomass-to-Liquid(BTL) process*. 2011, University of South Florida. p. 1-12.

129. Gardezi, S.A., et al., *Synthesis of Tailored Eggshell Cobalt Catalysts for Fischer–Tropsch Synthesis Using Wet Chemistry Techniques*. Industrial & Engineering Chemistry Research, 2011. **51**(4): p. 1703-1712.

130. Kang, J.S., et al., *Nickel-based tri-reforming catalyst for the production of synthesis gas*. Applied Catalysis A: General, 2007. **332**(1): p. 153-158.

131. Song, C. and W. Pan, *Tri-reforming of methane: a novel concept for catalytic production of industrially useful synthesis gas with desired H2/CO ratios*. Catalysis Today, 2004. **98**(4): p. 463-484.

132. Choudhary, V.R., K.C. Mondal, and T.V. Choudhary, *Oxy-methane reforming over high temperature stable NiCoMgCeOx and NiCoMgOx supported on zirconia–haffnia catalysts: Accelerated sulfur deactivation and regeneration*. Catalysis Communications, 2007. **8**(3): p. 561-564.

133. Choudhary, V.R., K.C. Mondal, and T.V. Choudhary, *Oxy-CO2 Reforming of Methane to Syngas over CoOx/CeO2/SA-5205 Catalyst*. Energy & Fuels, 2006. **20**(5): p. 1753-1756.

134. Choudhary, V.R., K.C. Mondal, and T.V. Choudhary, *Methane reforming over a high temperature stable-NiCoMgOx supported on zirconia–hafnia catalyst*. Chemical Engineering Journal, 2006. **121**(2–3): p. 73-77.

135. Choudhary, V.R., K.C. Mondal, and A.S. Mamman, *High-temperature stable and highly active/selective supported NiCoMgCeOx catalyst suitable for autothermal reforming of methane to syngas*. Journal of Catalysis, 2005. **233**(1): p. 36-40.

136. Song, C., et al., *Tri-reforming of methane over Ni catalysts for CO2 conversion to Syngas with desired H2CO rateios using flue gas of power plants without CO2 separation*. Studies in Surface Science and Catalysis, 2004. **153**: p. 315-322.

137. Pino, L., et al., *Hydrogen production by methane tri-reforming process over Ni–ceria catalysts: Effect of La-doping*. Applied Catalysis B: Environmental, 2011. **104**(1–2): p. 64-73.

138. Carl-Jochen, W., *Hydrogen energy — Abundant, efficient, clean: A debate over the energy-system-of-change*. International Journal of Hydrogen Energy, 2009. **34**(14, Supplement 1): p. S1-S52.

139. Raudaskoski, R., et al., *Catalytic activation of CO2: Use of secondary CO2 for the production of synthesis gas and for methanol synthesis over copper-based zirconia-containing catalysts*. Catalysis Today, 2009. **144**(3–4): p. 318-323.

140. Aresta, M. and I. Tommasi, *Carbon dioxide utilisation in the chemical industry*. Energy Conversion and Management, 1997. **38, Supplement**(0): p. S373-S378.

141. Aresta, M., A. Dibenedetto, and C. Pastore, *Biotechnology to develop innovative syntheses using CO₂*. Environmental Chemistry Letters, 2005. **3**(3): p. 113-117.

142. Laosiripojana, N., W. Sutthisripok, and S. Assabumrungrat, *Synthesis gas production from dry reforming of methane over CeO2 doped Ni/Al2O3: Influence of the doping ceria on the resistance toward carbon formation*. Chemical Engineering Journal, 2005. **112**(1–3): p. 13-22.

143. Takeguchi, T., et al., *Autothermal reforming of methane over Ni catalysts supported over CaO–CeO2–ZrO2 solid solution*. Applied Catalysis A: General, 2003. **240**(1–2): p. 223-233.

144. Xu, S. and X. Wang, *Highly active and coking resistant Ni/CeO2–ZrO2 catalyst for partial oxidation of methane*. Fuel, 2005. **84**(5): p. 563-567.

145. Chen, J., et al., *Effect of preparation methods on structure and performance of Ni/Ce0.75Zr0.25O2 catalysts for CH4–CO2 reforming*. Fuel, 2008. **87**(13–14): p. 2901-2907.

146. Montoya, J.A., et al., *Methane reforming with CO2 over Ni/ZrO2–CeO2 catalysts prepared by sol–gel*. Catalysis Today, 2000. **63**(1): p. 71-85.

147. Roh, H.-S., et al., *Highly active and stable Ni/Ce–ZrO2 catalyst for H2 production from methane*. Journal of Molecular Catalysis A: Chemical, 2002. **181**(1–2): p. 137-142.

148. de Leitenburg, C., et al., *The effect of doping CeO2 with zirconium in the oxidation of isobutane*. Applied Catalysis A: General, 1996. **139**(1–2): p. 161-173.

149. Roh, H.-S., et al., *Catalyst deactivation and regeneration in low temperature ethanol steam reforming with Rh/CeO₂–ZrO₂ catalysts*. Catalysis Letters, 2006. **110**(1): p. 1-6.

150. Roh, H.-S., K.-W. Jun, and S.-E. Park, *Methane-reforming reactions over Ni/Ce-ZrO2/θ-Al2O3 catalysts*. Applied Catalysis A: General, 2003. **251**(2): p. 275-283.

151. Srisiriwat, N., S. Therdthianwong, and A. Therdthianwong, *Oxidative steam reforming of ethanol over Ni/Al2O3 catalysts promoted by CeO2, ZrO2 and CeO2–ZrO2*. International Journal of Hydrogen Energy, 2009. **34**(5): p. 2224-2234.

152. Gao, J., et al., *Production of syngas via autothermal reforming of methane in a fluidized-bed reactor over the combined CeO2–ZrO2/SiO2 supported Ni catalysts*. International Journal of Hydrogen Energy, 2008. **33**(20): p. 5493-5500.

153. Zhuang, Q., Y. Qin, and L. Chang, *Promoting effect of cerium oxide in supported nickel catalyst for hydrocarbon steam-reforming*. Aplied Catalysis, 1991. **70**: p. 1-8.

154. Nagai, Y., et al., *Structure Analysis of CeO2-ZrO2 Mixed Oxides as Oxygen Storage Promoters in Automative Catalysts*, in *R&D Review of Toyota CRDL*. 2002. p. 20-27.

155. Shannon, R.D. and C.T. Prewitt, *Effective ionic radii in oxides and fluorides*. Acta Crystallographica Section B, 1969. **25**(5): p. 925-946.

156. Laosiripojana, N. and S. Assabumrungrat, *Methane steam reforming over Ni/Ce–ZrO2 catalyst: Influences of Ce–ZrO2 support on reactivity, resistance toward carbon formation, and intrinsic reaction kinetics*. Applied Catalysis A: General, 2005. **290**(1–2): p. 200-211.

157. Zhu, T. and M. Flytzani-Stephanopoulos, *Catalytic partial oxidation of methane to synthesis gas over Ni–CeO2*. Applied Catalysis A: General, 2001. **208**(1–2): p. 403-417.

158. Sidjabat, O. and D.L. Trimm, *Nickel–magnesia catalysts for the steam reforming of light hydrocarbons*. Topics in Catalysis, 2000. **11-12**(1): p. 279-282.

159. Trimm, D.L., *Design of industrial catalysts*. 1980, New York: Elsevier Scientific Pub. Co.

160. Rossignol, S., F. Gerard, and D. Duprez, *Effect of the preparation method on the properties of zirconia-ceria materials*. Journal of Materials Chemistry, 1999. **9**(7).

161. Li, J., et al., *Preparation of Nano-NiO Particles and Evaluation of Their Catalytic Activity in Pyrolyzing Biomass Components†*. Energy & Fuels, 2007. **22**(1): p. 16-23.

162. Brunauer, S., P.H. Emmett, and E. Teller, *Adsorption of Gases in Multimolecular Layers*. Journal of the American Chemical Society, 1938. **60**(2): p. 309-319.

163. Dorset, D.L., *X-ray Diffraction: A Practical Approach*. Microscopy and Microanalysis, 1998. **4**(05): p. 513-515.

164. Ravel, B. and M. Newville, *ATHENA, ARTEMIS, HEPHAESTUS: data analysis for X-ray absorption spectroscopy using IFEFFIT*. Journal of Synchrotron Radiation, 2005. **12**(4): p. 537-541.

165. Newville, M., *IFEFFIT : interactive XAFS analysis and FEFF fitting*. Journal of Synchrotron Radiation, 2001. **8**(2): p. 322-324.

166. Delgass, W.N., et al., *Spectroscopy in Heterogeneous Catalysis*. 1979, N.Y.: Academic Press Inc.

167. Defosse, C., F. Delannay, and M. Dekker, *X-ray Photoelectron Spectroscopy, in Characterization of Heterogeneous Catalysts*. F ed. 1984, N.Y.

168. Niemantsverdriet, J.W., *Frontmatter*, in *Spectroscopy in Catalysis*. 2007, Wiley-VCH Verlag GmbH. p. I-XII.

169. Xu, B.-Q., et al., *Nano-MgO: novel preparation and application as support of Ni catalyst for CO2 reforming of methane*. Catalysis Today, 2001. **68**(1–3): p. 217-225.

170. Sánchez Escribano, V., et al., *Characterization of cubic ceria–zirconia powders by X-ray diffraction and vibrational and electronic spectroscopy*. Solid State Sciences, 2003. **5**(10): p. 1369-1376.

171. Binet, C., A. Badri, and J.-C. Lavalley, *A Spectroscopic Characterization of the Reduction of Ceria from Electronic Transitions of Intrinsic Point Defects*. The Journal of Physical Chemistry, 1994. **98**(25): p. 6392-6398.

172. Ranga, G.R., *Structural, redox and catalytic chemistry of ceria based materials*. Bulletin of teh Catalysis Society of India, 2003. **2**: p. 122-134.

173. Souza, M.M.V.M. and M. Schmal, *Combination of carbon dioxide reforming and partial oxidation of methane over supported platinum catalysts*. Applied Catalysis A: General, 2003. **255**(1): p. 83-92.

174. Xu, J., et al., *Methane steam reforming for hydrogen production using low water-ratios without carbon formation over ceria coated Ni catalysts*. Applied Catalysis A: General, 2008. **345**(2): p. 119-127.

175. Goswami, Y.D., F. Kreith, and K. J.F, *Principles of Solar Engineering*. 2nd ed. 2000, New York, NY: Taylor and Francis Group.

176. Petri, R. and T.D. Clarr, *High Temperature Molten Salt Thermal Energy Storage Systems for Solar Applications*. 1980, NASA.

177. Gil, A., et al., *State of the art on high temperature thermal energy storage for power generation. Part 1—Concepts, materials and modellization*. Renewable and Sustainable Energy Reviews, 2010. **14**(1): p. 31-55.

178. Boger, T., A.K. Heibel, and C.M. Sorensen, *Monolithic Catalysts for the Chemical Industry*. Industrial & Engineering Chemistry Research, 2004. **43**(16): p. 4602-4611.

179. Kolb, G., et al., *Heliostat Cost Reduction Study*. 2006, SANDIA Laboratories.

180. Boerrigter, H., *Economy of Biomass-to-Liquids (BTL) Plants*. 2006, ECN Biomass, Coal & Environmental research.

Appendices

Appendix A: Solar Calculations

Month	n (days)	δs	Latitude	hsr (radians)	hsr (degrees)	a	b	d	hcoll (Deg)	hcoll (radians)	rt	CR	rd	hss	Hh	Ho,h	KT	Dh/Hh	Dh	Hc
June	166	23.31	33.43	-1.86	-106.52	0.2921	0.7720	-1.49	-104.52	-1.82	1.12	678	1.60	1.86	30090	40986	0.73	0.36	10908.62	16350.85
July	196	21.52	33.43	-1.83	-105.09	0.2799	0.7836	-1.44	-103.09	-1.80	1.13	678	1.60	1.83	27370	40154	0.68	0.35	9703.50	15380.24
August	227	13.78	33.43	-1.73	-99.32	0.2319	0.8292	-1.27	-97.32	-1.70	1.18	678	1.65	1.73	25440	37022	0.69	0.32	8197.10	16578.56
September	258	2.22	33.43	-1.60	-91.46	0.1693	0.8887	-1.04	-89.46	-1.56	1.33	678	1.80	1.60	21920	31768	0.69	0.28	6097.94	18166.72
October	288	-9.60	33.43	-1.46	-83.59	0.1113	0.9438	-0.83	-81.59	-1.42	1.60	678	2.08	1.46	17600	25397	0.69	0.23	4120.38	19538.54
November	319	-19.15	33.43	-1.34	-76.75	0.0653	0.9875	-0.67	-74.75	-1.30	1.98	678	2.48	1.34	12950	19998	0.65	0.20	2535.73	19292.71
December	349	-23.34	33.43	-1.28	-73.45	0.0449	1.0070	-0.59	-71.45	-1.25	2.22	678	2.74	1.28	10560	17587	0.60	0.18	1872.65	18335.89
January	15	-21.27	33.43	-1.31	-75.11	0.0550	0.9973	-0.63	-73.11	-1.28	2.09	678	2.60	1.31	11580	19070	0.61	0.19	2161.18	18601.03
Febuary	45	-13.62	33.43	-1.41	-80.8	0.0920	0.9622	-0.76	-78.8	-1.38	1.73	678	2.22	1.41	15330	23715	0.65	0.22	3349.49	19108.69
March	74	-2.82	33.43	-1.54	-88.14	0.1442	0.9125	-0.95	-86.14	-1.50	1.42	678	1.90	1.54	19870	29953	0.66	0.26	5158.25	18509.83
April	105	9.41	33.43	-1.68	-96.28	0.2072	0.8527	-1.18	-94.28	-1.65	1.23	678	1.70	1.68	25440	35820	0.71	0.31	7763.88	18089.33
May	135	18.79	33.43	-1.90	-108.65	0.3103	0.7547	-1.55	-106.65	-1.86	1.06	678	1.51	1.90	28850	39589	0.73	0.37	10803.27	14200.35

Design value Hc
occurs around 17% time 19107 KJ/m2-day

Appendix B: Permissions

ELSEVIER LICENSE
TERMS AND CONDITIONS

Mar 13, 2012

This is a License Agreement between Devin M Walker ("You") and Elsevier ("Elsevier") provided by Copyright Clearance Center ("CCC"). The license consists of your order details, the terms and conditions provided by Elsevier, and the payment terms and conditions.

All payments must be made in full to CCC. For payment instructions, please see information listed at the bottom of this form.

Supplier	Elsevier Limited The Boulevard,Langford Lane Kidlington,Oxford,OX5 1GB,UK
Registered Company Number	1982084
Customer name	Devin M Walker
Customer address	2625 Fiddlestick Cir. Lutz, FL 33559
License number	2838930124857
License date	Jan 30, 2012
Licensed content publisher	Elsevier
Licensed content publication	Renewable and Sustainable Energy Reviews
Licensed content title	Review and analysis of biomass gasification models
Licensed content author	Maria Puig-Arnavat,Joan Carles Bruno,Alberto Coronas
Licensed content date	December 2010
Licensed content volume number	14
Licensed content issue number	9
Number of pages	11
Start Page	2841
End Page	2851
Type of Use	reuse in a thesis/dissertation
Portion	figures/tables/illustrations
Number of figures/tables/illustrations	1
Format	both print and electronic
Are you the author of this Elsevier article?	No
Will you be translating?	No
Order reference number	None
Title of your thesis/dissertation	Catalytic Trireforming of Biomass-derived syngas to Produce Desired H2:CO Ratios for Fuel Applications
Expected completion date	Apr 2012
Estimated size (number of pages)	100
Elsevier VAT number	GB 494 6272 12
Permissions price	0.00 USD
VAT/Local Sales Tax	0.0 USD / 0.0 GBP
Total	**0.00 USD**
Terms and Conditions	

Appendix B (Continued)

JOHN WILEY AND SONS LICENSE TERMS AND CONDITIONS

Mar 13, 2012

This is a License Agreement between Devin M Walker ("You") and John Wiley and Sons ("John Wiley and Sons") provided by Copyright Clearance Center ("CCC"). The license consists of your order details, the terms and conditions provided by John Wiley and Sons, and the payment terms and conditions.

All payments must be made in full to CCC. For payment instructions, please see information listed at the bottom of this form.

License Number	2833730358267
License date	Jan 21, 2012
Licensed content publisher	John Wiley and Sons
Licensed content publication	Wiley Books
Licensed content title	Fundamentals of Industrial Catalytic Processes, 2nd Edition
Licensed content author	C. H. Bartholomew (Brigham Young University, Provo, UT), Robert J. Farrauto (Engelhard Corporation, Iselin, NJ)
Licensed content date	Oct 1, 2005
Type of use	Dissertation/Thesis
Requestor type	University/Academic
Format	Print and electronic
Portion	Figure/table
Number of figures/tables	1
Number of extracts	None
Original Wiley figure/table number(s)	Table 6.34
Will you be translating?	No
Order reference number	None
Total	**0.00 USD**
Terms and Conditions	